WASHINGTON UNIVERSITY

SEVER INSTITUTE OF TECHNOLOGY

MICROMIXING IN SACCHAROMYCES CEREVISIAE AEROBIC FERMENTATION

BY

Shao-Jian Ye

Prepared under the direction of Professor E. H. Dunlop

A research proposal presented to the Department of Chemical Engineering of Washington University in partial fulfillment of the requirements for the degree of

DOCTOR OF SCIENCE

January, 1985

Saint Louis, Missouri

WASHINGTON UNIVERSITY
SEVER INSTITUTE OF TECHNOLOGY

ABSTRACT

MICROMIXING IN SACCHAROMYCES CEREVISIAE AEROBIC FERMENTATION

by Shao-Jian Ye

ADVISOR: Professor E. H. Dunlop

January, 1985

Saint Louis, Missouri

This paper presents a detailed micromixing study of fermentation in a Virtis fermenter. The fermenter characterized by the experimental technique, which is investigated and developed previously, is used for the fermentation of Baker's yeast (Saccharomyces cerevisiae) under the conditions of glucose-limitation. Complex gas-liquid micromixing effects and biological effects, hitherto unreported, are observed.

The conclusions of the paper point out that even in a laboratory scale fermenter with perfect macromixing, micromixing is still incomplete. In the gas-liquid-two-phase fermenter, increasing agitation improves micromixing but increasing gas flow may improve or deteriorate micromixing. The incompleteness in micromixing deteriorates glucose uptake of Saccharomyces cerevisiae, leading to poorer cell budding, lower biomass yield and protein synthesis rate. A diffusion-reaction model is used to predict glucose uptake and cell-population concentration under steady state of continuous culture. Also proposed is the future work extending the results to five different injection ports and a series of dilution rate.

TABLE OF CONTENTS

TABLE OF CONTENTS
(continued)

TABLE OF CONTENTS
(continued)

TABLE OF CONTENTS
(continued)

LIST OF TABLES

LIST OF FIGURES

LIST OF FIGURES
(continued)

LIST OF FIGURES
(continued)

MICROMIXING IN SACCHAROMYCES CEREVISIAE AEROBIC FERMENTATION

1. INTRODUCTION

1.1 BACKGROUND TO THE RESEARCH

Fermentation, a process frequently used in biotechnology, involves three important components: fermenters, strains (living organisms) and media. In conventional fermenters, the cells of size about 5 microns may be conceptually thought of as sitting in eddies, the smallest of which is typically about 100 microns. Since biochemical reactions are fast and the diffusion rates of substrates and metabolites are slow, nutrients are rapidly depleted and metabolites rapidly accumulated inside the eddies. Therefore, these eddies can be thought of as stagnant pools which segregate the microbes from the rich nutrient source outside the eddies. Hence in fermentation media, there are actually two different kinds of growth environments: macroenvironments outside the eddies which are relatively rich in nutrients, and microenvironments inside the eddies which are relatively poor for the growth of microbes. Although the mixing outside these eddies may be perfect, mixing inside the eddies (micromixing) may not yet be complete. Therefore, no matter how good the overall average growth conditions are, microbial growth still depends on nutrient and metabolite diffusion, and is comparatively slow.

With respect to strains, Saccharomyces cerevisiae is sensitive to glucose level in the media. These concerns raise two main serious obstacles to the efficient growth of microbes:

1. limited substrates provide less nutrients for the growth and reduce the biochemical reaction rate (governed by Michaelis-Menten kinetics);

2. locally-overproduced metabolites reverse the reactions and may be toxic to the enzymes of the microbes.

Imperfect mixing will make these problems become worse as the fermenters are scaled up. It will lead to reduced yields and higher energy consumption in large scale fermentation. Increasing power input to stirrers is not an efficient solution to this problem, because the smallest eddy size is proportional to the energy input raised to the minus one quarter power.

To enhance micromixing (i.e. the mass transfer from macroenvironments to microenvironments in which microbes grow), it is necessary to further investigate the principles of micromixing, particularly in multiphase bioreactors.

1.2 PURPOSE AND OBJECTIVE OF THE RESEARCH

The objective of the research is to relate engineering variables to biological responses in fermentation in terms of micromixing or eddy size. As a first step, the effects of engineering variables on micromixing in a conventional fermenter must be investigated; secondly, the fermenter so characterized can be used to carry out fermentations to find the biological responses, if any; thirdly, the biological responses need to be related to the engineering variables. The characterization technique used involves a very fast reaction between a slight excess of

reactant A (1-naphthol) and reactant B (p-diazobenzene sulfonate). Under perfect mixing conditions, the reaction forms a mono-substituted azo dye. Under less than perfect mixing conditions, a disubstituted azo dye is formed even in the presence of excess 1-naphthol. The product concentrations can be measured by visible spectrophotometry.

A set of mathematical models based on diffusion-reaction mechanisms can then be used to relate the product distribution to the micromixing conditions in terms of eddy size. Also proposed is a model predicting the growth of Baker's yeast as function of micromixing.

1.3 POSSIBLE APPLICATIONS OF MICROMIXING STUDY

The micromixing study in biological reactors will have some applications to other biological processes. Specifically, the study will have fundamental scientific applications for the studies of:

1. micromixing effects in gas-liquid systems;

2. mechanisms of substrate (oxygen) transport in Saccharomyces cerevisiae aerobic fermentations;

3. micromixing effects on Saccharomyces cerevisiae metabolism and dynamic growth;

4. micromixing and shear effects in stirred tank reactors;

Technically, micromixing study in biological reactors will provide some indications on a finer scale, which are still not very clear, for the improved design of biological reactors. Further, enhancing micromixing in bioreactors can improve the efficiency of large scale biological processes so that relatively high yield and low energy consumption can be obtained.

2. BACKGROUND TO MICROMIXING STUDY

2.1 MICROMIXING CONCEPT AND ITS HISTORICAL BACKGROUND

It has long been recognized [1,2,3,67,77,90] that turbulent mixing is very important to momentum, energy and mass transfer. Theoretically, mixing in a reactor depends upon two interrelated and interactive aspects [12,14,82-85]: 1. macromixing - mixing but only on a macroscopic scale; and 2. micromixing - mixing on a molecular scale (Figure 2.1). In continuous reactors, macromixing may be regarded as a process of particles intermingling in flow, each particle remaining as a distinct and separate aggregate of molecules and retaining its identity as it passes through the process [4]. It can also be defined by the residence time distribution (RTD) [82]. On the other hand, micromixing may be viewed as a transition from segregation by age to segregation by life expectation [5,14,83,85]. In other words, whether the fluid elements have a tendency to aggregate and be surrounded by elements of the same age (state of aggregation), and whether the fluid mixes early or late as it flows through the vessel (earliness of mixing) [6].

Macroscale mixing has been long investigated by classical fluid mechanics and chemical engineering methods. The concept of micromixing, however, has only begun to receive attention during the past 10 or 15

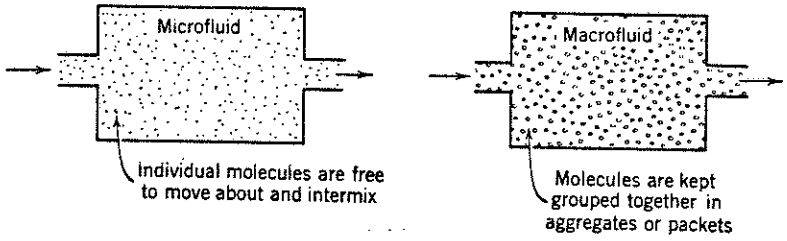

Figure 2.1. Flow of idealized microfluid and macrofluid. Tracer measurements cannot distinguish between them; however, for chemical reactions these fluids may behave differently. [6]

years. The phenomenon of micromixing is relatively easy to understand but the mathematics used for modelling and predicting the level of micromixing achieved is quite complex. It has its bases in macromixing and/or a number of historically recognized areas of scientific endeavor, for example mixing and turbulence.

In 1952, Danckwerts [7] defined the concept of the Intensity of segregation at the molecular level. The measurement of the intensity of segregation has been developed and widely applied by Danckwerts [8] and Hiby [9].

In 1958, Kramers [10] showed that RTD alone was not enough to calculate chemical conversion unless the reaction order was equal to one. This case is illustrated in Figure 2.1a. Danckwerts [11] proposed the concept of segregation which indicates that in the same vessel, there are clumps of fluid with different concentrations, caused by incomplete mixing. As opposed to one extreme of segregation - ''complete segregation'', Zwietering [12] introduced the concept of ''maximum mixedness'' or ''no segregation''. Danckwerts pointed out that the state of segregation was determined by: (a) the scale of segregation and (b) the degree of segregation (so-called intensity of micromixing). As for the earliness of mixing, complete segregation requires that the completely segregated clumps flow until mixing occurs at the outlet (or as the fluid is sampled for analysis), i.e. there is segregation throughout the entire system up to the outlet, or late mixing. Maximum mixedness requires the intimate micromixing of the clumps at the earliest stage, i.e. early mixing. These two bounds on mixing may result in the same RTD, but the conversions of the reactions in the two systems can be different [13], as shown in Figure 2.2b.

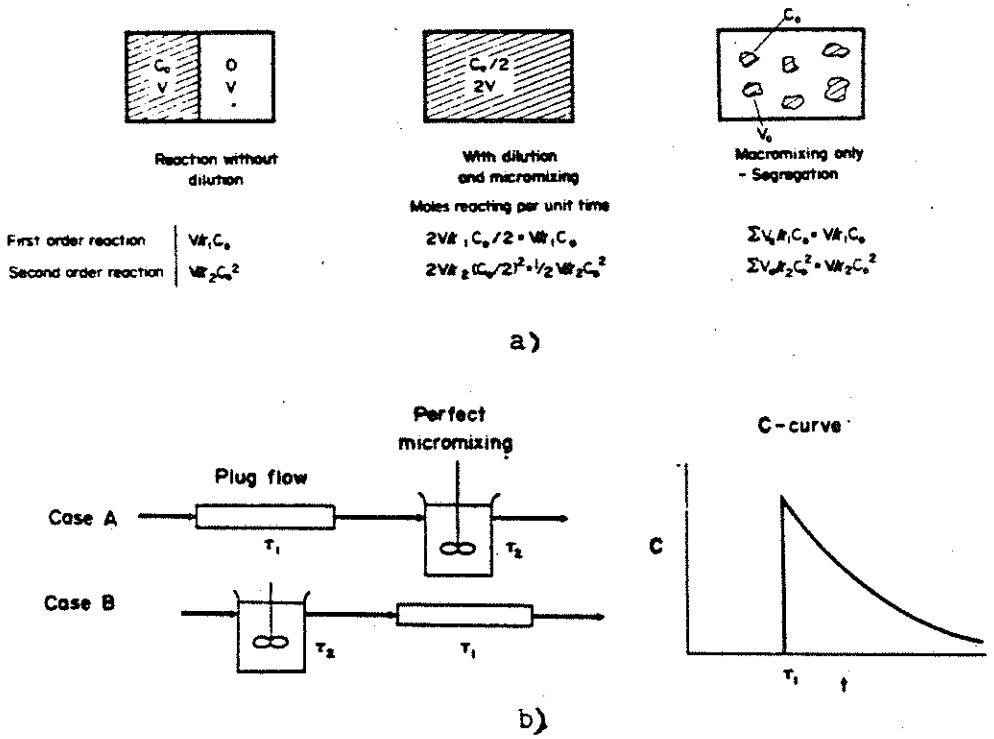

Figure 2.2. a). Influence of state of mixing on first and second order reaction rate [4]. b). Kramer's example of a PRF and CSTR in series (Note that the C-curve is the same for both cases) [7].

Between these two extremes, several classes of models have been proposed for intermediate level of micromixing, with arbitrary RTD. For example, Weinstein and Adler [14], and Villermaux and Zoulalian [15] consider the reactor contents to be comprised of two parts - a segregated region and a maximally mixed region (environment models). Another approach is to consider that mixing is accomplished either by coalescence-and-redispersion mechanisms or by diffusion. Based upon the population balance concept, the coalescence-and-redispersion mechanism considers that during mixing the liquid is broken into small ''droplets''. These droplets have a boundary but may not be different in composition from a neighboring droplet or from the bulk. The droplets then coalesce and redisperse with a characteristic frequency, depending upon the energy input. These ''droplets'' can be thought of

as eddies. Aubry and Villermaux [16] gave a simplified version that only considered mean micromixing coalescence effects, but that appears to give similar results to the more complicated population balance equations. Other descriptions of micromixing are based upon the physical bases of the ultimate microturbulence and molecular diffusivities of the fluid elements. For example, Nauman [17] proposed that the ultimate molecular mixing events before reactions should be based upon molecular diffusion within the smallest eddies - presumably determined by the mixing and/or turbulence level. In this case, the micro-timescale would be the diffusion time and a segregation number could be defined as the ratio of the micro- to macro-timescale. Nauman chose the reactor mean residence time as the macrotime but Truong and Methot [18] consider the inverse of a characteristic first order (or pseudo first order) rate constant to be a better one. Alternately, Ott [19], Nabholz et al [20,21,22] and Bourne [23,25-31] used the ratio of diffusion to reaction time for fast reactions with mass transfer the controlling mechanism.

As another approach, turbulent momentum and mass transfer theories are also applied to determine velocity fluctuations and to relate them to concentration fluctuations, thus to local reaction rates [1,32,33].

Finally, the so-called fluid flow models are also used wherein a simplified fluid mechanical model is built by spatial interconnection of zones, each having well defined macro- and micro-mixedness [34,35,36].

2.2 MICROMIXING IN STIRRED TANK REACTORS - SELECTION OF SIMULATION MODEL

In stirred tank reactors, micromixing process may be interpreted by the three successive or simultaneous stages initially proposed by Beek and Miller in 1959 [37]:

1. Distribution of one fluid throughout the other, and homogenization of overall composition without decreasing local concentration variations;

2. Reduction of the size of the regions with uniform composition and increase of contact areas between regions of different composition;

3. Mixing by molecular diffusion.

Since the process in stage 1 is really concerned with macromixing, we will assume that it is very fast in perfectly macromixed reactors.

Two different mechanisms may be involved in stage 2:

1. Laminar Stretching of Aggregates(Figure 2.3a). Under laminar viscous friction, aggregates are gradually stretched out and folded up, but their volume remains constant. The fluid ends up with a lamellar or striated texture characterized by an average striation thickness.

2. Turbulent Erosion of Aggregates(Figure 2.3b). Under the influence of turbulent shear, the aggregates are gradually eroded and they shrink as they lose matter to the environment.

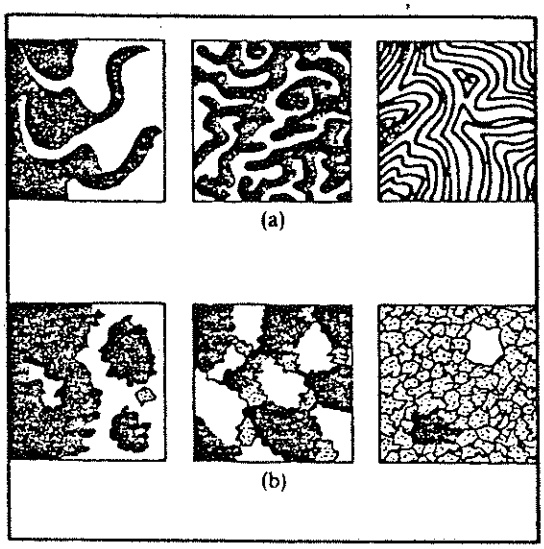

Figure 2.3. (a) laminar mixing: stretching out of aggregates leading to a striated structure; (b) turbulent mixing: erosion of fresh fluid aggregates leading to ultimate aggregates containing a mixture of reactants. [136]

In reality, micromixing may be obtained by a combination of stage 2 and 3, and the behavior of aggregates should be somewhere between laminar stretching and turbulent erosion, depending upon the local mixing situation or fluid flow characteristics. Although molecular diffusion is significant to micromixing in fast reactions, step 2 is also very important to defining the dimension of micromixing zones and/or time scale. A diffusion - reaction model proposed by Bourne [28] is used here to simulate the formation of micromixing zone. It is simple, has physical sense and gives good predictions [26-31].

2.3 TECHNIQUES USED IN MICROMIXING STUDY - SELECTION OF METHOD

Experimental techniques characterizing micromixing processes can be divided into two categories: 1) physical methods, e.g. electrical conductivity [40,41], light absorption, fluorescence [42], etc., and 2) chemical methods such as azo-coupling [23,26], nitration of aromatic hydrocarbons [22], bromation of resorcin [24], etc. The spatial resolution of physical methods (optical, electrical microprobes) is often poor [41] and is difficult to apply to multiphase systems. Chemical methods are much more powerful because the reactant species act as molecular probes for micromixing. For example, if the reactor is partially segregated, the extent of reaction will be a function of segregation:

$$X = \lambda X_{macro} + (1 - \lambda)X_{micro} \qquad (2.1)$$

or in more complex function form,

$$X = \lambda f_1(X_{macro}) + (1 - \lambda)f_2(X_{micro}) \qquad (2.2)$$

where X_{macro} and X_{micro} are the limiting extent of reaction observed in a well macromixed reactor and λ is a ratio constant.

This also stands for the yield of final product and is the basis

for the determination of λ, or conversely for the prediction of X [23,26].

To experimentally characterize a micromixing process using chemical reactions, some other practical criteria must also be satisfied [43]: $t_R << t_D$; distribution of products depending on segregation; irreversible reactions; known mechanism; easy analysis and regeneration; safe and inexpensive chemicals; etc.

The chemical reaction technique of fast, competitive, consecutive reaction was extensively used by Bourne and coworkers [23,25-31], especially the coupling of 1-naphthol (A) and p-diazobenzene sulfonate (B). This reaction technique was further developed in the micromixing study in this work.

2.4 RELATIONS BETWEEN MICROMIXING AND SYSTEM CHARACTERISTICS - SELECTION OF INVESTIGATED VARIABLES

Micromixing effects are very complex. For convenience, these effects can be summarized as three interrelated, interacting aspects [44]: material properties (diffusivity [23,27], viscosity [28], surface tension [45], etc), chemical characteristics (rate constant [23,27], order, complexity and linearality of rate equations [46], conversion level [47], etc.) and engineering variables (reactant feed port [26,28], premixed and unpremixed feed streams [40], agitation and gas flow [26,28,48,49,50], RTD [58], multiphase phenomena [52-55], etc.). The complexity not only results from the separate effects of these parameters but also from the interactions of one on another. For example, in fast reactions, the relative ratio of reaction rate constant and diffusivity determines the importance of micromixing. When this ratio is very large, i.e. rate constant is very large or reaction is

very fast, or diffusivity is very small, or micromixing zones are big, the diffusion rate would be much lower than the reaction rate and diffusion is the controlling mechanism. On the other hand, when this ratio is small, i.e. slow reactions, small eddy size or small micromixing zone, or greatly enhanced mass transfer by a surface active agent or by emulsification [56], kinetics is the controlling mechanism and macromixing is more important. Since the chemical reaction technique was used in this work, some chemical parameters of the reactions need to be investigated. In addition, agitation, gas flow and injection ports in a stirred tank fermenter were chosen as the main engineering variables for investigation. This is because:

1. most industrial fermenters are multiphase stirred tank reactors;

2. previous work showed that in stirred tanks, the distribution of the eddy size and energy dissipation is very uneven [41,67];

3. some mixing results with Baker's yeast fermentation showed that in stirred tanks, mixing is important to biomass yield [58,100];

4. the applications of the reaction technique to the study of stirred tanks was well developed [25,26].

2.5 EFFECTS OF MICROMIXING ON BIOLOGICAL SYSTEMS

Micromixing is expected to be of great importance in biochemical reactors because of the characteristics of biological systems.

Biological materials are generally very viscous, high surface tension solid (cell)-liquid-gas suspension, nonnewtonian fluids with complex colloid characteristics. Biochemical reactions are very fast and highly non-linear, complex whilst the diffusion of reaction species are comparatively slow. Sedimentation, aggregation, dispersion and coalescence of cells, gas bubbles and liquid droplets generally occur

during the agitated fermentation processes. Individual biochemical reactions are usually very fast but overall reactions, e.g. cell growth, are relatively slow. It has been shown by mathematical modelling [59,86,87,88,89,93] that the effect of various levels of micromixing on conversion may be considerable for growth processes obeying Michaelis-Menten kinetics. Chen [59] found that segregation was strongly unfavorable to the conversion of substrates and to the growth process; Fan et al [87] drew the same conclusion.

The study of micromixing has more and more applications in processes such as copolymerization [91,92]; autocatalytic reactions [93,94]; competitive, consecutive reactions [22,95]; biological growth processes [59,60,86-89,93], etc. As biotechnology develops, the study of micromixing in large scale biological processes will have important applications.

3. CHARACTERIZATION TECHNIQUE - AZO-DIAZO REACTION

To experimentally study the micromixing process in a stirred tank fermenter, the chemistry of the 1-naphthol and diazotized sulphanilic acid coupling reactions need to be fully understood and good analytical techniques need to be developed.

3.1 AZO-DIAZO COUPLING REACTION OF 1-NAPHTHOL WITH DIAZOTIZED SULPHANILIC ACID

The kinetics of the coupling of 1-naphthol (A) with diazotized sulphanilic acid (B) was investigated by Bourne and coworkers [25,26]. Their results showed that the first substitution occurs in the p-, and not in the o- position (Figure 3.1).

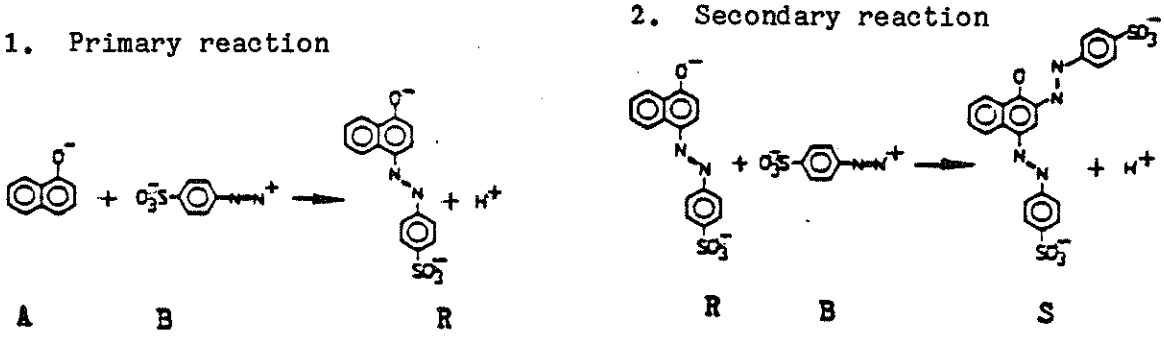

Figure 3.1. The reaction

The first step of the reaction, $A + B \xrightarrow{k_1} R$, is extremely fast and the second step of the reaction, $R + B \xrightarrow{k_2} S$, is relatively slow ($k_1 >> k_2$). Therefore, the first step of the reaction is diffusion controlled but the second step is the kinetically controlled. If a small volume of B (1 volume fraction for this study) is injected into a large volume (10 volume fraction), excess of A, B will disperse into A and form B-rich patches when A and B are partially segregated. Then, R is formed and accumulated locally inside the pateches, because the first

step reaction is very fast compared to the diffusion of R. Part of R will be converted to S as it contacts B inside the patches, and the rest of R will diffuse out of the zones. The smaller the size of the zones, the faster R diffuses out and the less R is formed (Figure 3.2).

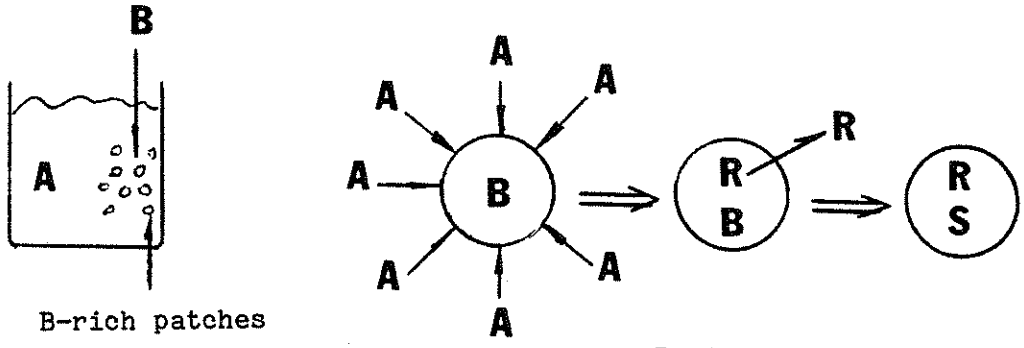

Figure 3.2. Micromixing with 1-naphthol (A) and Diazotized sulphanilic acid (B) reaction.

Therefore, the yield of S, which depends on the zone size and rate constant ratio, is a measure of segregation, and the micromixing index:

$$X_{s,micro} < X_s < 1 \qquad (X_s = 2c_s/(c_R + 2c_s)) \qquad (3.1)$$

However, azo-coupling reactions have complex pH and ionic effects [23,25,26,61,62,63,64,65]. The rate constant k_s is affected by an acid-base equilibrium in one of the two reactants. There exists therefore an optimum pH at which the product of the concentrations of the reactive species is maximized and thus, the reaction rate is a maximum for given total reagent concentrations. The optimum pH calculated was 10.1 for the primary coupling (10.0 in the literature [25,26]) and 9.6 for the secondary coupling. Further, increasing ionic strength would cause a decrease in the rate of reaction in the case of the diazonium ion (negative salt effect), but an increase in the case of the diazotated ion (positive salt effect) (see Appendix 9.1).

In addition to the complexity of the pH and ionic effects, another difficulty is that previous work using this reaction for a micromixing study was based upon a reference absorption spectrum of impure product diazo-dye or 2,4-bis-4'-sulphophenylazo-1-naphthol [25,44]. A stoichiometric mixture solution of R and B was used as S. Elementary analysis showed that the molecular ratio of the mixture differred from the pure product in the literature [25]. Therefore, the work done here had to include purifying the diazo-dye to obtain an accurate reference absorption spectrum.

3.2 MODIFICATION OF THE REACTION TECHNIQUE

3.2.1 Preparation of the Azo- and Diazo-dyes

The preparation methodology used for this work was similar to that used previously [25]. The intermediate product from the primary reaction is azo-dye or monoazo-dye, chemically 4-4'-sulphophenylazo-1-naphthol. It was made by adding diazotized sulphanilic acid to naphthol, and then purified by recrystallization (up to eight times) until paper chromatography of the dye showed one spot. The crystals were then dried in a vacuum oven at 50 ^{o}C. Preparation of diazo-dye S (2,4-bis-4'-sulphophenylazo-1-naphthol) followed the procedure described in [25] but the solvent used was 95% ethanol. In brief, the dye was repeatedly washed with 1:1 (v/v) ethanol/ water solution twelve times until paper chromatography of the dry product solution showed only one spot. The drying procedure was the same as that for monoazo-dye R. The melting points of samples from each crystallization were measured. The dried crystals were stored dessicated and in the dark at room temperature. The melting points for R samples are shown in Table 3.1.

Table 3.1 Melting Point of Monoazodye R

(4-4'-sulphophenylazo-1-naphthol)

Crystallization #	Melting Point ^{o}C
1	——
2	259
3	270
4	270
5	272
6	272
7	272
8	272

The melting points for S samples are shown in Table 3.2 (next page). All the melting point were measured by Thomas Hoover Capillary Melting Point Apparatus (made by Arthur H. Thomas Co.). The mean melting point of the resulting S was 249.8 ^{o}C.

Paper chromatography was done on pre-washed Whatman No. 3 filter paper at room temperature about 75^{o}F. The solvent system was butyl acetate/pyridine/ammonia solution (concentrated)/water 30:47:3:20 [23]. Saturated aqueous solution (R or S) was pointed on the filter paper by pipets (0.02 ml) to form 0.4 cm diameter spots.

Table 3.2 Melting Point of Diazodye S

(2,4-Bis-(4'sulphohenylazo)-1-naphthol)

Crystallization Times	Melting Temperature °C				
	Sample 1	2	3	4	5
1	239	240	241	240.5	239.5
2	239.5	239	239.5	239	239
3	244.5	245	244	244	243
4	247	247.5	247	246.5	244.5
5	245	249	250	249.5	249
6	249	250	249.5	249	250
7	249.5	250	249.5	249	250
8	249.5	250	249.5	249.5	250
9	249.5	249.5	250	249.5	--
10	250	249.5	250	249.5	--
11	250	250	249.5	249.5	--

3.2.2 Analytical Technique

The analytical technique was modified in this work [40]. All the spectra of the solutions prepared (buffered in 10 mols/m³ both of Na_3CO_2 and $NaHCO_3$, I= 40 g ion/m³) were measured in a 1 cm quartz cell by a Cary 210 spectrophotometer. The wavelengths used were from 400 to 600 nm in 5 nm increments, with sufficient time allowed for the readings to stabilize to 4 significant figures.

The extinction coefficients of R and S were calculated by the Lambert-Beer law:

$$E_i = \varepsilon_i dc_i \qquad (3.2)$$

or

$$\varepsilon_i = E_i/dc_i \qquad (3.3)$$

and are shown in Table 3.3:

Table 3.3 Extinction Coefficients for R (Monoazodye) and S (Diazodye)

Wavelength (nm)	ε_R (m^2/mol)	ε_S (m^2/mol)	Wavelength (nm)	ε_R (m^2/mol)	ε_S (m^2/mol)
400	458.6	683.0	505	3082	1588
405	541.9	751.7	505	3139	1580
410	630.1	836.3	515	3164	1589
415	724.2	924.4	520	3143	1620
420	828.9	1029	525	3078	1665
425	927.2	1132	530	2966	1716
430	1030	1238	535	2803	1773
435	1138	1339	540	2608	1830
440	1284	1444	545	2369	1877
445	1354	1523	550	2113	1921
450	1463	1605	555	1839	1948
455	1582	1665	560	1572	1944
460	1712	1712	565	1282	1918
465	1860	1741	570	1021	1917
470	2018	1754	575	795.2	1878
475	2185	1752	580	599.6	1821
480	2362	1736	585	428.4	1744
485	2537	1710	590	301.0	1655
490	2709	1689	595	203.7	1550
495	2849	1648	600	134.3	1430
500	2972	1616			

For monoazo-dye, the absorption maximum was at 515 nm which was the same as that in Kozicki's work. For diazo-dye, the absorption maxima were at 472 and 556 nm, and the minimum at 508 nm, which are different from the literature values [25]. Figure 3.3 shows this difference. This difference ultimately made the X_s values calculated by these extinction coefficients 0.011 units lower than those calculated by using Kozicki's extinction coefficients (Figure 3.4). It appears that Kozicki's procedure of mixing stoichiometric amounts of monoazo compound (R) with the azosulfonate left about 9.2 wt% of monoazo compound in what was labelled pure diazo compound (S).

To check the accuracy and precision of the technique, a series of synthetic mixturesof R and S were made by mixing different volume ratio of 3.084×10^{-5} mol/l of R and 4.615×10^{-5} mol/l of S solution (in the same buffer system). The volume ratio of R/S was: 99/1, 98/2, 97/3, 96/4, 95/5, 94/6, 93/7, 92/8, 91/9, 90/10, 80/20/ 70/30, 60/40, 50/50, 40/60, 30/70, 20/80, 10/90, 9/91, 8/92, 7/93, 6/94, 5/95, 4/96, 3/97, 2/98, 1/99. For these synthetic mixtures, linear regression of Lambert-Beer law for a two compound mixture:

$$E = \varepsilon_R d c_R + \varepsilon_S d c_S \qquad (3.4)$$

or

$$E/\varepsilon_R d = c_R + \varepsilon_S/\varepsilon_R c_S \qquad (3.5)$$

allowed the calculation of the concentrations of R and S. The values calculated were then compared with the weighted data. The literature analytical procedure [25] was modified so that the extinction coefficients from 460 to 600 nm in 5 nm increments were used in the calculations. Table 3.4 shows the regression results from the synthetic mixtures.

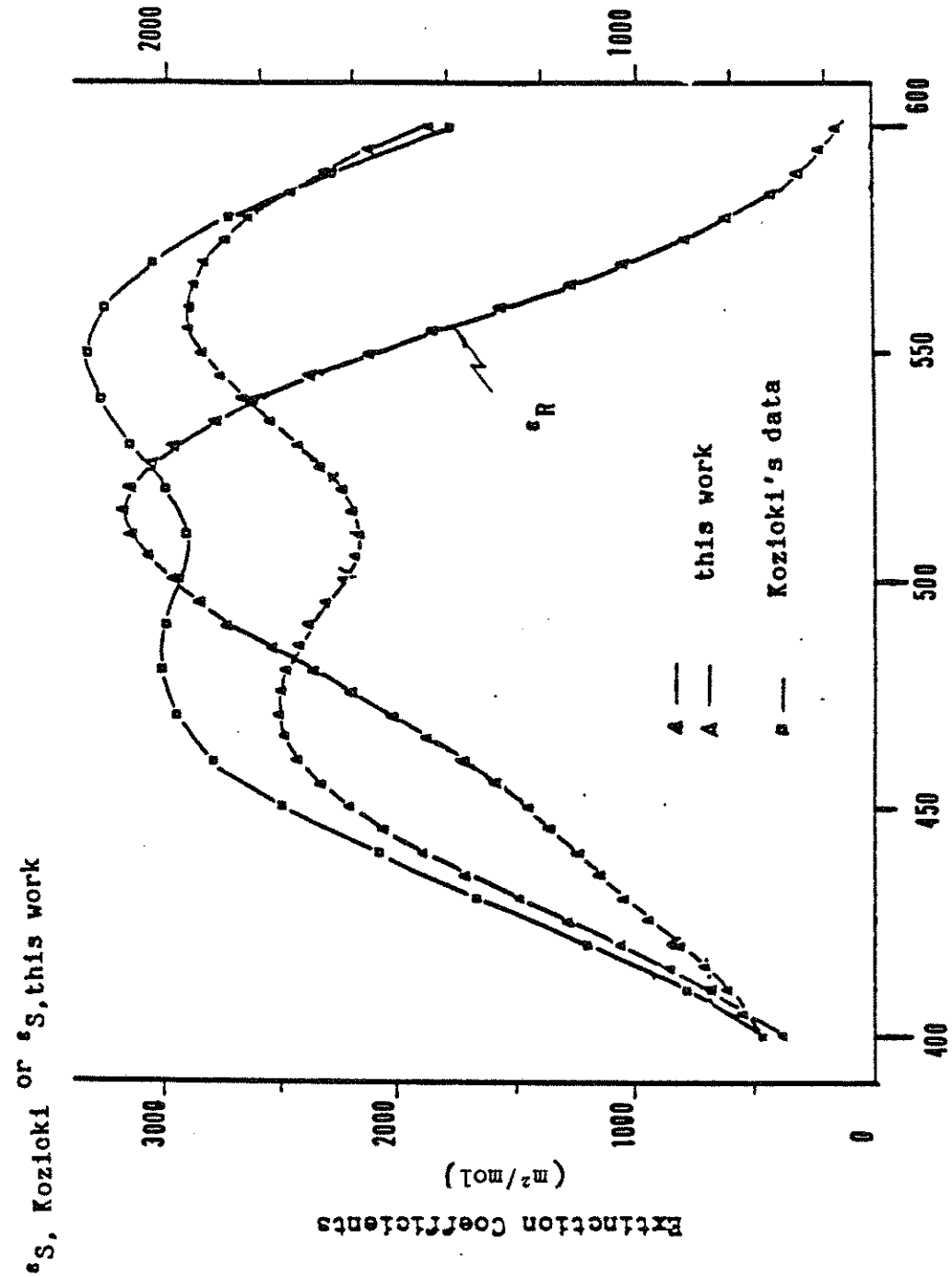

Figure 3.3 Visible spectra of R and S

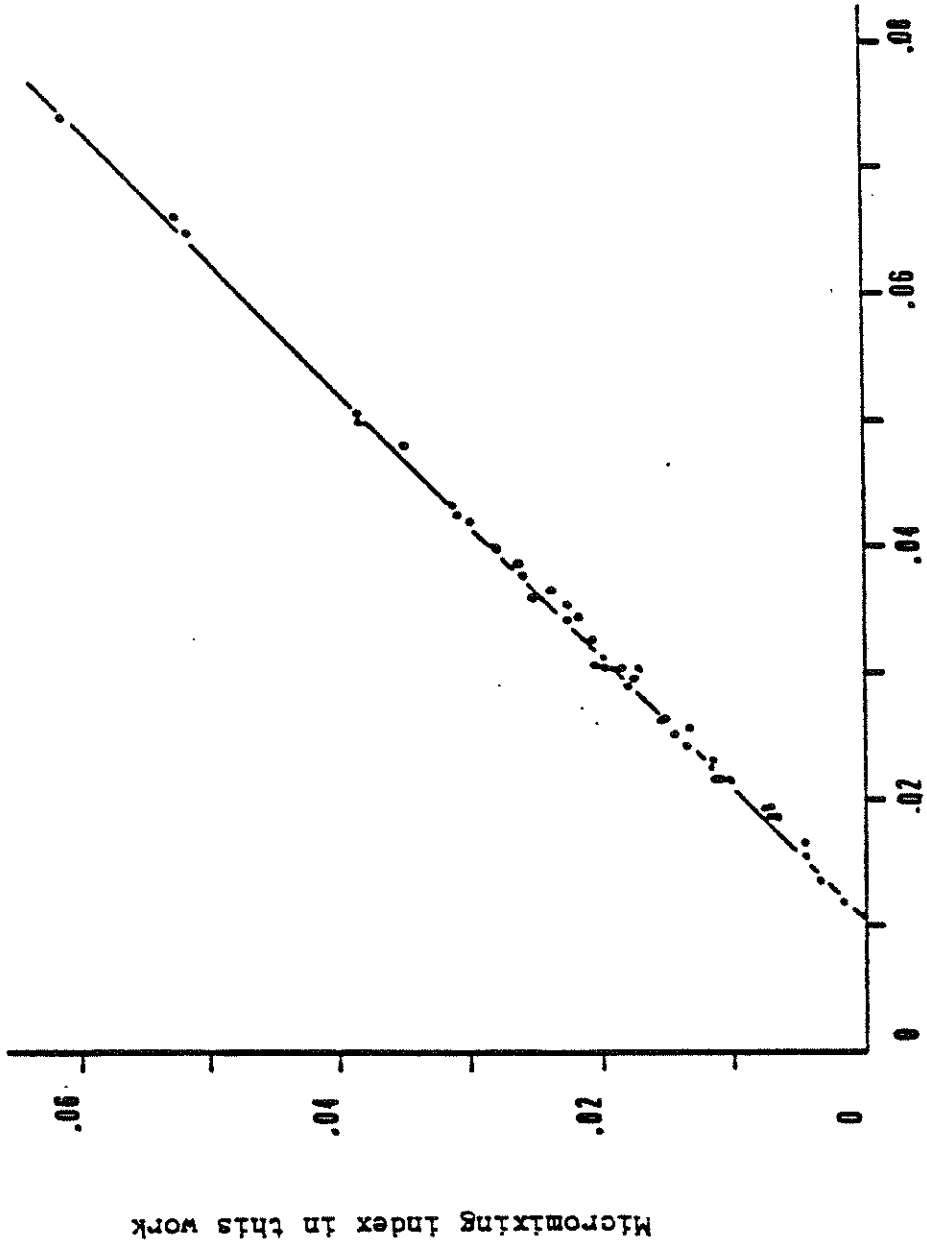

Figure 3.4. Micromixing index in this work vs that calculated by Kozicki's extinction coefficeints

Table 3.4 Regression Analysis Results of Synthesis R and S Mixture

R/S Ratio	Correlation Coefficient	Total Mass calculated	Total Mass weighed	Total Mass error (%)
99/1	0.938	0.03099	0.03074	0.8
98/2	0.988	0.03114	0.03045	2.2
97/3	0.871	0.03129	0.03123	0.19
96/4	0.945	0.03144	0.03163	0.6
95/5	0.971	0.03159	0.03184	0.79
94/6	0.980	0.03178	0.03112	2.08
93/7	0.975	0.03191	0.03179	0.36
92/8	0.983	0.03206	0.03144	1.94
91/9	0.986	0.03221	0.03224	0.093
90/10	0.927	0.03236	0.03253	0.49
80/20	0.997	0.03389	0.03351	1.15
70/30	0.998	0.03543	0.03469	2.08
60/40	0.999	0.03696	0.03686	0.27
50/50	0.999	0.03849	0.03842	0.18
40/60	0.999	0.04002	0.04054	1.3
30/70	0.999	0.04155	0.04232	1.8
20/80	0.999	0.04308	0.04361	1.2
10/90	0.999	0.04461	0.04578	2.6
9/91	0.999	0.04476	0.04535	1.3
8/92	0.999	0.04492	0.04551	1.3
7/93	0.999	0.04507	0.04584	1.7
6/94	0.999	0.04523	0.04539	0.35
5/95	0.999	0.04538	0.04640	2.2

Table 3.4 (continued)

R/S Ratio	Correlation Coefficient	Total Mass calculated	Total Mass weighed	Total Mass error (%)
4/96	0.996	0.04553	0.04660	2.3
3/97	0.997	0.04568	0.04668	2.1
2/98	0.996	0.04583	0.04605	0.4
1/99	0.996	0.04599	0.04740	3.06

Figures 3.5 to 3.7 show the strong diagonal relations of the R and S concentrations and X_s values calculated by the extinction coefficients of this work versus those weighted in synthetic mixtures of R and S.

3.3 DISCUSSION

3.3.1 Assay of Product

As the extinction coefficients of R and S are very similar in the range of wavelengths from 400 nm to 450 nm, the linearity of the regression equation here was very poor. Therefore, the extinction coefficients of R and S from 460 to 600 nm were used for the product analyses.

It was found that the required standards for regression could be well satisfied for the X_s values from 0.0068 to 0.95. If X_s is lower than 0.0068, linearity would then be poor. On the other hand, if X_s was higher than 0.983, concentrations calculated would differ greatly from the real values. Therefore, other analytical methods, e.g. HPLC should be developed to overcome this problem.

3.3.2 By-product of the Reaction

Paper chromatography showed that in the reaction, a third, weak

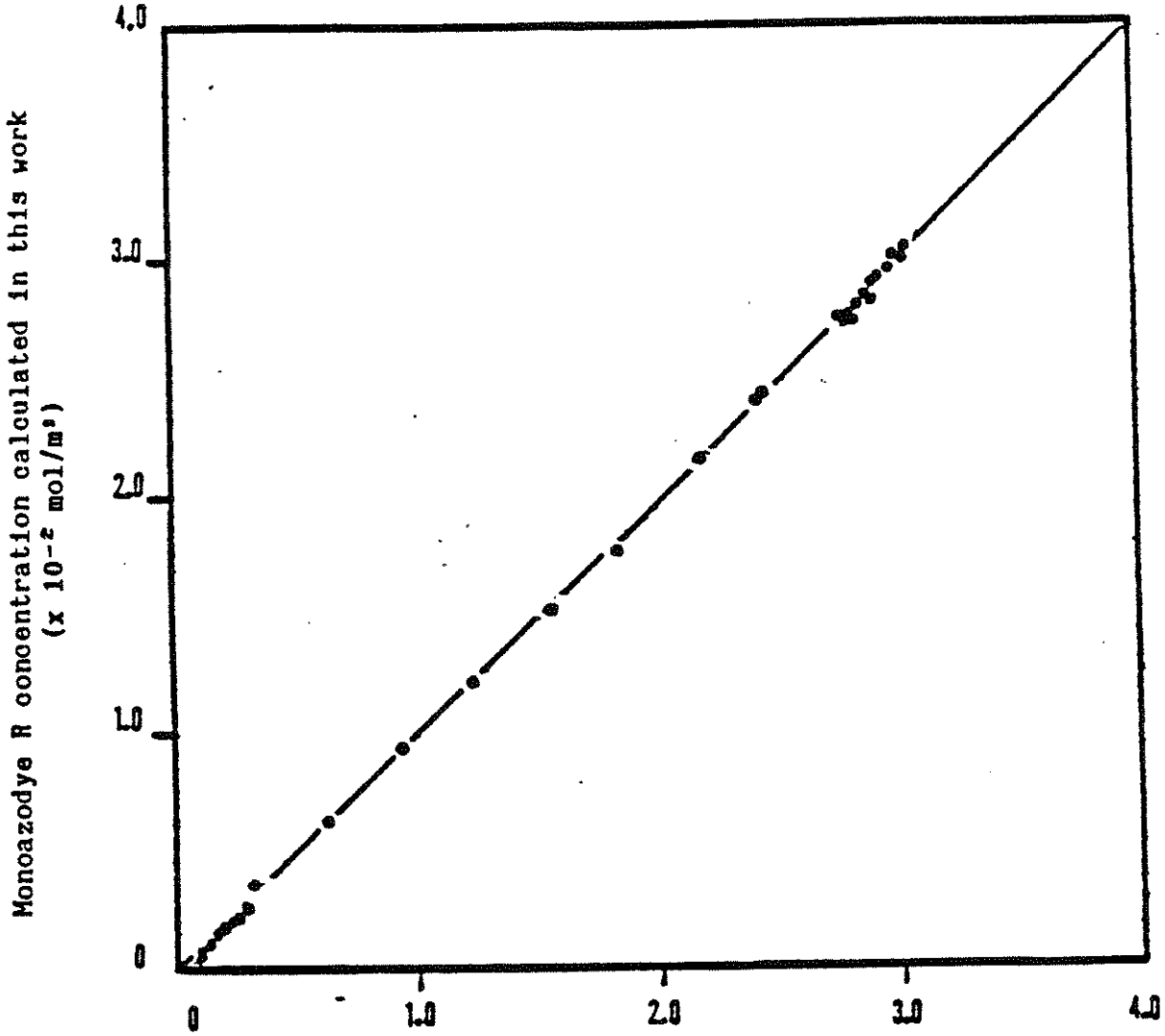

Figure 3.5. Monoazodye R concentration calculated vs. that weighed in R and S synthetic mixture

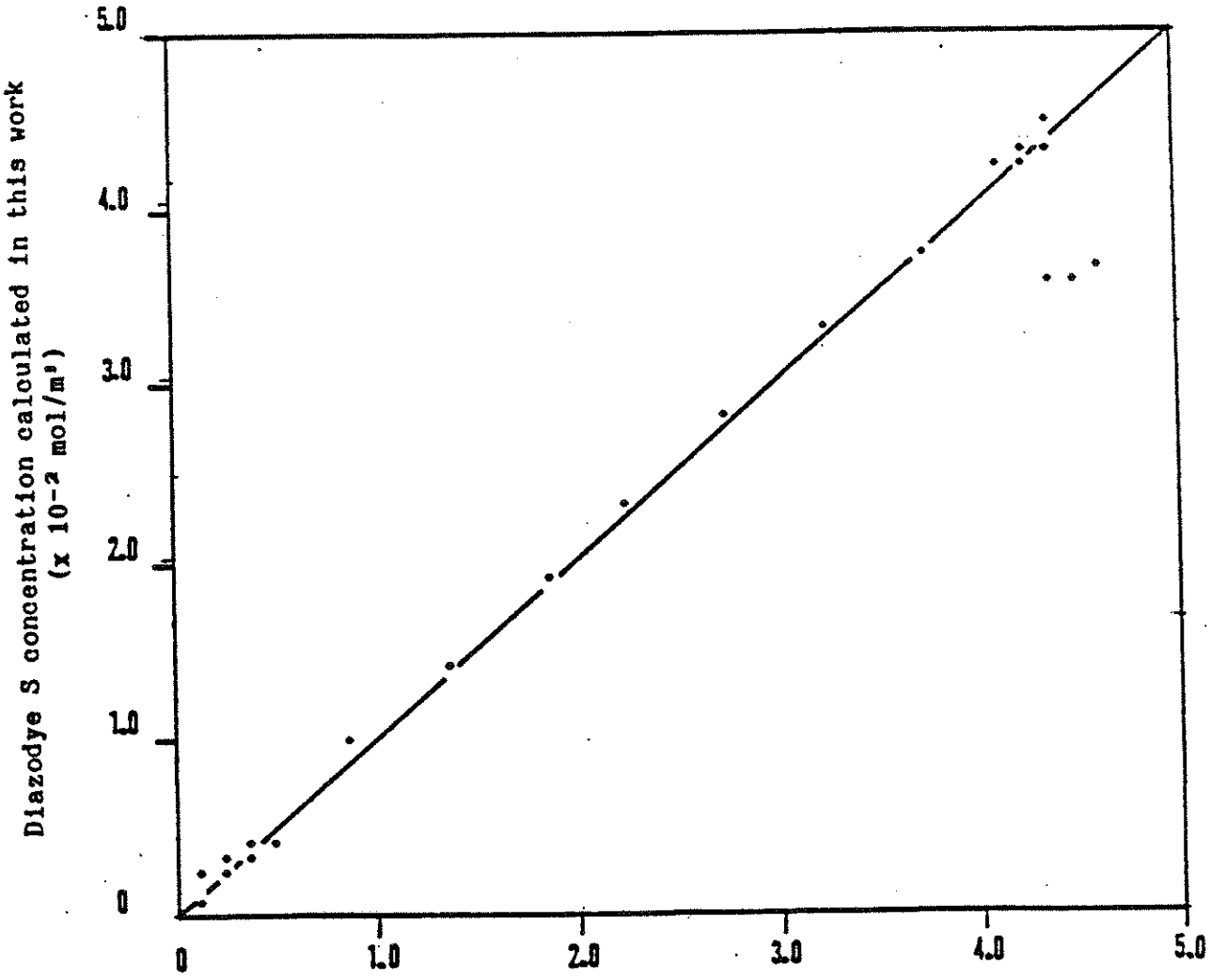

Figure 3.6. Diazodye S concentration calculated vs. that weighed in R and S synthetic mixture

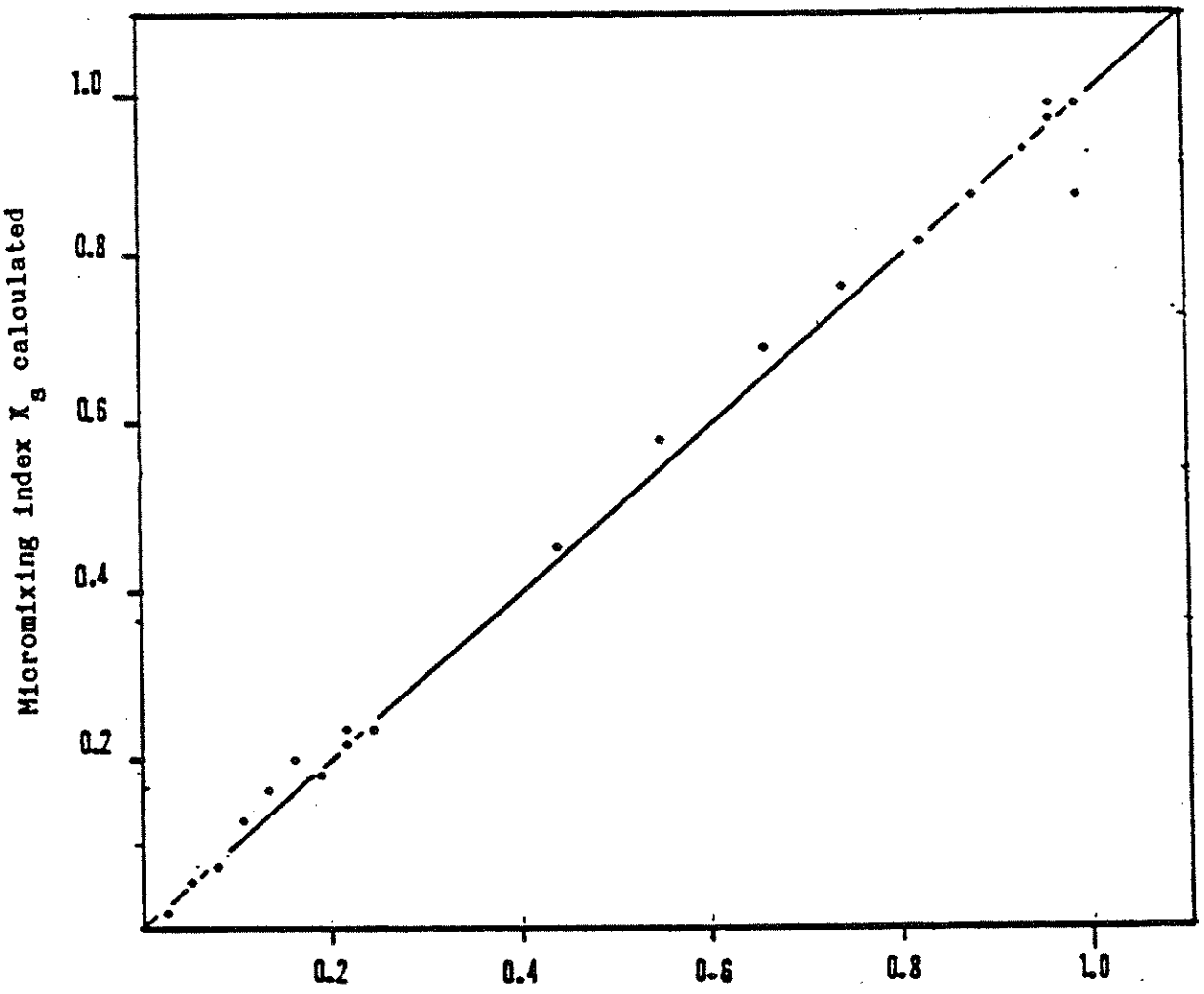

Figure 3.7. Micromixing index X_s calculated vs. that weighed in R and S synthetic mixture

absorbent component caused deterioration of the correlation coefficient and mass balance. It was suspected that stainless steel (or Fe ion) may catalyze the formation of the third component, and after coating (with silicone grease) metal surface on the inside of the fermenter, the problem was overcome.

3.3.3 Reaction Characterization

As with the previous work, results have been expressed in terms of X_s, the yield of S. This relationship is convenient since it allows material balance on B and avoids analysis of the unreacted A which was always present in these experiments, even after complete reaction of B. A further advantage of X_s is as an experimental index of mixing that can be subsequently used empirically for other systems. It should be made clear that as an empirical parameter, X_s could equally well have been defined as the conversion of naphthol. This alternate ratio would have a significant impact on the numerical value of the mixing index (e.g. X_s based on naphthol conversion$\doteq$1/2 X_s based on azide conversion) but would be equally useful in the understanding of mixing for competitive reactions.

3.3.4 Effects of Temperature

Increasing temperature not only raises the concentration of S because of the equilibrium balance but also increases the concentration of the third component which is unfavorable to mass balance. This study was preformed at 30 ^{o}C and good results were obtained.

4. MICROMIXING STUDY - CHARACTERIZATION OF A FERMENTER

To characterize micromixing with 1-naphthol (A) and p-diazobenzene sulphonate (B) experimentally, a perfectly macromixed fermenter with incomplete micromixing should be used. This is satisfied in this work by:

1. using instantaneous fast reaction of 1-naphthol and p-diazobenzene sulphonate such that mass transfer instead of kinetics is the controlling mechanism.

2. designing experiments where hydrodynamic conditions are well controlled: small stirred reactors with high power input as recommended by Villermaux [43].

A small size Virtis fermenter (model 43-100) with 3 liter working volume was used with a single high-power-input Rushton stirrer (Figure 4.1). Some macromixing characteristics were also investigated as necessary.

4.1 MACROMIXING STUDY OF THE FERMENTER

The fermenter was classified in a number of methods which are mainly related to the macroscale characteristics of mixing: flow pattern, gas holdup, and reduced power input. The internal circulation time was estimated for batch operation and the RTD was measured for continuous operation. The liquid phase used was water at 30 ^{o}C and the gas used was nitrogen at the same temperature.

Three different agitation and injection systems were used. The dimensions of System I (two overlapping 44 mm stirrers) and II (76 mm stirrer) are given in [44]. System III has two injection ports: stirrer side and fermenter bottom. Its dimensions are: diameter of impeller =

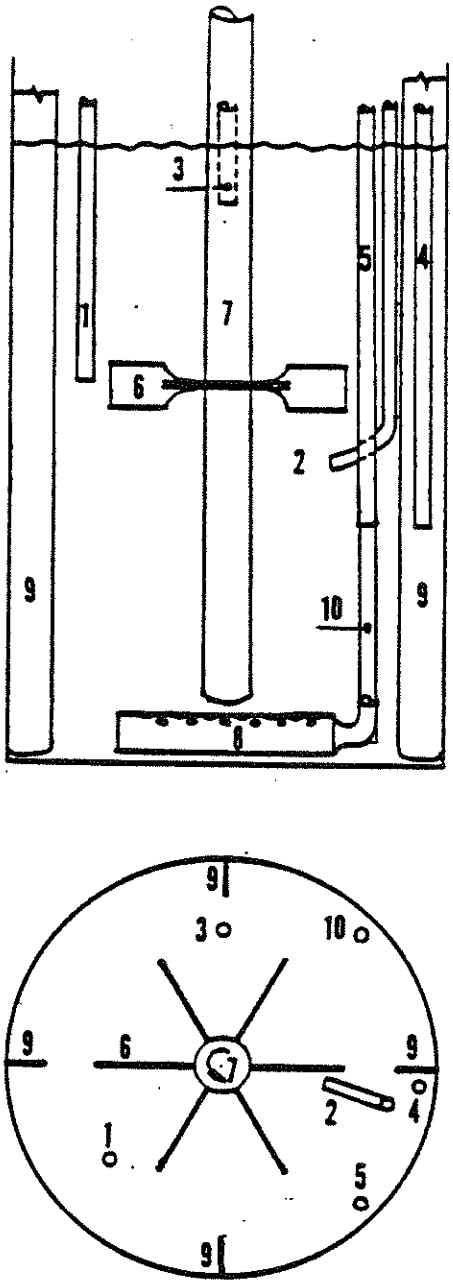

Figure 4.1. Dimension of fermenter Virtis model 43-100

1 - Stirre Side (STS);
2 - Stirrer Bottom (STB) (below stirrer)
3 - Surfaoe (SUR);
4 - Front of Baffle (BA1)
5 - Between Baffles (BA2)
6 - Turbine
7 - Stirrer Shaft
8 - Gas Sparger
9 - Baffles
10 - Fermenter bottom

44 mm, width of the stirrer side feed port to circle of stirrer = 15 mm, fermenter bottom feed port to center line = 60 mm, with height = 15 mm.

4.1.1 Reduced Power Number And Flooding Point

Power consumption of the fermenter was measured using a Simpson iron-vane type AC voltmeter and ammeter connected to the stirrer motor. Because of static friction, the reduced power input (power consumption with gas divided by that without gas) was used to indicate the characteristics of the fermenter. The results are shown in Figure 4.2 for gassed system. The flooding point of the fermenter at the fixed gas flow rate was about 600 rpm.

4.1.2 Effects Of Initial A-to-B Molar Ratio

The initial A-to-B molar ratio also affects the X_s values. Figure 4.3 shows this effect for System I at 120 rpm. The experimental procedure was the same as that used in micromixing study (see below, p. 35) but changed the total feeding volume of B. The addition rate of B was set at 100 cc/min, total volume of B fed changed and the gas flow rate was zero and the space above the liquid phase in the fermenter was purged by nitrogen. It was interesting to notice that when the reaction was close to the equivalent point of A and B, X_s increased dramatically. To reduce the sensitivity to this effect, the flat portion conditions should be used and in this work, the initial molar ratio was 1.05 for the fermenter characterization. On the other hand, to increase the formation of S so as to improve the accuracy of analysis, the molar ratio used should be close to one.

4.1.3 Residence Time Distribution in Continuous Operations (System III)

For System III with agitation of 120 rpm and gas flow rate of 10 lpm, the RTD was measured by the use of azo-dye as an inert tracer.

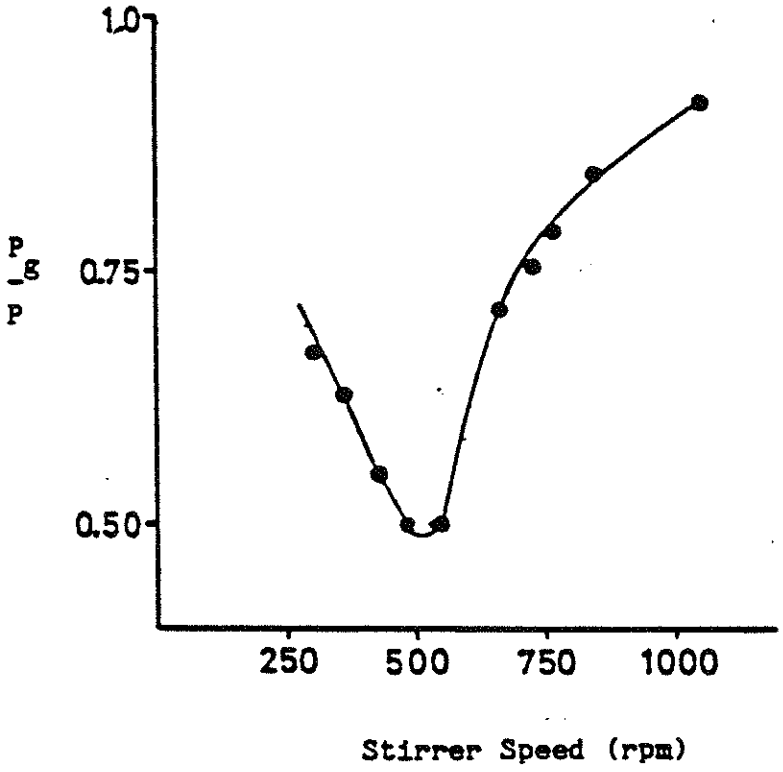

Figure 4.2. Reduced power vs. stirrer speed for 8 lpm (2.67vvm) gas feed rate

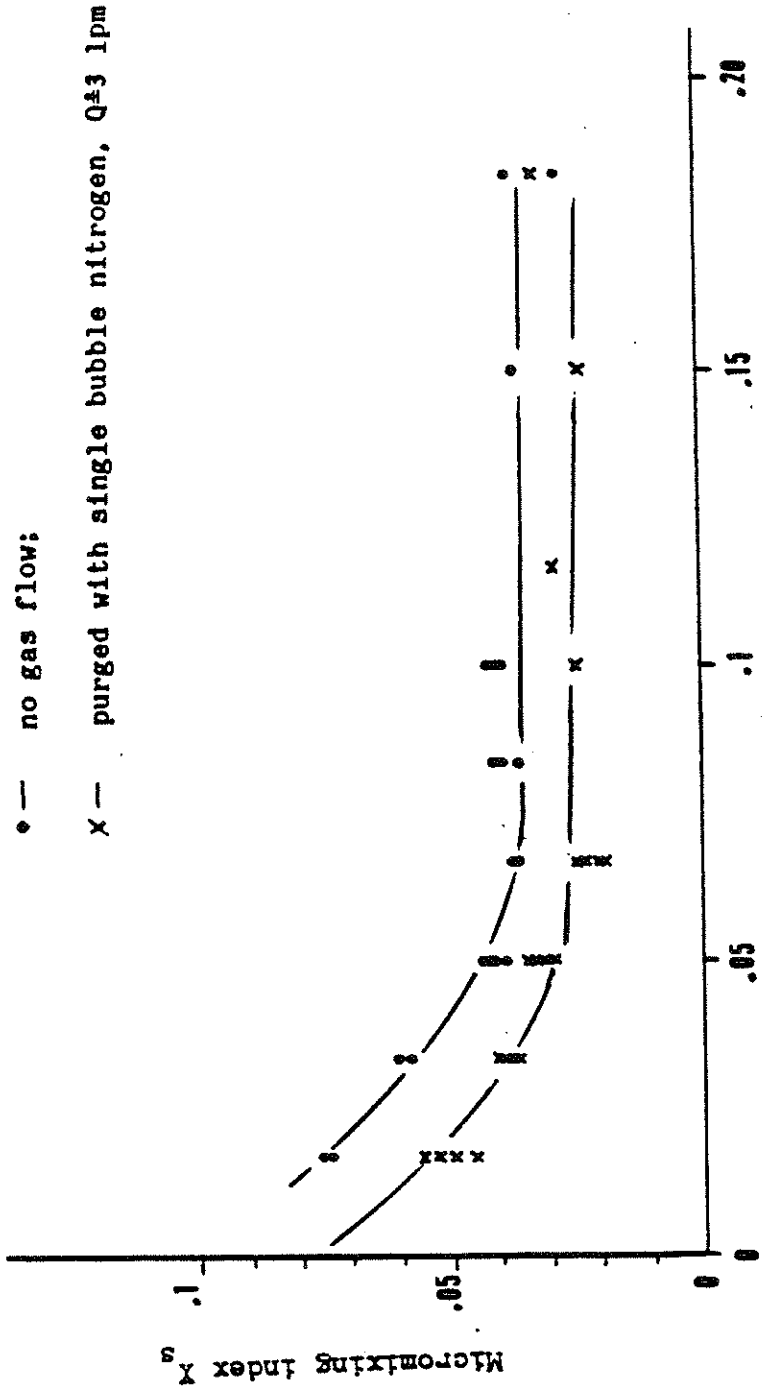

Figure 4.3. Micromixing index X_s vs. $N_{A_o}/N_{B_o} - 1$

Azo-dye was buffered in the same system at pH 10.15. Two extreme injection ports were chosen: stirrer side as the best one and fermenter bottom as the worst one, so that other ports are better macromixed than the bottom port. Also, these two ports were used for the fermentation experiments so that the micromixing effects on fermentation could be maximized. The fermenter was initially filled with 3 liters of the buffer solution. Step input feed of azo-dye, and discharge of the overflow fluid, were controlled by two Masterflex pumps. Radial positioning of the discharge tubing at the fluid surface did not affect the effluent concentrations, as shown in Table 4.1a.

Figure 4.4 shows that two different injection ports of tracer did not affect the RTD although their micromixing indices are different (see later, p. 46).

In Figure 4.5, the data from the F-curve is plotted and compared to Tank in Series model [68]. The figure shows that the data corresponds to N (number of tank) = 1 or the dispersion number (D'/uL) related is close to infinity, which stands for perfect macromixing (Table 4.1b).

4.1.4 Effects Of Kinetic Control, Circulation Time in Batch Operations

Since in System II the small volume fermenter has an oversized stirrer and high energy input, the size of the micromixing zone may be small and the experiments may be in the combined kinetic-and-diffusion controlled regime. Under these conditions, product distribution is determined by the reaction rate kinetics. Integration of the reaction rate equations [44] show that in the kinetic region, X_s is only 0.00116 at t = 30 ^{o}C. Therefore, the kinetic resistance is negligible.

Based upon Bryant's results in a stirred tank fermenter [69], the effects of fluid internal circulation can be estimated by:

Table 4.1a. Absorbence of Samples at Different Radial Positions

Radius to Center	20 mm	40 mm	60 mm
$Absorbence_{515\ nm}$	0.243	0.247	0.246

Remark: Radius to center is the width of sample port to center line. The absorbence was measured in 1 cm cuvet by Spectronic 710 (Bausch and Lomb).

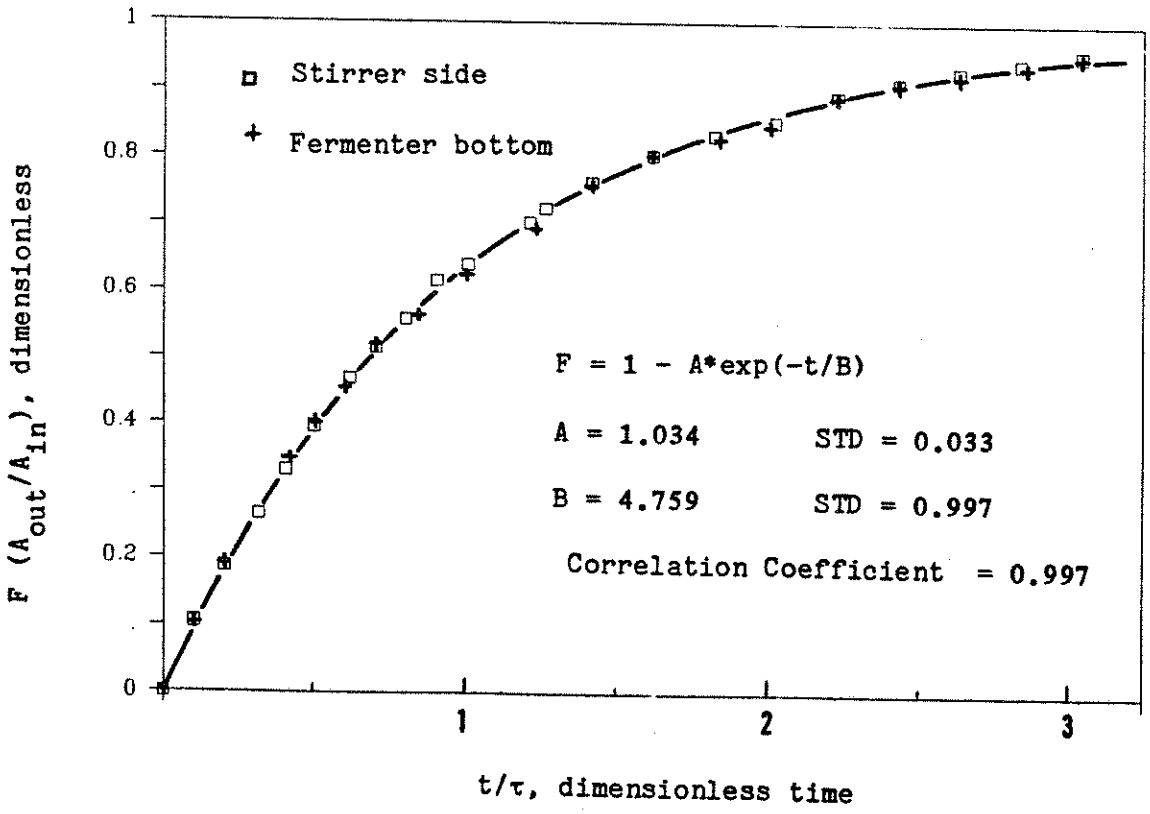

Figure 4.4 F-curve of macromixing study for stirrer side (50 microns) and fermenter bottom (160 microns) (System III).

Table 4.1b. RTD Measurement Results of System III

Mean Residence Time (hour)	Mean Residence Time (hour)	Dead Volume (ml)	Dispersion Coefficient (D'/uL)
4.76	4.759	0	well mixed (D'/uL->∞)

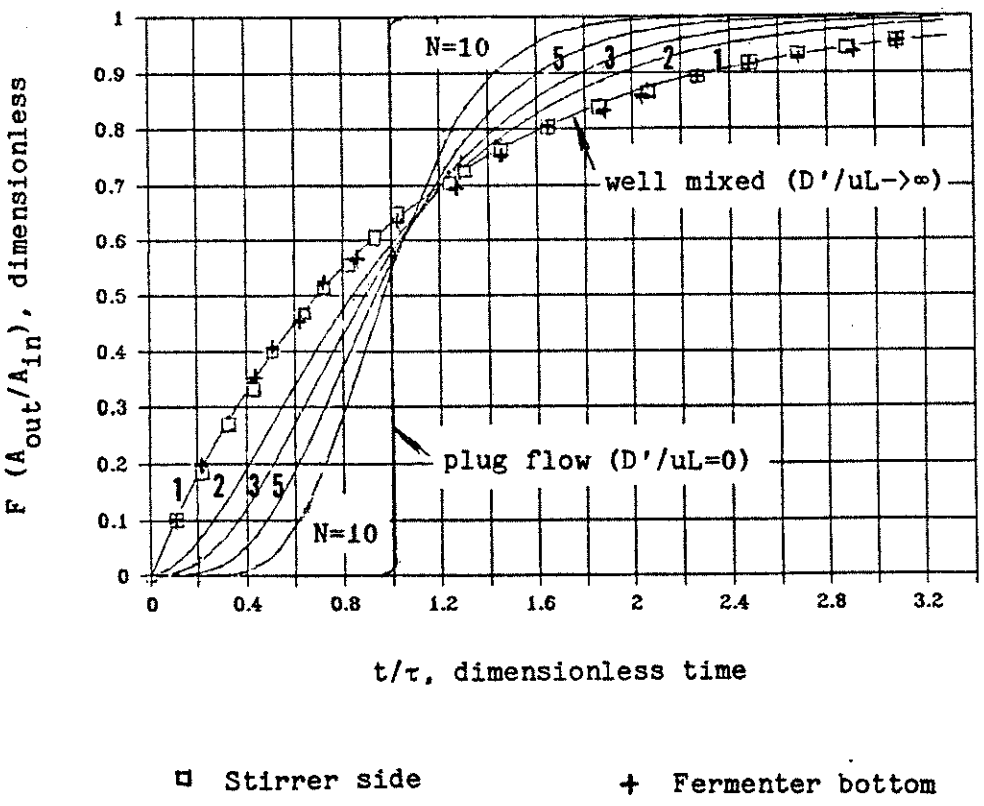

Figure 4.5. Comparison of experimental F-curve of System III (50μ stirrer side port and 160 μ bottom port) with the Tank in Series Model

$$\bar{t}_c \triangleq V/(Nd^3) \qquad (4.1)$$

Under the typical batch-operation conditions used in this study, the mean circulation time is very small. Because of the effects of kinetic control, internal circulation are negligible, and because macromixing is perfect, λ in Equations (2.1), and (2.2) is very small so that the equations as follows hold:

$$X_s = X_{micro} \quad \text{or} \quad X_s = f(X_{micro}) \qquad (4.2)$$

As a first approximation, X_s is simply used as the micromixing index in this work.

4.2 MICROSCALE CHARACTERISTICS OF THE FERMENTER

4.2.1 Experimental Setup

The experimental setup for the micromixing study is illustrated by Figure 4.6. The experimental procedure followed was to charge the vessel with 3 liters of the naphthol (A) solution and thermally equilibrate to 30.0 $\pm$0.2 °C. The reactions were conducted at 30 °C and final pH = 10.15 (obtained by buffering the naphthol solution with 10 mM of both Na_2CO_3 and $NaHCO_3$, I=40). The initial concentration of 1-naphthol was 5.78 x 10^{-5} M and for the diazotized sulfanilic acid, 55 x 10^{-5} M. The procedure used for preparation of these reagents was as reported in [25,26]. All solutions were degassed with N_2 overnight prior to use. Gas flow rate was set at the desired value on a rotometer and manually maintained at that rate during thermal equilibration and subsequent portions of the run. The feed rate of the azosulfonic acid (B) solution at 30 °C through the desired feed port was also maintained manually. No indications of backmixing into the feed pipe [19] were observed at the feed rate which

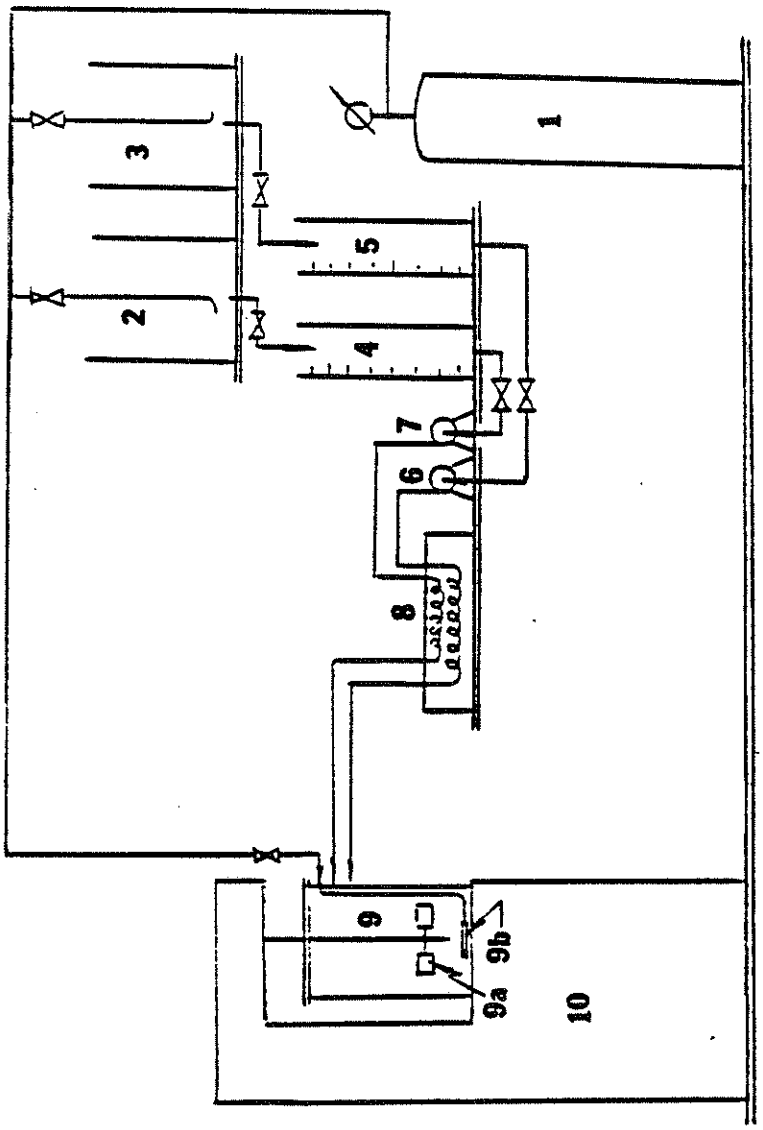

Figure 4.6. Equipment setup for semi-continuous micromixng study

1 - nitrogen cynlinder 2,3 - reactant A, B storage tank
4,5 - volumetric flask for reactant A, B 8 - water bath
6,7 - feed pump of reactant A, B 9b - gas sparger
9 - fermenter vessel 9a - turbine
10 - fermenter control

gave a linear velocity of 1.01 to 10.5 cm/sec. After completion of the addition, the mixture was stirred for an additional 5 minutes and then sampled for analysis. Repeat measurements were made for a number of conditions and indicate a relative error (standard deviation) of 5% in X_S.

Different criteria from the literature were used for acceptance of the results. In most cases the significance of the regression was >99.5%, with correlation coefficient larger than 0.90 (less than 5% of the analyses did not satisfy this higher level of significance, with correlation coefficient 0.72 to 0.88). Material balances were also calculated and averaged 96.0% with a standard deviation of 1.6% (n=62). Since the degree of freedoms are different (d.f.=28 here from 460 to 600 nm in 5 nm increments and d.f.=13 in Kozicki's work from 470 to 600 nm in 10 nm increments), the criteria used here are equivalent to a minimum regression coefficient of 95% and mass balance between 95% to 105% which were the criteria Bourne used in his work [25,26].

As with the previous work, results have been expressed in terms of $X_S = 2c_S/(c_R+2c_S)$. The analytical procedure and standards for the assay of products were the same as described previously.

4.2.2 Micromixing Study

4.2.2.1 Experiments of System I (Two Overlapping 44 MM Stirrers)

This micromixing study was performed with two overlapping 44 mm diameter Rushton stirrers for two different injection ports under nonflooding conditions. These two injection ports were: stirrer side and stirrer bottom as shown in Figure 4.1. The experimental conditions were the same as those specified above; volumetric gas flowrate and B-feed rate used are shown in Table 4.2.

Table 4.2. Orthogonal Design of Effects of Agitation, Injection Port, Reactant Addition Rate on Micromixing Index

Injection Port	Agitation (rpm)	Gasflow (vvm)	Feed Rate (cc/min)	X_s
stirrer bottom	600	2	100	0.0221
†stirrer side	600	1.33	10	0.0185
†stirrer side	600	1.33	10	0.0175
stirrer side	420	0	100	0.0166
stirrer bottom	420	2	10	0.013
stirrer bottom	120	1.33	100	0.0247
stirrer side	120	0	10	0.0416
*stirrer bottom	120	0	100	0.0420
*stirrer bottom	120	0	100	0.0433
*stirrer bottom	120	0	100	0.0388
*stirrer bottom	120	0	100	0.0412

The data with ''*'' is taken from Figure 4.3. The data points with ''†'' are the repeated measurements.

The results of GLM (General Linear Models) analysis of the design are listed in Table 4.3 (by use of SAS [70,71,72]).

Table 4.3. GLM Analysis Results of Orthogonal Design on Fermenter with System I

SOURCE	TYPE I SS	DF	F	PR>F	TYPE IV SS	F	PR>F
IP	7.0×10^{-7}	1	0.18	0.70	5.9×10^{-6}	1.59	0.15
N	0.0011	2	148	0.001	2.93×10^{-4}	39.3	<0.01
Q	0.000231	2	30.9	0.01	0.00024	32.2	<0.01
R	0.0000159	1	4.25	0.131	0.0000159	4.25	0.13
model	0.00135	6	60.3	0.0032			
error	0.0000112	3					
total	0.00136	9					

R-SQE 0.992 STD DEV 0.00193 X_s MEAN 0.0302 C.V. 6.4

The two injection ports and the addition rate of B did not have significant effects on X_s, so that the data averaged over agitation speed and gas flowrate are shown in Figures 4.7 and 4.8.

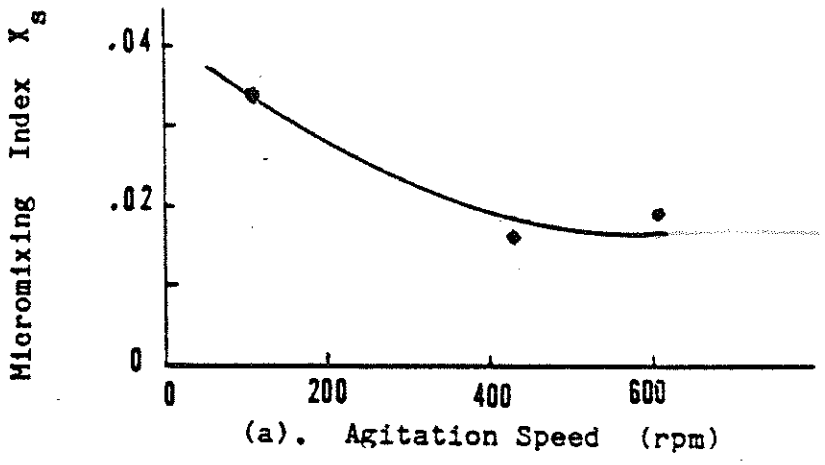

Figure 4.7. Micromixing index vs. agitation speed.

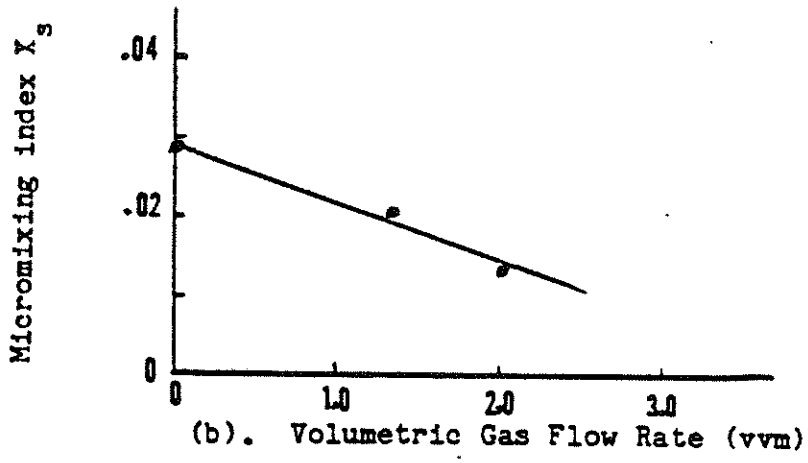

Figure 4.8 Micromixing index vs. gas flowrate.

4.2.2.2 Experiments of System II (With 76 MM Stirrer)

A micromixing study was also conducted with a 76 mm diameter Rushton stirrer for five different injection ports under flooding conditions. These five injection ports were: stirrer side and stirrer bottom, surface, front of baffle and between baffles as shown in Figure 4.1. This work used a 3x3 (3^2) factorial experimental design and the two variables controlled were: agitation speed (rpm) 500, 650 and 800 (stirrer Reynolds number $4.8x10^4$, $6.3x10^4$ and $7.7x10^4$), gas flow (vvm) 2.0, 2.67 and 3.33 (gas superficial velocity 0.0065, 0.0087 and 0.0108 m/sec.); The addition rate of B was 100 cc/min. Other experimental conditions were the same as those used in the small-size stirrer study.

The results of the effects of agitation and gas flow are shown in Figure 4.9 and 4.10, as a function of agitator speed averaged over gas feed rate, and in Figure 4.11 and 12 as a function of gas feed rate averaged over agitator speed, for each of the injection points.

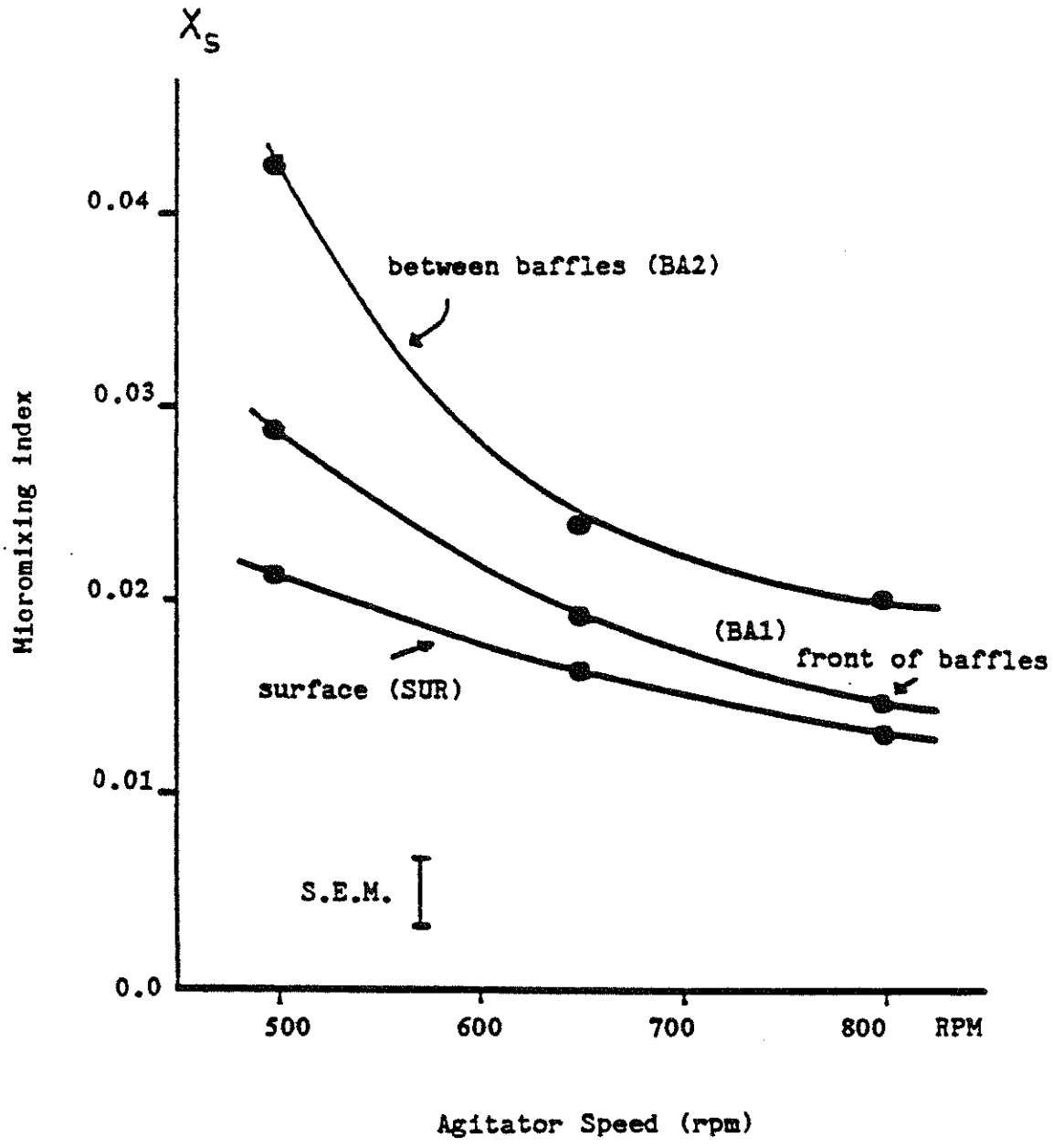

Figure 4.9. Micromixing index vs. agitator speed for indicated feed port

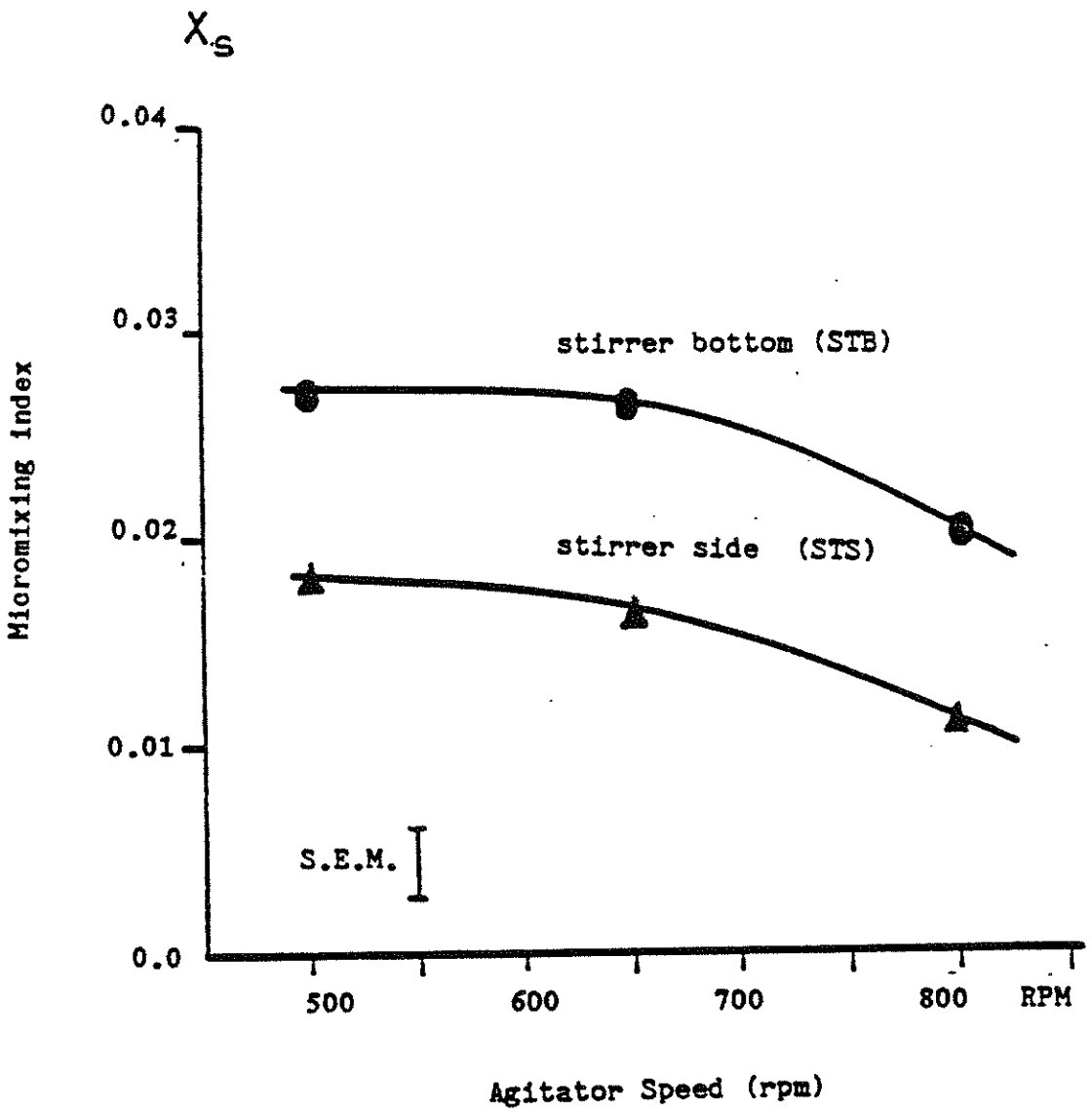

Figure 4.10. Micromixing index vs. agitator speed for indicated feed port

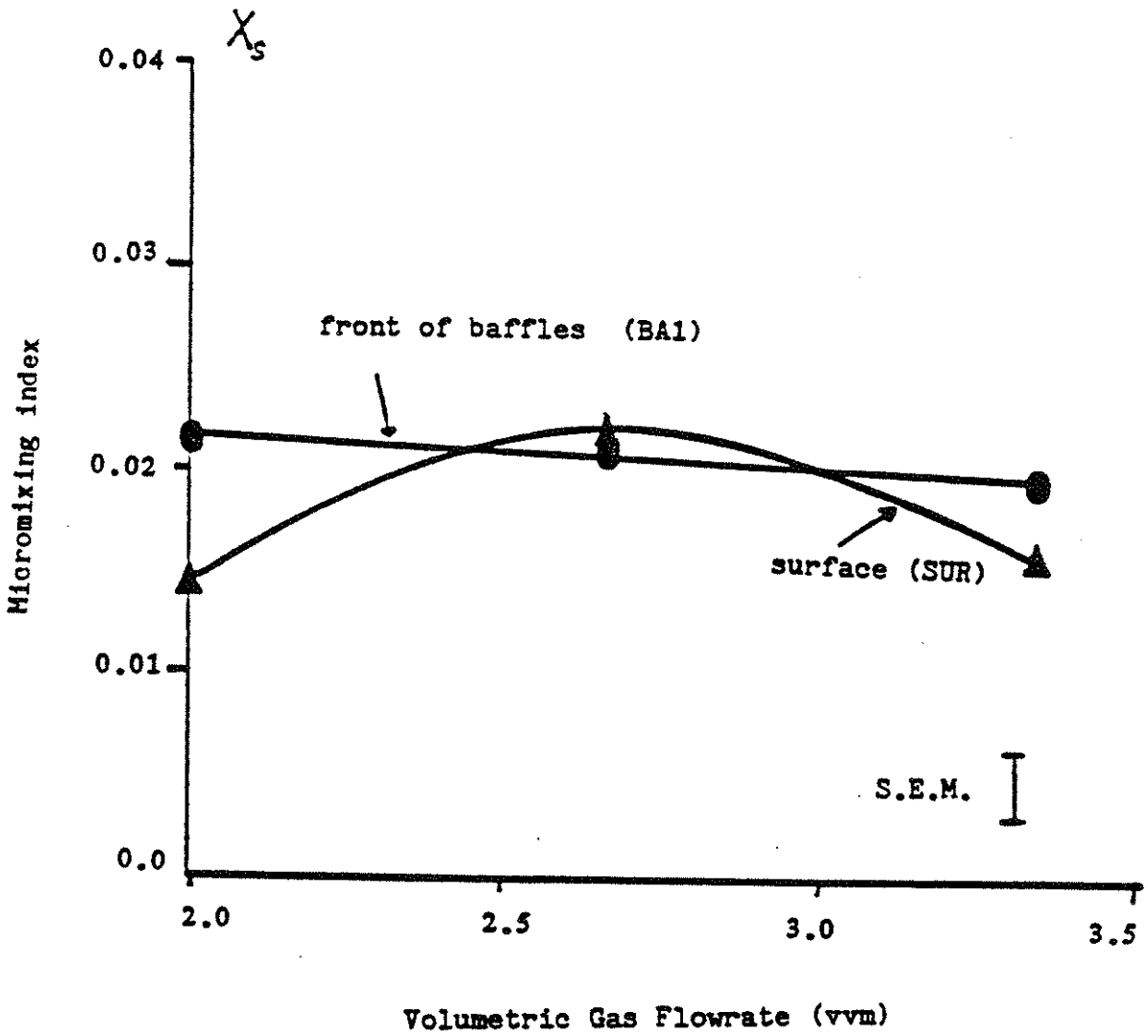

Figure 4.11. Micromixing index vs. gas flowrate for indicated feed port

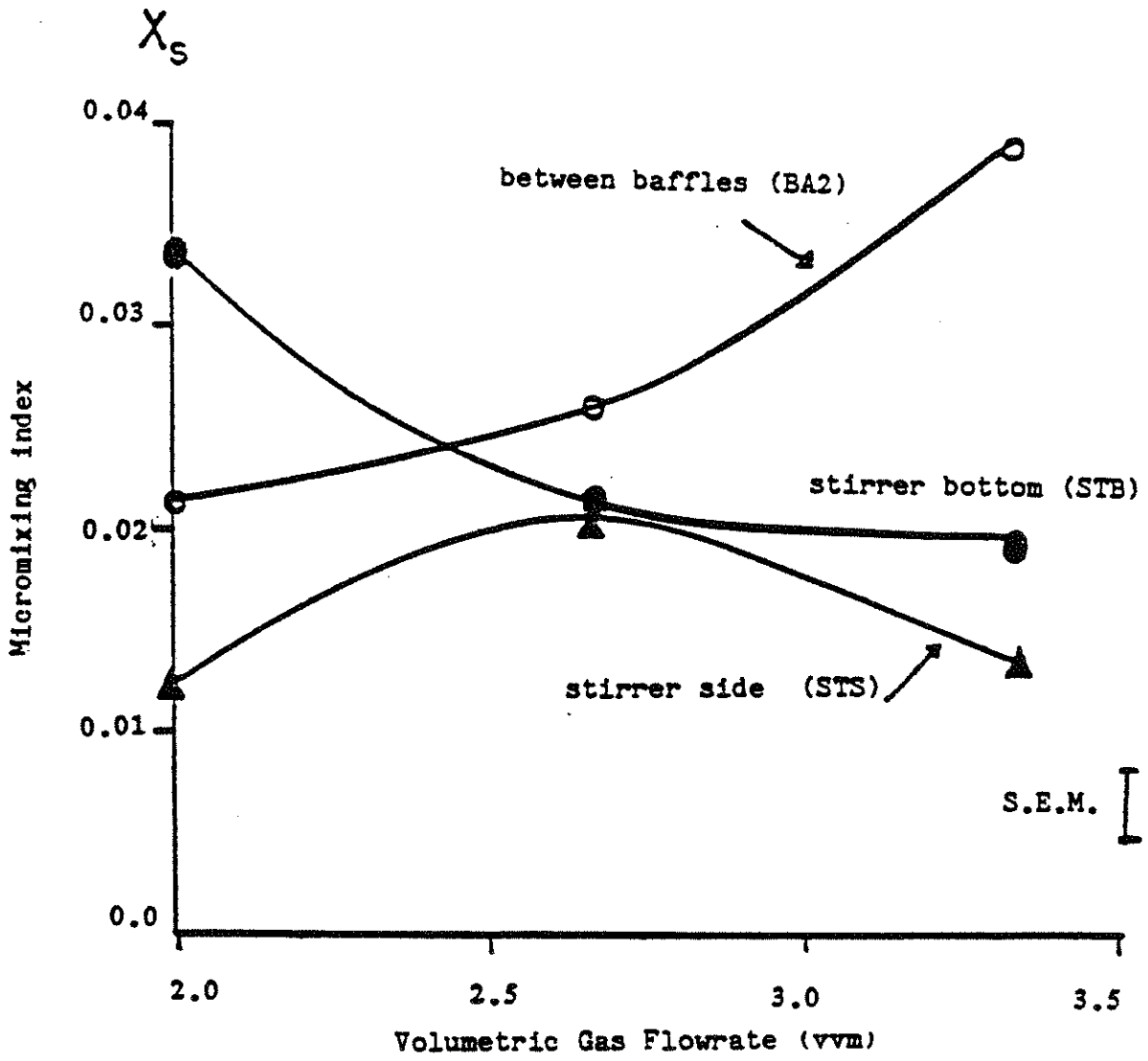

Figure 4.12 Micromixing index vs. gas flowrate for indicated feed port

Inspection of these figures shows decreasing, increasing and maximal values for X_s with increasing gas flow rate for the various injection points and a more regular decrease in X_s with increasing agitator speed.

The individual data points that go into making up the three by three matrix for each injection point are more complex than is suggested by these averages. The complex response function across all of the injection ports has been observed and for a single injection port, the data is listed in [44].

For all data of the five injection ports, ANOVA (Analysis of Variance) was used to analyze the data and the results obtained are listed in Table 4.4.

Table 4.4. ANOVA Results of Fractorial Design on Fermenter with System II

SOURCE	TYPE I SS	DF	F	PR>F	R-SQE 0.785
IP	0.000983	4	4.36	0.0142	STD DEV 0.007508
N	0.000884	2	7.84	0.0042	Xs MEAN 0.021
Q	0.0000458	2	0.41	0.673	C.V. 35.68
IP*N	0.0005384	8	1.19	0.362	
IP*Q	0.000830	8	1.84	0.142	
N*Q	0.0000207	4	0.09	0.984	
model	0.0033	28	2.09	0.0621	
error	0.000902	16			
total	0.0042	44			

The ANOVA results show that for these five injection ports, there are definite differences between the injection points, and that

agitation has significant effects on micromixing but gas flow is not important. However, the interaction of gas flow and injection ports suggests the the gas-liquid phases may behave differently at different positions of the fermenter.

4.2.2.3 Experiments of System III (One 44 MM Stirrer)

When the agitation speed was 120 rpm and the gas flow rate was 10 lpm, the RTD of System III showed that the fermenter was perfectly macromixed. Under these operating conditions with very long mean residence time (4.7 hours), although the F-curves of two different injection ports showed no difference in the inert tracer study, chemical characterization showed that the X_s values of the two ports had a significant difference, being 0.078 at the stirrer side and 0.248 at the fermenter bottom.

4.3 DISCUSSION

4.3.1 Macro- and Micro-mixing

In batch reactors, mixing on the macroscale can be characterized by flow pattern, stirrer Reynolds number, fluid mean circulation time, etc. In continuous reactors, mixing on the macroscale can be fully understood from the RTD. The experimental evidence clearly shows that when mass transfer is the controlling mechanism, even though macromixing is perfect, micromixing may not be complete. The system used in this work was carefully controlled so that the net effects of micromixing could be determined. For large scale continuous reactors with incomplete macro- and micro-mixing, the effective diffusivity can be use in the diffusion-reaction equation to evaluate the macromixing effects.

4.3.2 Distribution Of Micromixing Zone

To quantify the differences between the injection ports, their

ranking order and the distribution or overlapping of the micromixing zones characterized by these five injection ports, multiple range testing (Duncan or Waller-Duncan method from the SAS software package) was used. The testing results showed that there are definite differences between the injection points, with a rank ordering, from best to worst, of stirrer side, surface, front of the baffle, stirrer bottom and between baffles. Further, there are three overlapping but distinguishable groups of injection points at the 0.05 level of significance. At this level the stirrer side is equivalent to the surface; surface, front of baffle and stirrer bottom are equivalent; and front of baffle, stirrer bottom and between baffles are equivalent [44]. These overlapping mixing zones are not unexpected (see for example [58]). It has been proposed that the whole picture of micromixing can consist of several different micromixing zones or cells [75,76], where each one has a different degree of micromixing and exchange mass with each other. Some more work need to be done to improve the knowledge of this aspect.

4.3.3 Effects Of Agitation

It is not surprising to see that micromixing was improved with the increase of agitation (Figure 4.7 to 10). It is in agreement with previous work on mass transfer rate, for example, the relationship between mass transfer coefficient and agitator speed (rpm) [77]. It appears from the current study that when the agitator speed was very high, increasing power consumption did not improve micromixing very much for the locally-high-turbulent regions, e.g. the side of stirrer, but did dramatically improve micromixing in poor mixing regions, e.g., in the baffle area. These results suggest different regions inside the

fermenter may have different mass transfer mechanisms and that eddies ($Re_1 \doteq 1$) in the diffusion layers of the droplets (or eddies) play the most important role in mass transfer (Bulicka and Prochaz [78]).

4.3.4 Effects Of Gas Flow

The presence of the gas phase complicated the picture of micromixing. The flow pattern of the fermenter was such that at fixed gas flow rate before the flooding point, gas was broken up into very fine bubbles. The dispersion of gas into the bubbles and the mixing of gas-liquid formed a mixing zone around the stirrer. The top and the bottom portions of the fermenter were relatively stagnant and the bottom portion was worse than the top portion in apparent mixing. The mixing zone expanded when the agitation speed was increased. When the agitation speed was increased to 600 rpm, the mixing zone around the stirrer expanded and connected to the top portion, forming a cone-shape mixing zone which was in agreement with the Duncan test.

For a gassed system under nonflooding conditions, the experimenta results of System I showed that increasing gas flow improves micromixing. Under these conditions, the gas flow rate was low (between 0 to 6 lpm or 0 to 2 vvm or superficial velocity of 0 to 0.0065 m/sec.) and the gas phase mostly consisted of dispersed gas phase.

Previous work by Madden et al. [79] showed that the coalescence-dispersion frequency in a stirred tank is proportional to the rpm and gas holdup. Increasing agitation and gas flow rate caused the system to approach the flooding conditions (rpm $\doteq$ 600, gas flowrate is 6 to 10 lpm or 2 to 3.33 vvm or superficial velocity of 0.0065 to 0.0108 m/sec.). Under these conditions, the reduced power measurements shown in Figure 4.2 suggest that the mixing index results reflected the

crossover from dispersed gas phase to flooded gas phase operation. It is not surprising that complex micromixing response is observed.

In Figure 4.11 and 4.12, the mixing index for the surface and bottom of stirrer injection points show maxima. Maxima in gas transfer coefficients with increasing gas flow are well documented [67] with an explanation proposed that there are two types of bubbles - active and dead - of which the latter have been depleted of absorbable reactant. However, in this system the gas is nitrogen and is not a reactant. It appears that the gas must contribute both dispersive and absorptive components to the mixing. As the gas flow rate increases towards the transition to flooding, and mixer controlled gas dispersion corresponding to a decrease in the reduced power, the mixing is poorer. Above this transition, where reduced power increases, the mixing improves. Coalescence of the gas is an energy absorptive process since the surface area per unit of volume decreases. The injection point having the poorest mixing and highest coalescence - between the baffles - has an increasing mixing index (poorer mixing) with increasing gas flow rate.

The stirrer side injection point is the highest shear zone and gave the best mixing, as expected. Similarly, the two baffle locations on the periphery of the mixer proved to be relatively poor in mixing. The surface injection point receives a strong down thrust from both the stirrer and the build up in front of the baffle. The relatively good mixing obtained from this injection point may be highly dependent on the small size of this vessel. The stirrer bottom injection point is probably adversely affected by the gas purge.

In general, the point to point changes in mixing appear to be related to the changes in bubble interfacial area per unit of bubble

volume [80]. Increasing or high values of this ratio result in relatively poor mixing, whereas decreasing or low values of this ratio results in better mixing. As noted above, the detailed response of X_s to the interaction of agitator speed and gas flow rate is more complex than is shown in Figures 4.9 to 4.12 [44]. But even at that detail the mixing can be qualitatively understood from the expected influence of the interaction of gas flow rate and agitator speed on the bubble interfacial area per unit of volume.

4.3.5 Deformation Of Micromixing Zone And Local Power Dissipation

It is interesting to look at the relationship between the experimental mixing index X_s and the mixing modules M as proposed by Bourne and coworkers, despite the fact that this system is far more complex than was envisioned for the model. In Figures 4.13 and 4.14 are presented the calculated X_s values of a sheared reaction zone model from reference [29], together with the experimental results from this work. P for the unaerated vessel is taken from standard power number vs Reynolds number curves [73] and the reduced power fraction for the gassed system is taken from this work. Similar results are found in [81].

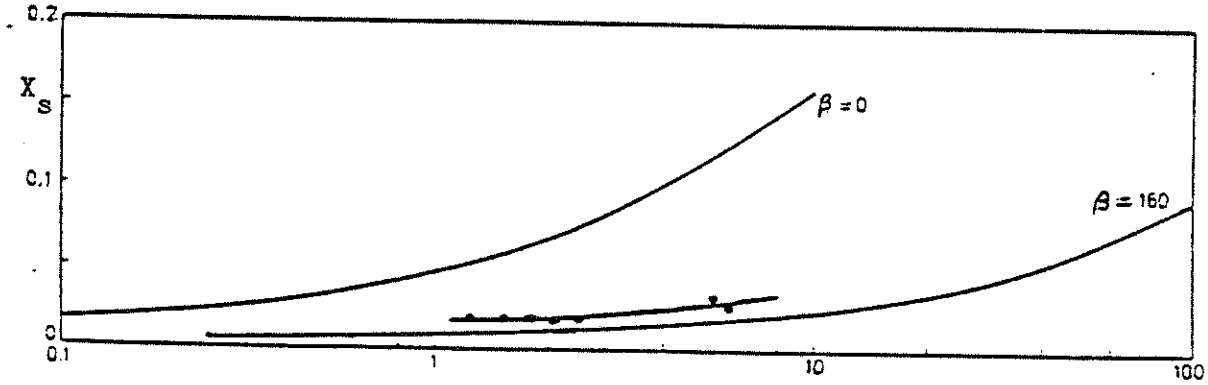

Figure 4.13. Calculated and experimental micromxiing index. Micromixing zones near stirrer tip and at stirrer bottom are highly stretched

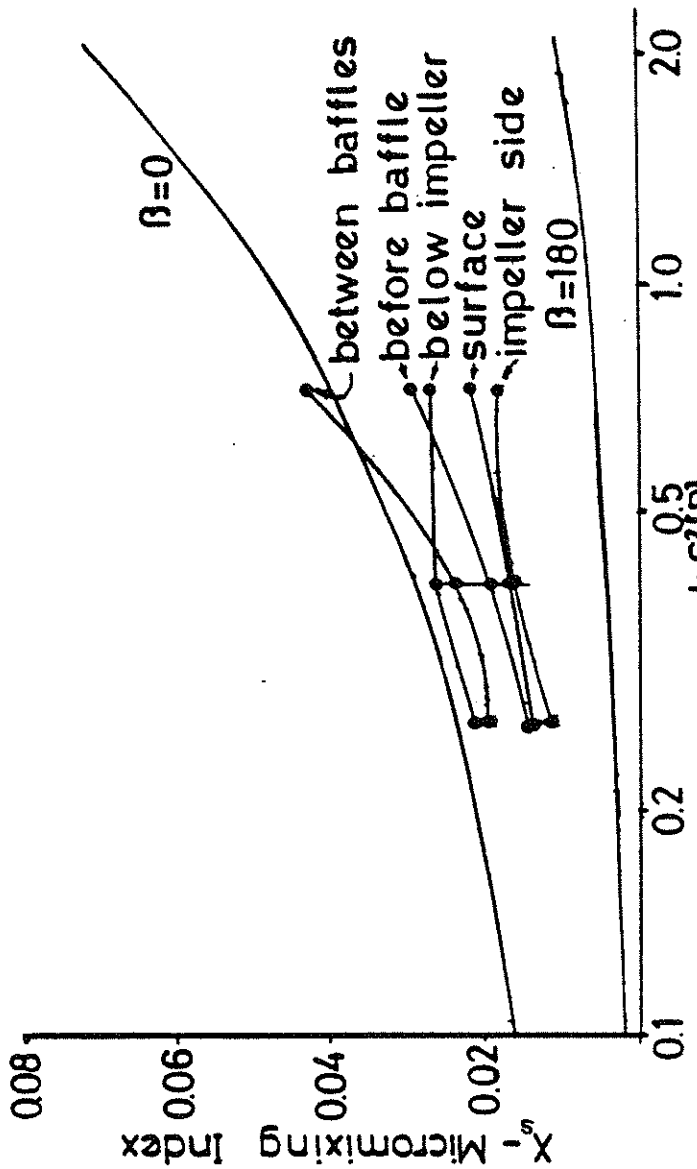

Figure 4.14. Calculated and experimental micromixing index

The variance of M arising from changes in gas flow rate is small with respect to the variance due to changes in stirrer speed and has been ignored.

The experimental results are within the range of the model albeit somewhat compressed. Further, the slopes of the lines connecting the data points for each injection port are semi-quantitatively what is expected. Those near the baffles and wall more nearly parallel the low shear model line, whereas those ports in higher shear zones more nearly parallel the high shear model line. These results confirm the relations with local velocity profile and concentration fluctuations in the work recently published by Villermaux [41].

If local power dissipation values could have been used, the semi-quantitative results would not be materially affected since all points for an injection point would be shifted in the same direction by approximately the same amount.

Overall power consumption is often used as a parameter to indicate the engineering response for mixing situations. The study of micromixing can provide some ideas for the design and scaleup of new fermenters, in which the overall power consumption may be smaller than what is used in the conventional fermenter. On the other hand, overall power consumption seems not to have an apparent relationship with the local power dissipation, and the relations between the local power input and Kolmogroff eddy size is in question [41].

As a theoretical approach, it may be desirable to apply the Coalescence-Dispersion theory to investigate multiphase micromixing, in light of the complex response from the two-phase experiment found in this work, and the behavior of liquid droplets and of gas bubbles.

5. MODELLING OF MICROMIXING EFFECTS ON GLUCOSE UPTAKE AND YEAST GROWTH

5.1 INTRODUCTION

To relate the micromixing index X_s, which is the yield of final product S of the 1-naphthol and diazotized sulphanilic acid reaction, to micromixing zones, which are in the same order of magnitude of turbulent free eddy size, several different mechanisms can be used, e.g. coalescence-dispersion or diffusion models.

To connect the zone size to the biological responses of Baker's yeast fermentation, especially glucose uptake under the influence of micromixing, effective glucose concentration on the cell surface, which depends on the molecular mixing can be calculated also by the diffusion mechanism, and then the biomass production can be related to the effective glucose concentration.

For the modelling of micromixing with the reaction in this work, based on the micromixing - instantaneous reaction mechanisms in stirred tank reactors, a diffusion-reaction model proposed by Bourne et al. [27,29] is useful to correlate X_s to the zone size.

As for the biological responses, if we want to relate glucose uptake to yeast growth, the Monod equation can not be simply used to correlate the specific growth rate of Baker's yeast and substrate (glucose) level, and Fiechter and von Meyenburg [112] found a wide deviation from the Lineweaver-Burke plot (reciprocal of specific growth rate versus the reciprocal of residual glucose concentration).

A lot of effort has been made to try to model the biological processes and the growth of Saccharomyces cerevisiae. Most of the

models developed for Saccharomyces cerevisiae involve modifications of the Monod model and are oriented toward describing batch growth and/or continuous culture steady state behavior [121-127]. However, few of them are related to the engineering aspects in Saccharomyces cerevisiae fermentations and there has been surprisingly little effort to do so, which is believed very important for large scale processes.

Young and Bungay [128,129] conducted some investigations of the continuous culture dynamics of Saccharomyces cerevisiae. They found that the greatest complexity of the dynamic response was associated with the transfer function relating the specific growth rate and the glucose concentration.

To simulate the glucose uptake and yeast growth under the influence of micromixing, the importance and the controlling mechanisms of glucose transport must be clearly understood so that the mathematical equation can be set up for this purpose.

5.2 GLUCOSE UPTAKE MECHANISM OF SACCHAROMYCES CEREVISIAE IN MICROMIXING.

Conceptually, micromixing improves nutrient transport to the yeast and it is necessary to investigate the nature of nutrient uptake. In yeasts, glucose is the main regulatory substrate under aerobic conditions [103]. Growth of glucose-sensitive yeast, e.g. Baker's yeast, is governed by glucose regulation. Based upon the mechanisms of micromixing in stirred tank and glucose transport in Saccharomyces cerevisiae, glucose transfer into the cells in stirred tank fermenter can be simplified by several steps as follows (Figure 5.1 and 2.3):

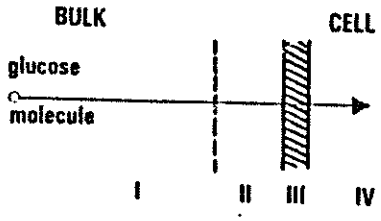

I - bulk fluid II - micromixing zone (eddy)

III - cell membrane IV - cell inside

Figure 5.1. Scheme for the glucose transport from the liquid bulk into the cell.

1. macromixing (or turbulent mixing) - glucose transfer from bulk fluid to the edge of eddies. In stirred tank, it can be represented by:

   a. distribution of injection medium through the broth and homogenization of average composition without decreasing local concentrations gradients

   b. reduction of size of the regions of uniform composition and increase of contact areas between regions of different composition.

2. micromixing - glucose transfer from the edge of eddies to the surface of cell wall by molecular diffusion;

3. glucose transfer across the cell membrane;

4. biochemical reactions inside the cell.

The first step may affect the micromixing zone formation and the second step determines the glucose concentration profile inside the micromixing zone.

Step 1, 2 and 3 are generally regarded as transport steps in the biological literature. From a determination of sugar distribution

volumes Conway and Downey [130] found that galactose and arabinose enter the cell-wall space, but are not distributed in one hour to an appreciable extent in the cell way. However, addition of the same concentration of glucose to the suspension of Saccharomyces cerevisiae resulted in their total uptake in 3 to 5 minutes (Rothstein [131]). For the penetration of glucose at low concentrations in Saccharomyces cerevisiae, Heredia et al. [132] estimated an acceleration factor of 10^6 and more than it would be expected by assumption of physical diffusion. In spite of this high rate of glucose penetration, little or no glucose can be detected within the cell (because of the fastness of biochemical reactions) so that the transport step is the rate - limiting step [129,131,133,134].

Under perfectly macromixed conditions, step 2 is the controlling step compared to step 1, 3 and 4, and micromixing is most important to the glucose uptake of Saccharomyces cerevisiae. Based upon this, a mathematical model is proposed to relate the growth of Baker's yeast to micromixing, combining with the diffusion-reaction model proposed by Bourne [27,29] for estimating the micromixing eddy size.

5.3 MODELLING OF YEAST GROWTH IN MICROMIXING

5.3.1 Estimation of the Size of Micromixing Zone

The size of micromixing zone (or eddy) can be calculated by the model developed previously [27,29]. Experimentally, it is characterized by 1-naphthol and diazotized sulphanilic acid reaction.

Based on the diffusion-reaction mechanism of micromixing process in stirred tank described previously, a set of partial differential equations, with the patches of B-rich fluid being the control volume, can be set up to simulate the micromixing [29,74]:

$$\frac{\partial c_i}{\partial t} + U\frac{\partial c_i}{\partial x} = D\frac{\partial^2 c_i}{\partial x^2} + R_i \qquad (5.1)$$

Accumulation + Convection = Diffusion + Generation by Reaction

In a conventional fermenter, although stirrer Reynolds number is relatively high, the Reynolds number of p-diazobenzene sulfonate rich zones or micromixing zones are very low (smaller than 10 for zone size below 200 micron) and they are still subject to laminar flow. In a laminar shear flow with a uniform one dimensional velocity gradient, the thickness of a given aggregate decreases with its age: e.g. for a filament stretching with a constant velocity. Ottino [39] recently considered the problem in great detail and proposed a lower bound for the stretching time in a newtonian fluid. Therefore, for the final formed segregates, only laminar flow field is considered for the computer simulation.

Standard result [38] showing the uniform shear acting on a slab reduces its thickness by the equation as follows:

$$\delta_o/\delta = (1 + (\gamma t)^2)^{0.5} \qquad (5.2)$$

The velocity profile in the shrinking lamina is:

$$U = U_\delta(x/\delta) \qquad (5.3)$$

where U_δ equals to $d\delta/dt$. Substituting Eqn (5.2) into (5.3) gives:

$$U = -\frac{x\gamma^2 t}{1+(\gamma^2 t^2)} \qquad (5.4)$$

Thus Eqn (5.1) becomes:

$$\frac{\partial c_i}{\partial t} = D\frac{\partial^2 c_i}{\partial x^2} + R_i + \frac{x\gamma^2 t}{1+(\gamma^2 t^2)}\frac{\partial c_i}{\partial x} \qquad (5.5)$$

After introducing the dimensionless terms:

$$T = tD/\delta_o^2 \qquad X = x/\delta \qquad C_i = c_i/c_o \qquad (5.6)$$

Eqn (5.5) becomes:

$$\frac{\partial C}{\partial T}i = (1 + \gamma^2 t^2)\frac{\partial^2 C}{\partial X^2}i + \frac{\gamma^2 R}{Dc_0}i \qquad (5.7)$$

The convective term in Eqn (5.1) and (5.5) no longer appears in Eqn(5.7), and this is a useful simplification when solving Eqn (5.7) numerically.

The generation term by reaction is given by the rate equations:

1-naphthol (A) $$R_A = -k_1 c_A c_B \qquad (5.8)$$

Diazotized Sulphanilic Acid (B) $$R_B = -k_1 c_A c_B - k_2 c_R c_B \qquad (5.9)$$

Monoazodye (R) $$R_R = k_1 c_A c_B - k_2 c_R c_B \qquad (5.10)$$

Diazodye (S) $$R_S = k_2 c_R c_B \qquad (5.11)$$

The governing equation (5.7) becomes:

$$\frac{\partial C_A}{\partial T} = (1+\beta^2 T^2)\frac{\partial^2 C_A}{\partial X^2} - \frac{k_1}{k_2}\left(\frac{k_2 c_{B0}\delta_0^2}{D}\right)C_A C_B \qquad (5.12)$$

$$\frac{\partial C_B}{\partial T} = (1+\beta^2 T^2)\frac{\partial^2 C_B}{\partial X^2} - \frac{c_{A0}}{c_{B0}}\left(\frac{k_2 c_{B0}\delta_0^2}{D}\right)C_B[(k_1 C_A/k_2)+C_R] \qquad (5.13)$$

$$\frac{\partial C_R}{\partial T} = (1+\beta^2 T^2)\frac{\partial^2 C_R}{\partial X^2} + \left(\frac{k_2 c_{B0}\delta_0^2}{D}\right)C_B[(k_1 C_A/k_2)-C_R] \qquad (5.14)$$

where $\beta = \gamma\delta_0^2/D$. When $\beta=0$, stretching is neglected. When β is large, the slab is highly stretched. The initial slab thickness $2\delta_0$ will be estimated as equal to λ_k, i.e. $\delta_0 = 0.5(\nu^3/\varepsilon)^{1/4}$. The laminar shear rate in a turbulent fluid can be estimated [135] from $\gamma \doteq 0.5(\varepsilon/\nu)^{1/2}$. The mixing modulus (or segregation number), $k_2 c_{B0}\delta_0^2/D$, will subsequently be denoted by M. It is the ratio of characteristic diffusion time and characteristic reaction time:

$$k_2 c_{B0}\delta_0^2/D = \frac{m^3}{\text{mol. reaction time}}\Big|\frac{\text{mol.}}{m^3}\Big|\frac{m^2}{m^2/\text{diffusion time}}$$

$$= \frac{\text{diffusion time}}{\text{reaction time}}$$

and the micromixing index $2c_S/(c_R + 2c_S)$ will be expressed as X_s.

The governing equations are solved numerically with the initial and boundary conditions for batch and continuous operations and the results are expressed with X_s as function of M [27,29].

Although the relation between the micromixing index X_s and the micromixing zones, which is in the order of magnitude of Kolmogroff eddy size, depends on the mathematical model, yet it is desirable to give a quantitative descriptions of the eddy (or micromixing zone) size distribution calculated from the experimental micromixing index X_s inside the fermenter. It is shown in Figure 5.2a where the unsheared case was used.

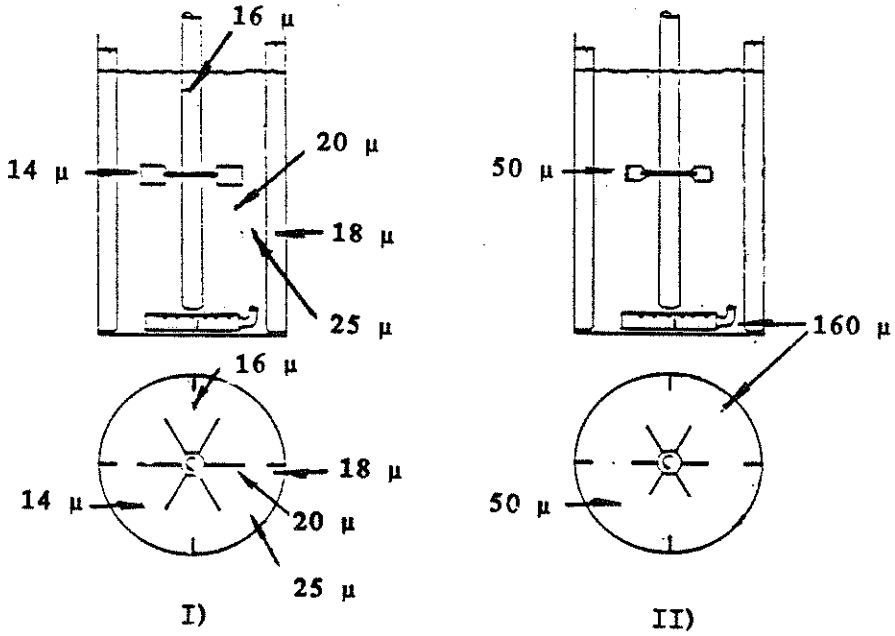

Figure 5.2a. Micromixing zone (eddy) size distribution. I) System II with mean values; II). System III.

5.3.2 Effective Glucose Concentration in Micromixing

For a system where the substrate diffusion coefficient is independent of substrate concentration (or extreme diluted solution), where the enzyme is distributed evenly on the surface and all enzyme molecules are equally active, the mass transfer rate at steady state equals to the reaction rate or glucose uptake rate [96]. Then, the overall mass transfer rate per unit volume from bulk fluid to cell surface, N', is:

$$N' = k_l a\,(S_o - S_s) = \frac{V_{max}\,X\,S_s}{K' + S_s} = \text{constant} \qquad (5.15)$$

which also equals to the mass transfer rate from the micromixing zone to the cell surface.

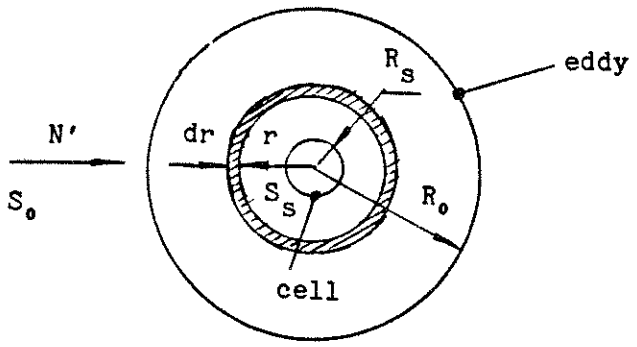

Figure 5.2b. Mass flux inside the micromixing zone (eddy).

By taking a differential element of the micromixing zone, as shown in Figure 5.2b., we have,

$$N' = \frac{4\pi r^2}{(4/3)\pi r^3}\, D\, \frac{dS}{dr} \qquad (5.16)$$

Integrating from the cell surface to the zone edge gives:

$$3D(S_o - S_s) = \frac{N'}{2}(R_o^2 - R_s^2) \tag{5.17}$$

or,

$$N' = \frac{6D(S_o - S_s)}{R_o^2 - R_s^2} \tag{5.18}$$

When glucose is limited, S_s will be very small compared to K'. Therefore, we have,

$$N' = \frac{6D(S_o - S_s)}{R_o^2 - R_s^2} = \frac{V_{max} X S_s}{K' + S_s} \doteq \frac{V_{max} X S_s}{K'} \tag{5.19}$$

which gives the glucose concentration on the cell surface:

$$S_s = \frac{S_o}{1 + \frac{V_{max} X}{6 D K'}(R_o^2 - R_s^2)} \tag{5.20}$$

5.3.3 Yeast Growth and Glucose Utilization

The population concentration in steady state continuous culture is indeterminate so long as μ is constant [106]. By analogy with heterogeneous reactions, a effectiveness factor of glucose uptake in yeast, η, is defined by:

$$\eta = \frac{\text{actual rate (limited by diffusion)}}{\text{rate if not slowed by molecular diffusion}}$$

$$= \frac{R_{\text{with diffusion}}}{R_{\text{without diffusion}}} \tag{5.21}$$

and the effective cell-population-concentration ratio (cell-population-

concentration limited by diffusion divided by that without diffusion limitation) from the effective glucose uptake can be estimated proportional to the effectiveness factor η:

$$\frac{X_{\text{with diffusion}}}{X_{\text{without diffusion}}} \sim \eta^{\gamma} \tag{5.22}$$

where γ is a power constant, and is taken as one here.

By applying Michaelis-Menten type kinetics to the glucose uptake rate equation, the effectiveness factor η is:

$$\eta = \frac{\left(\frac{S}{K' + S}\right)_{\text{with diffusion}}}{\left(\frac{S}{K' + S}\right)_{\text{without diffusion}}}$$

$$= \frac{\left(\frac{S_s}{K' + S_s}\right)}{\left(\frac{S_o}{K' + S_o}\right)} \tag{5.23}$$

Substituting Eqn (5.20) into Eqn (5.23) gives:

$$\eta = \frac{\dfrac{S_o}{\left(1 + \dfrac{V_{max}\, X}{6\, D\, K'} (R_o^2 - R_s^2)\right)}}{\left[K' + \dfrac{S_o}{\left(1 + \dfrac{V_{max}\, X}{6\, D\, K'} (R_o^2 - R_s^2)\right)}\right]} \cdot \frac{1}{\left(\frac{S_o}{K' + S_o}\right)} \tag{5.24}$$

$$= \frac{\dfrac{1}{\left(1 + \dfrac{V_{max}\, X}{6\, D\, K'} (R_o^2 - R_s^2)\right)}}{\left[K' + \dfrac{S_o}{\left(1 + \dfrac{V_{max}\, X}{6\, D\, K'} (R_o^2 - R_s^2)\right)}\right]} \cdot (K' + S_o)$$

$$= \frac{K' + S_o}{(K' + S_o) + \dfrac{V_{max}\, X}{6\, D\, K'} (R_o^2 - R_s^2)} \qquad (5.24)$$

By rearranging we have:

$$\eta = \frac{1}{1 + \dfrac{V_{max}\, X}{6D(K' + S_o)} (R_o^2 - R_s^2)} \qquad (5.25)$$

or by substituting Eqn. (5.22),

$$\frac{X}{X_{max}} = \frac{1}{\left[1 + \dfrac{V_{max}\, X}{6D(K' + S_o)} (R_o^2 - R_s^2)\right]^{\gamma}} \qquad (5.26)$$

Introducing the dimensionless variables,

$$\alpha = \frac{3D(K' + S_o)}{V_{max}\, X_{max}\, R_s^2}, \quad \xi = \left(\frac{R_o}{R_s}\right)^2 - 1, \quad \bar{X} = X/X_{max} \qquad (5.27)$$

Eqn (5.26) becomes:

$$\bar{X}\,(1 + \xi/(2\alpha)\bar{X})^{\gamma} = 1 \qquad (5.28)$$

The equation is solved by Newton method [137], and the results are given in Figure 5.6. When $\gamma = 1$, Eqn. (5.28) gives:

$$\bar{X} = ((\alpha/\xi)^2 + 2\alpha/\xi)^{0.5} - \alpha/\xi \qquad (5.29)$$

Figure 5.3 shows the values of $\bar{X}$ (or η) versus those of ξ with the parameters indicated in the figure. The factors affecting $\bar{X}$ in the model are: V_{max} - maximum glucose uptake rate (g glucose/g cell.sec.); X_{max} - maximum cell concentration (g/l); S_o - bulk fluid glucose concentration (g/l); ξ - dimensionless (radius)^2 of eddy; γ - power constant.

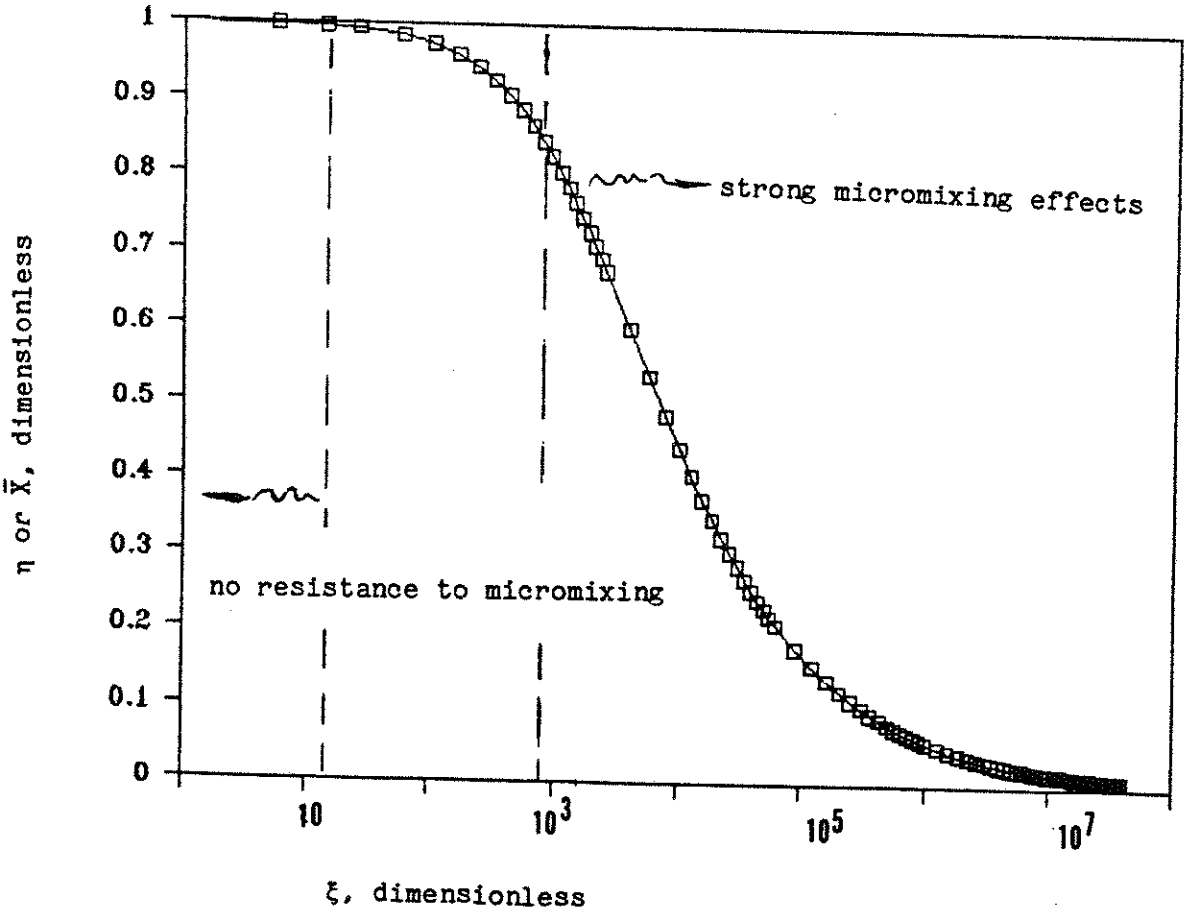

V_{max}= 0.0012 ggs, R_s=2 μ, X_{max}= 5g/l, S_o=0.03 g/l, γ=1, K'=0.05 g/l

Figure 5.3. η or $\bar{X}$ versus ξ

5.4 TESTING THE MODEL

The model is tested by changing the magnitude of the parameters such as maximum glucose uptake rate V_{max}, bulk glucose concentration, Michaelis-Menten kinetic constant K', maximum cell-population concentration X_{max} and the constant γ in Eqn. (5.22). Figures 5.4 to 5.8 show the results.

Figure 5.4 and 5.5 show that under the experimental conditions (see Chapter 6), in which S_o < 40mg/l and X_{max} is estimated as 5.5 g/l (derivation in Appendix 9.3), S_o and X_{max} are not the important factors affecting η or $\bar{X}$. However, V_{max}, K', and γ have significant effects on $\bar{X}$, as shown in Figures 5.6 to 5.8.

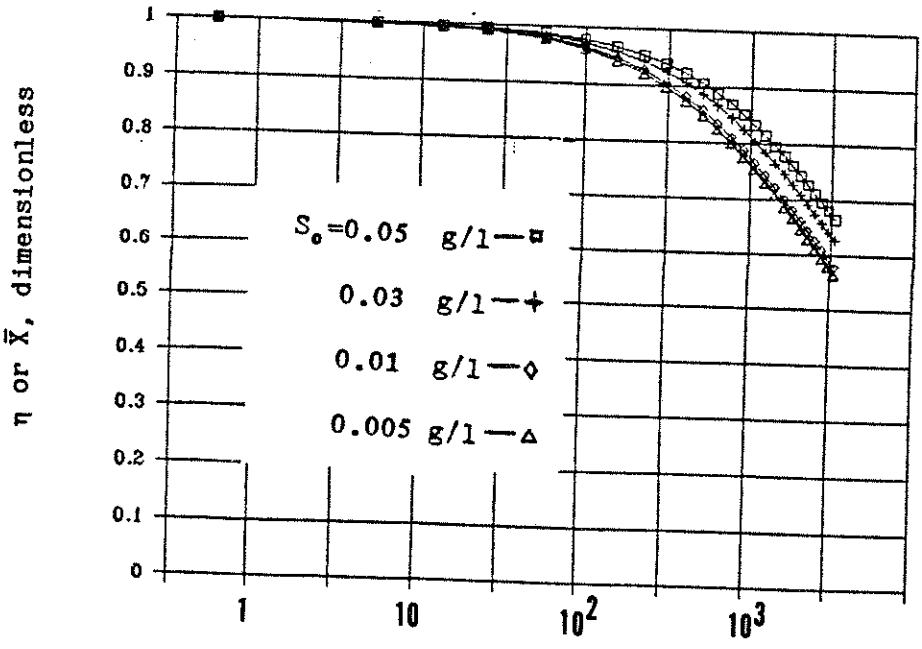

V_{max}= 0.0012 ggs, R_s=2 μ, X_{max}= 5g/l, γ=1, K'=0.05 g/l

Figure 5.4. η or $\bar{X}$ versus ξ with S_o as parameter.

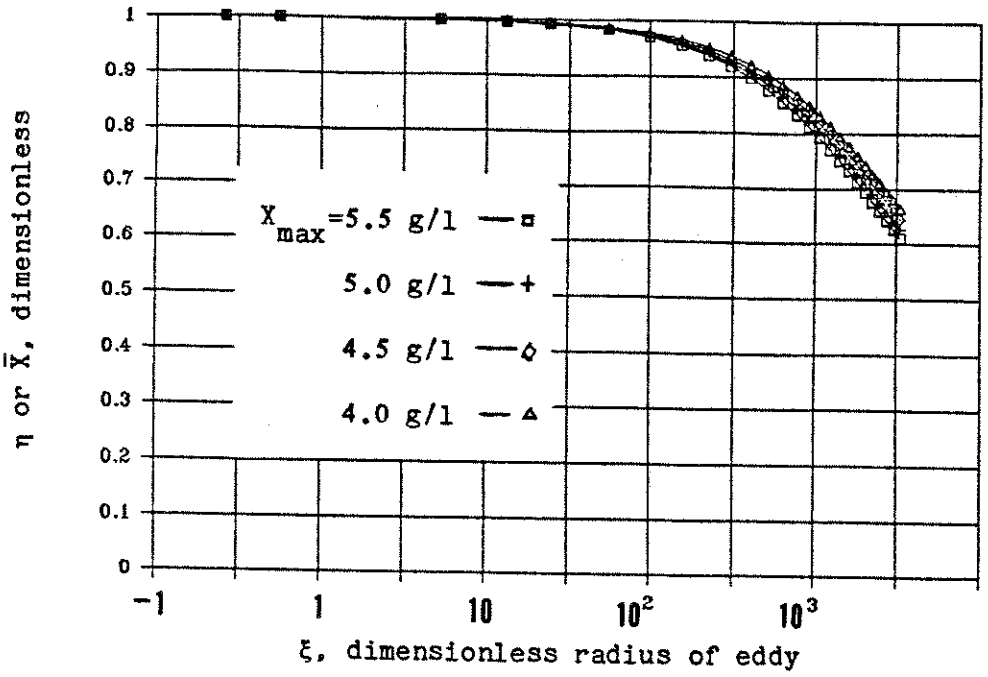

V_{max}= 0.0012 ggs, R_s=2 μ, S_o=0.03 g/l, γ=1, K'=0.05 g/l

Figure 5.5. η or $\bar{X}$ versus ξ with X_{max} as parameter.

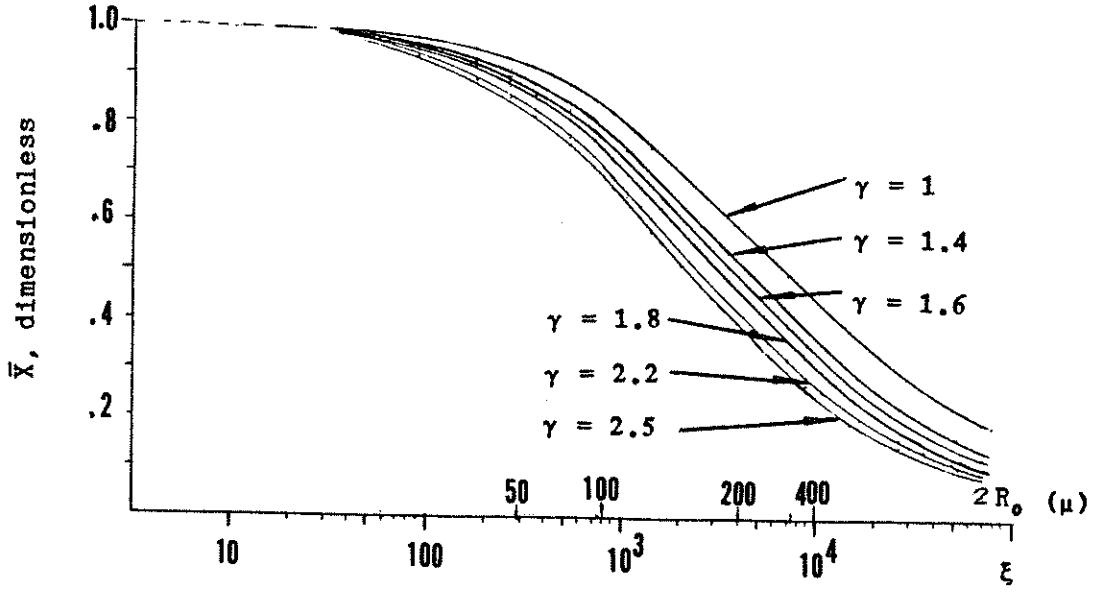

V_{max}= 0.0012 ggs, R_s=2 μ, X_{max}= 5g/l, S_o=0.03 g/l, K'=0.05 g/l

Figure 5.6. $\bar{X}$ versus ξ with γ as parameter.

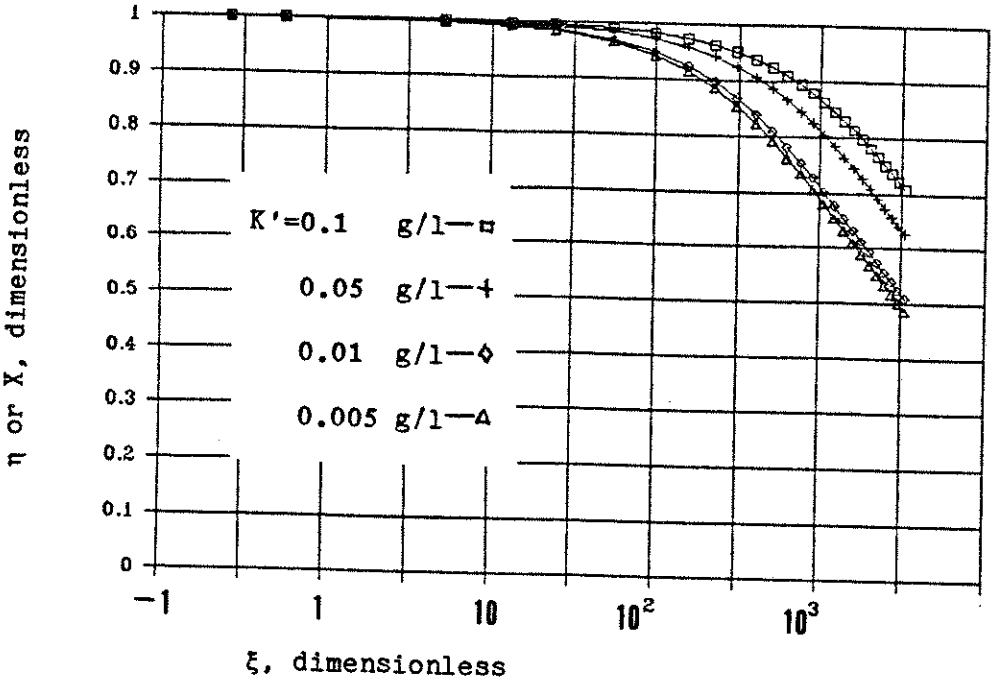

V_{max}= 0.0012 ggs, R_s=2 μ, X_{max}= 5g/l, S_o=0.03 g/l, γ=1

Figure 5.7. η or $\bar{X}$ versus ξ with K' as parameter.

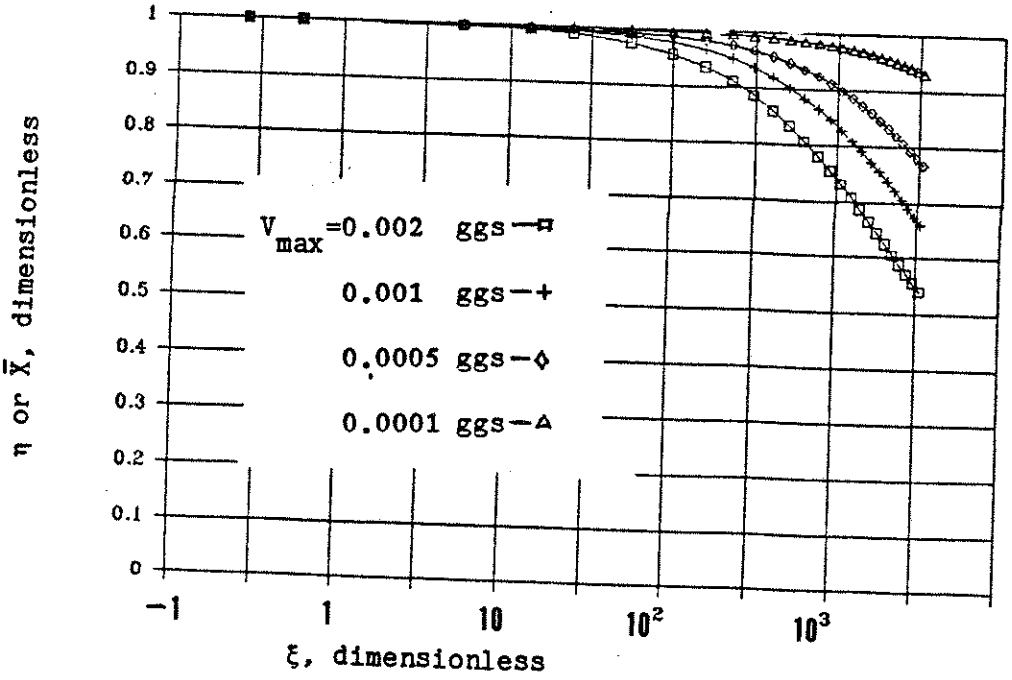

R_s=2 μ, X_{max}= 5g/l, S_o=0.03 g/l, γ=1, K'=0.05 g/l

Figure 5.8. η or $\bar{X}$ versus ξ with V_{max} as parameter.

5.5 DISCUSSION

Although the size of micromixing zone is in the same order of magnitude of eddy size, the relation between the size of micromixing zone and the eddy size is still not clear. Even with the microscale of eddy, Taylor, Corrsin and Kolmogroff give different definitions, which have different quantities of microscale for the same energy dissipation. Therefore, there is a problem as to the ultimate stage of mixing by molecular diffusion where it is not clear whether the diffusion mixing time is $t_m = t_s \sim (L_s^2/\varepsilon)^{1/3}$ or $t_m = t_D \sim \lambda_k^2/D$ [43]. This brings some difficulties to quantitatively describe micromixing by molecular diffusion.

The computation here is only valid for steady state and instantaneous fast reactions. The characteristic half-life for reaction can be estimated by [20,21]:

$$t_{1/2R} = 1/(k_1 c_{B0}) \tag{5.28}$$

The characteristic half-time for diffusion is estimated by [90]:

$$t_{1/2D} = 0.15\ R_k^2/D \tag{5.29}$$

For the chemical reaction, the half-life of the reaction is 0.0002 second. For the eddies near the impeller tip, the mean microscale of the eddy is about 14 microns (System II) and the half-life for molecular diffusion is 0.011 second. The eddy in the fermenter bottom area is about 160 microns, with its half-life for molecular diffusion being 1.4 second (System III). Compared to the internal circulation time in System III of 17.6 seconds (calculated by Eqn. (4.1), p. 36), the diffusion time of species in the 160 microns eddy is very short. Therefore, in the typical micromixing zone or liquid droplets, reaction time is much faster than the diffusion time, which is in turn faster

than the relative particle velocity. The cell particles may be simplified as stagnant particles inside the eddy and the diffusion-reaction model can be used.

Since the energy dissipation and eddy size distribution are not even inside the stirred tank reactors [26,28,41,67,44], it is oversimplified to use the calculation data from one single eddy size to predict the behavior induced by injecting media through a port with the same magnitude of micromixing zone size. However, it provides the baseline for the complex picture of micromixing inside the stirred tank reactors (multiple stirrer, uneven eddy size distribution). The total picture of micromixing can be obtained by combining the data of different eddy size over the whole micromixing zone distribution of the reactors [75]. By doing so, more correct results can be obtained but also tremendous work need to be done in a multiphase, microorganism and different mechanical configurations overlapped system and it is not the main objective of this work.

6. MICROMIXING EFFECTS ON BAKER'S YEAST AEROBIC FERMENTATION

6.1 INTRODUCTION

Although it is expected and some mathematical modelling [59,86,87,88,89,93] have shown that micromixing has significant effects on biochemical reactions, and various strategies [96,97] have been proposed for the design and scaleup of fermenters, little or no work has been done experimentally to investigate micromixing effects on biological growth. Previous work has emphasized mixing in fermentation [57,69,97,104] and most of them are based upon the complex effects of macro- and micro-mixing.

Taguchi [98] found that power input affected the oxygen availability in novobiocin fermentations. Bryant [69] discussed mixing and agitation in relation to the performance of fermenters and its characterization by determining the distribution of circulation rates. Recently, Fields and Slater [99] found that fluid mixing had some influences on respiratory patterns for extended growth of a methylotroph in an air-lift fermenter.

In Baker's yeast fermentation, Einsele et al [57] were able to isolate macromixing time from overall reaction time in the growth of Baker's yeast and found a relatively constant time for the sum of other resistance. Earlier, Hansford and Humphrey [58] showed an influence of mixing on cell yield of Baker's yeast at low dilution rates in continuous culture. They found that the yields at low dilution rates can be improved to a limited extent by using a multiple feed-distribution better mixing system. Various potential reactant feed ports were shown to be of importance in yeast growth. Fiechter [100] similarly reported

that on a continuous culture of Saccharomyces cerevisiae, critical dilution rate D_c was a function of substrate concentration S_{in} in the inflowing medium and overall mixing (macro- and micro-mixing), influenced by the degree of agitation, was the limiting parameter. It was demonstrated [97,104] that blade turbines in baffled vessels have poor mass-flow (mixing) characteristics. Stagnant zones behind the baffles and slow distribution of the entering glucose give rise to remarkable concentration profiles along the three axes of the reactor. Recently, Bajpai and Reuss [101] utilized the circulation time distribution and simple assumptions regarding the fluid segregation patterns in a stirred tank to model the continuous culture of baker's yeast.

The cell yield of Saccharomyces cerevisiae cultivated on a synthetic medium may also be influenced by mixing, or more specifically micromixing, not only from the previous experiment results but also from the characteristics of this yeast, for example, its sensitivity to the glucose level in the media [100,102,103].

In this work, fed-batch and continuous fermentations were tested and continuous culture was used for the micromixing study. This is because continuous fermentation provides better control over the operational variables; pH, temperature, agitation speed, gas flow rate, concentration and fed-rate of the injecting media, etc. can keep constant during the experiments.

6.2 EXPERIMENTAL METHODS

6.2.1 Mixing Study

The fermenter with System III in previous chemical characterization of the fermenter was used for yeast fermentation. RTD of the fermenter

was measured by azodye tracer as described in Chapter 4. Experimental results showed that injecting inert tracer into two different injection ports had the same RTD, but injecting reactant B into A through these two ports showed that micromixing was incomplete although the fermenter was perfectly macromixed under the experimental conditions.

Under the experimental conditions (N=120 rpm, Q=10 lpm), X_s was 0.0765 for stirrer side and 0.248 for fermenter bottom injection ports. These two values correspond to Kolmogroff eddy size 50 and 160 microns from the unsheared sphere model [27,29].

6.2.2. Organism

A strain of Budweiser Baker's yeast (Saccharomyces cerevisiae) was supplied by Anheuser-Busch Co. (St. Louis, MO).

6.2.3 Media

The shake flask and fermenter growth media contained (gram per liter): KH_2PO_4 2.81; EDTA 0.45; NH_4Cl 7.63; Citric Acid 0.105; $CaCl_2.2H2O$ 0.165; $FeCl_3.6H_2O$ 0.1125; $MnSO_4.3H_2O$ 0.051; $ZnSO_4.7H_2O$ 0.066; $CuCl_2.2H_2O$ 0.012; $Na_2MoO_4.2H_2O$ 0.0078; H_3BO_4 0.012; KI 0.0018; $CoCl_2.6H_2O$ 0.01204; $MgSO_4.7H_2O$ 0.59; Biotin 0.000053; Thiamine-HCl 0.005; Meso-inositol 0.047; Panthotenic Acid 0.023; Pyridoxine 0.0228; Glucose 11.4. pH was adjusted at 5 [105].

6.2.4 Fermenter

The dimensions of the fermenter with System III are shown in Figure 4.1, Chapter 4. A schematic diagram of the fermenter, its controls, and analytical devices are shown in Figure 6.1.

Temperature and pH were controlled by the automatic controlling units of the fermenter. The experimental temperature was 30 ± 1 °C and the pH was 3.3 ± 0.1.

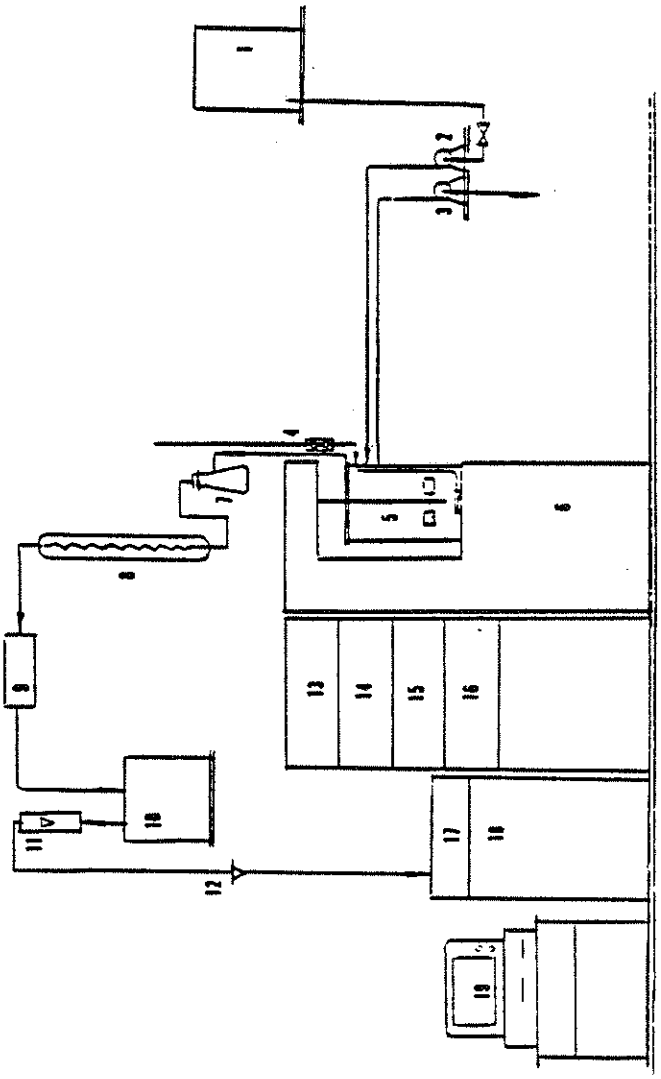

Figure 6.1. Fermentation Equipment Flowsheet for Micromixing Study
1 - medium tank; 2,3 - feeding and discharging pumps;
4,9, 12 - air filters; 5 - fermenter vessel
6, 13, 14, 15, 16 - control modulus ; 7, 10 - surge bottles
8 - condenser; 11 - flowmeter; 17 - ISSAC microprocessor
18 - gas analyzer; 19 - IBM PC

Agitation and air flow was controlled manually at the conditions used in the micromixing characterization, 120±10 rpm and 10±0.5 lpm.

Medium was injected through the 50 and 160 micron injection ports alternately, and the broth was discharged through a discharging port at the surface (i.e. surface port of System II), which kept the constant volume for the broth inside the fermenter. The feeding and discharging were carried continuously by two Cole-Parmer masterflex pumps.

Air was supplied through a Whatman Gamma-12 filter (4) and a multiple hole sparger. The exit gas passed through a water cooling coil (8) and a glass fiber filter (9), a flowmeter (11), a Gelman's Acrodisc filter (12) and then A Perkin-Elmer 1200 Multiple Gas Analyzer. Tank 10 was used to prevent damage to the gas analyzer by preventing overflow of broth into the analyzer.

The gas analyzer was used to analyze the exit gas compositions, ethanol, carbon dioxide, oxygen, nitrogen and H_2O reported. The data were processed by an ISSAC 2000 (Cyborg Corp.) micro-processor and an IBM personal computer.

6.2.5 Experiment Procedures

Fermentations were conducted by inoculating 3 liter medium with 800 ml broth (to shorten the batch cultivation time) taken from a shake flask culture in the exponential growth phase. 29 hours after inoculation, the batch operations was switched to continuous cultivation and medium was continuously fed through the 50 micron stirrer side injection port with a dilution rate (reciprocal of mean residence time) of 0.16/hr. After stabilizing the continuous cultivation for 28 hours (about 7 doubling times), the O.D. (optical density) at 660 nm showed that the culture had reached steady state. 31.5 hours into the

continuous culture, the injection port was then changed to the 160 micron port. The O.D. of the broth decreased from about 6.5 to 4.0 in about 2 hours and then remained steady. 40 hours after initiation of continuous culture, the injection port was changed back to the 50 micron port, and the O.D. increased from 4.0 to about 5.5 in 3 hours. To see the reproducibility, at 55 hours from the initiation the injection port was once again changed to the 160 micron port, the O.D. dropped again from 5.5 to 4.0 in 2.5 hours. This process is shown in Figure 6.2.

The experiment was performed under conditions where glucose was the only limiting nutrient. The residual glucose concentrations of all samples were lower than 40 mg/l and the dissolved oxygen level was above 6.25% of saturated concentration or 0.073 mmol/l (compared to the critical value of yeast, 0.0046 mmol/l [106]).

The experiment was not only evaluated on the overall biological responses (optical density or dried weight, respiratory quotient), but also on the cell contents, including total protein, aldolase and isocitrate dehydrogenase activity and pyruvic acid. The particle size populations from the samples of two different injection ports were also measured by Coulter Counter Model T_{AII} from Coulter Electronic, Inc..

6.2.6 Sample Analysis

Broth samples were collected through the front of baffle port as shown in Figure 4.1. The samples were then frozen for later analysis.

The broth samples were centrifuged at 3000 rpm at 5 °C by an IEC DPR-600 Centrifuge (Damon/IEC Division) for 10 minutes, and the supernatant was pipetted out and several types of analyses were performed by using the diagnostic reagent kids from Sigma Chemical Company (St. Louis) (Table 6.1, sampling at steady state).

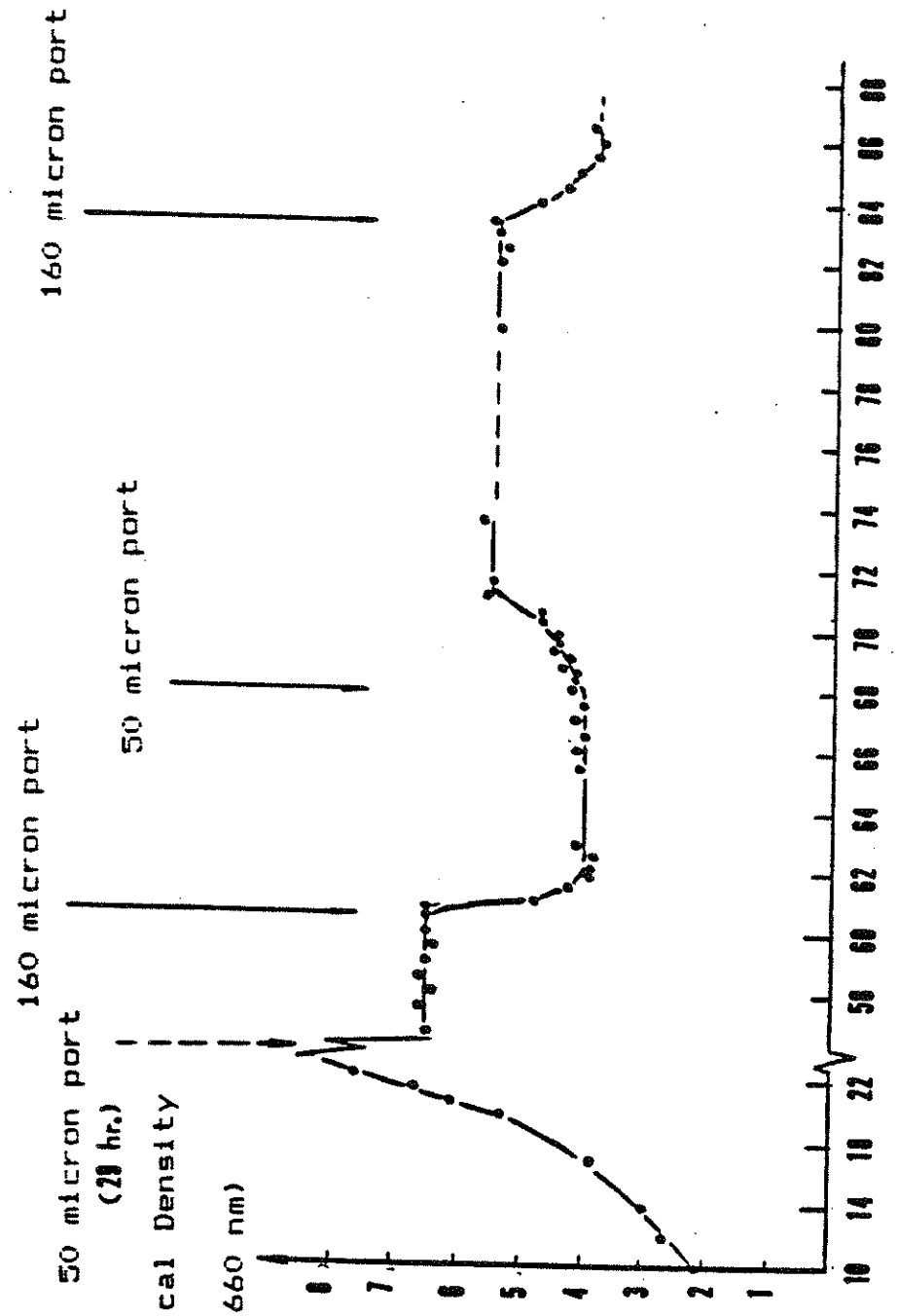

Figure 6.2. Cultivation of S. cerevisiae under glucose limitation
Dilution rate = 0.16 /hr; Glucose concentration in feed = 11 g/l;
Residual glucose concentration: all < 40 mg/l;
D.O. all > 6.25% saturation; pH = 3.3; temperature = 30 °C;
Agitation = 120 rpm; Gas flow = 10 lpm

The optical density at 660 nm wavelength of the broth samples was measured by Spectronic 710 (Bausch and Lomb) in 1 cm. cuvet. The paste cells after centrifugation were washed with 1:1 (broth/water volume ratio) iced water three times and then put into vacuum oven at about 70 °C. The dry wright of the cells showed a linear relation with the optical density measurement (Figure 6.2b).

Table 6.1 Analysis of Supernatant from Two Injection Ports

	Stirrer Side (50 μ)	*Stirrer Side (50 μ)	Fermenter Bottom (160 μ)
phosphorus (mg/l)	0.30, 0.28	0.33, 0.34	0.30, 0.35
residual glucose (mg/l)	33, 37, 37, 41	26, 33, 33, 33	11, 22, 15, 19
ethanol % (w/v)	0.14, 0.13, 0.10, 0.12	0.13, 0.14, 0.17, 0.14	0.09, 0.14 0.11, 0.13
pyruvic acid (mg/l)	2.4, 2.8, 2.4	1.1, 2.6, 2.5, 7.8	2.5, 2.7, 3.6, 3.4
soluble protein (mg/ml)	0.374	0.374	0.374

* Remark: samples after switching injection from the 160 micron port.

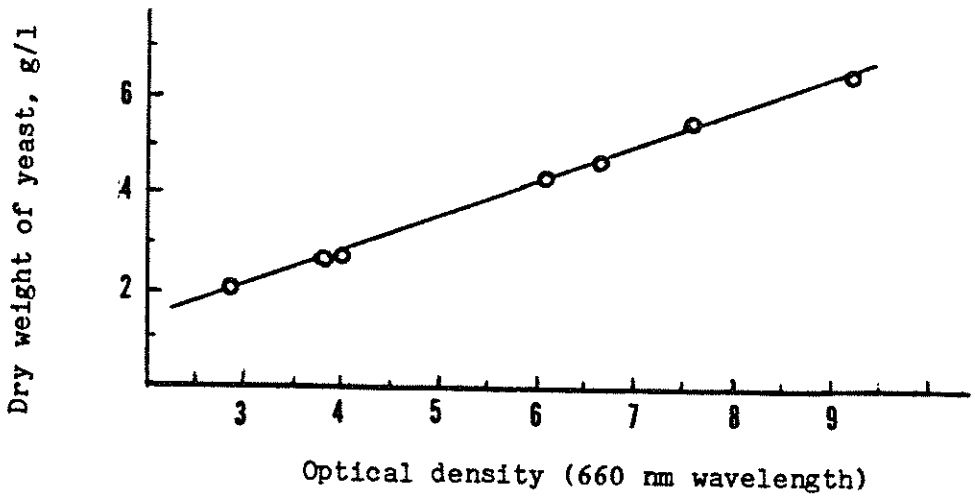

Figure 6.2b. Dry weight of yeast as function of optical density.

The cell content was analyzed by different methods. Total protein was measured by disrupting the cells in potassium hydroxide [107] and the biuret method [108] was used. To measure the activities of aldolase and isocitrate dehydrogenase, 2-glucronuridase and sonication with glass beads (150 μ) were alternately used to break the cell wall of yeast and then the enzyme activities were measured [109,110]. All the diagnostic reagents were provided by Sigma Chemical Company (St. Louis). The buffer system was 0.02 M Na_2HPO_4/NaH_2PO_4 at pH 6.53. PH change during disruption was smaller than 0.06. Microscope was used to check the disrupted cells. Table 6.2 shows the results with different cell disruption methods and similar results were obtained for both methods.

Table 6.2 Comparison of Cell Disruption Methods

Enzyme Method			Sonication with Glass Beads		
Time (hr)	% Disrupted	Aldolase (IU)	Time (min.)	% Disrupted	Aldolase (IU)
1.5	30	6.6	2	40	6.1
2.0	50	10.5	3.5	80	9.2
2.5	>95	10.8	5	>95	10.6
3.0	>95	10.7	6	>95	10.7

With the enzyme method, the samples were added 0.2 ml of the enzyme solution (10^8 unit/l) to the cell paste from 5 ml broth and then incubated at 37 °C, being shaken once 10 minutes. With the sonication, 80 % volume of 150 μ diameter glass beads was used and the samples were put into ice bath during sonication. Aldolase content of the samples was measured by the Spectronic 710 in 1cm cuvet at 540 nm.

6.3 DISCUSSION

6.3.1. Carbon Conversion, Yeast Growth and Micromixing

The experiment results in Figure 6.3 show that the dry weight of yeast was strongly influenced by the micromixing scale. A t-test showed very significance levels for these effects. Divided by the amount of glucose consumed, the data can be transferred to biomass yield (g dry weight/g glucose consumed). Figure 6.4 shows that the biomass yield had a strong relation with the injection ports or the size of eddies or the degree of micromixing.

Previous results from the literature show that when the dilution rate is lower than the critical dilution rate, oxidative metabolism of glucose predominates. The residual glucose concentration is below 50 mg/l, the biomass yield is near 0.4 to 0.5 dry mass per g glucose consumed, the R.Q. is one, and only traces of ethanol are evident [100,111-114] in this range. At the dilution rate higher than the critical value, the residual glucose concentration increases and the burden of energy generation shifts to the fermentation of glucose. In this range, the biomass yield is much lower, approaching 0.15 g dry mass per g glucose consumed, the RQ rises far above one, and large amounts of ethanol are produced. Moreover, the specific oxygen uptake rate, which increases linearly with dilution rate in the oxidative region, decreases with increasing dilution rate beyond the critical value [100,111-114]. The biomass yield data showed when glucose was fed through the 50 micron port, oxidation of glucose predominated and the biomass yield was close to 0.5 g dry mass/ g glucose. However, when switched medium feeding to the 160 micron port, the biomass yield dropped to 0.24 g dry mass/g glucose, which is close to the value with glucose repression

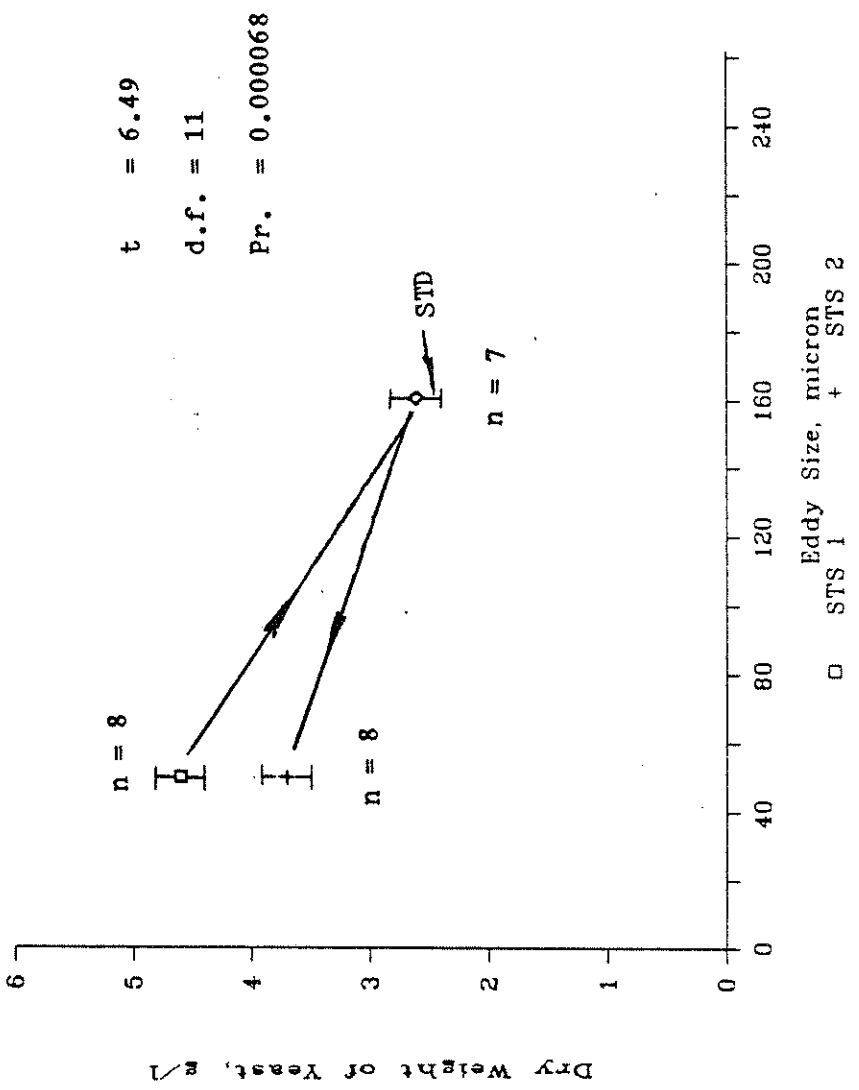

Figure 6.3. Dry weight of yeast as function of eddy size

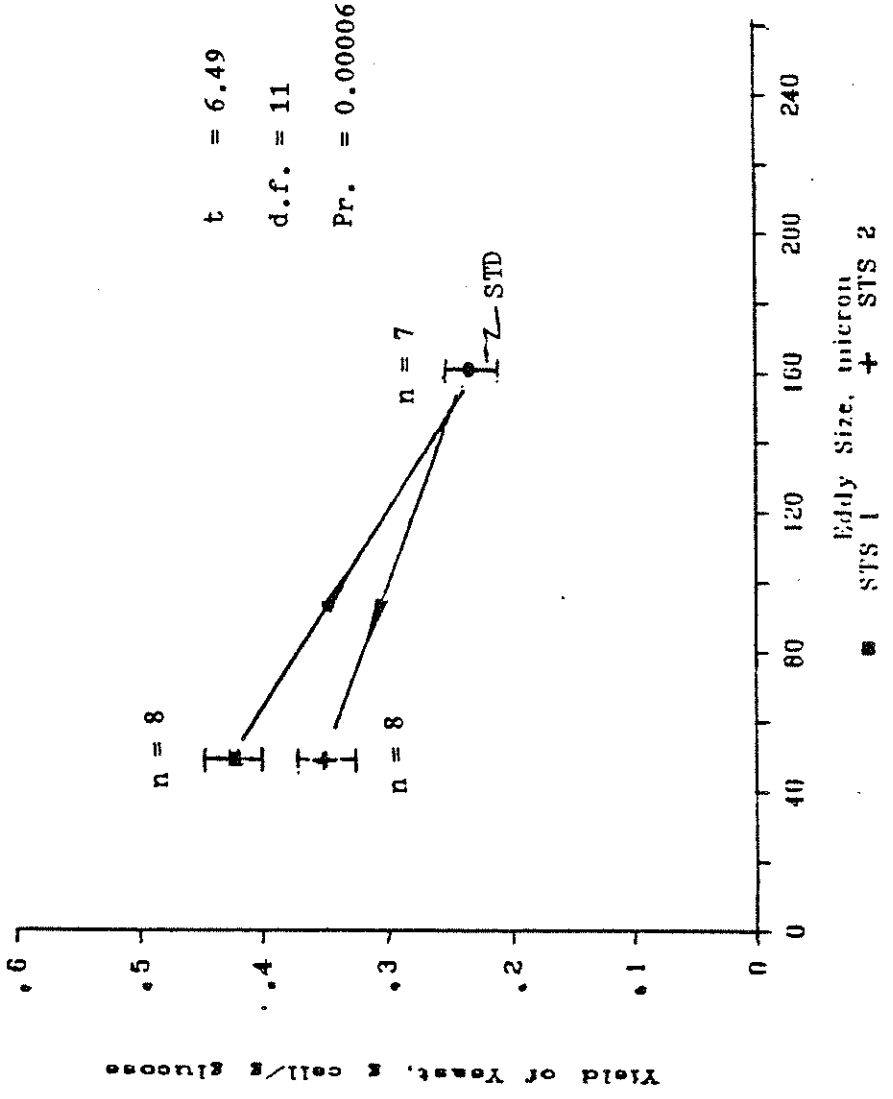

Figure 6.4. Biomass yield as function of eddy size

(Crabtree effects). This suggests that at the 160 micron port, some kind of combination of glucose repression and oxidation occurred. Since the critical dilution rate (typically is 0.2 - 0.32 /hr) marking the onset of the Crabtree effects has been found to be quite variable (growth supplements, such as glutamic acid, are reputed to raise the critical dilution rate by modifying key internal metabolic pools. It has also been reported that imperfect reactor mass-flow patterns, resulting in significant glucose concentration profiles, and inadequate oxygen transfer can reduce the critical dilution rate [100,102,103]), the biomass yield data suggests that incomplete micromixing may lead to locally-accumulated glucose which lowered the critical dilution rate, stimulating the Crabtree effects.

The biomass yield data are also in agreement with Hansford and Humphrey's findings [58] to some extent. They found that the continuous growth of Baker's yeast with a sugar nutrient at low dilution rates in a stirred tank varied with the position of the nutrient injection. They concluded that cells which encountered regions of high sugar concentration, such as those when nutrient was injected into the relative tranquil fluid in the lee of a baffle, diverted a greater proportion of substrate carbon into extracellular product via endogeneous metabolism. This behavior caused a reduction in the overall cell yield. The conflict between their results and this work is that they only observed the effects at low dilution rate (lower than 0.1). Since there are no micromixing data available about the fermenter they used, this work would give a better quantitative observation.

The relative portion of the fermenter inactivated by glucose repression can be estimated from the biomass yield data, assuming 0.15 g

dry mass/g glucose of biomass yield is 100% glucose repressed.

6.3.2. Micromixing and Respiratory Patterns

While the dry weight changed in hours after changed the feeding port, the exist gas compositions changed in minutes. The experimental results showed that the respiratory of yeast had a strong relation with micromixing and the values of R.Q. (respiratory quotient, mole ratio of carbon dioxide formed divided by oxygen consumed) from the gas analyzer showed a relation with the micromixing zone size (Figure 6.5). It is reported that the low RQ (0.4-0.7) stood for the oxidative metabolism of ethanol [115], and that if the residual glucose concentration was lower than 100 mg/l, ethanol produced was very small (especially around Dc) and increasing glucose level increased the production of ethanol [100,120]. Since the amount of glucose fed was very low (about 6 g/hr), the high glucose concentration seems to occur only locally and the Crabtree effects would occur locally. The carbon dioxide formation and oxygen consumption average over the whole fermenter will be trivial. It appears to be that feeding through the 160 micron port led the system to the edge of the Crabtree effects. However, if Crabtree effects really occurred, R.Q. should show higher values before it reached 0.4 to 0.7. More experiments are needed to carefully explain this phenomenon.

6.3.3 Micromixing and Yeast Budding

It is interesting to look at the relationship between dynamic growth-budding and micromixing. S. cerevisiae is a diploid yeast, oval in shape, which has rather complex modified life cycle called vegetative cell cycle in typical batch and continuous cultivation, as shown in Figure 6.6a [116].

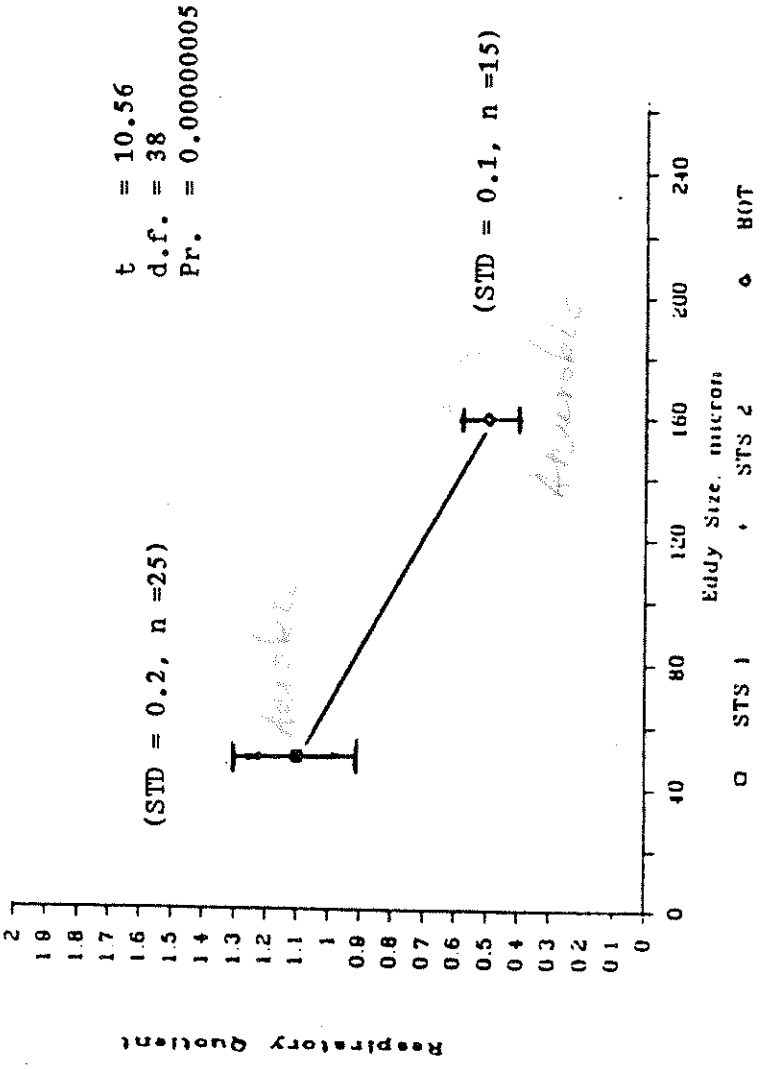

Figure 6.5 Respiratory quotient as function of eddy size

The cell cycle of S. cerevisiae consists of several distinct stages based on morphology and biochemical events (Figure 6.6b):

1. S phase, a period of DNA replication;

2. G2 phase, a period separating the end of DNA replication from nuclear division;

3. M phase, a period of nuclear migration and division;

4. G1 phase, a period separating nuclear division from DNA replication;

5. G1* phase, that portion of G1 separating nuclear division from cell division [117].

It is reported that S+G2+M phases are relatively invariant and the mean length of G1 phase in S. cerevisiae population is strongly dependent on the specific growth rate as shown in Figure 6.7 [117]. The higher the growth rate, the shorter is the budded period whilst the rest of the cell cycle keeps approximately constant time and the higher is the percentage of the budded cells. This is shown in Figure 6.8 [118]. Particle population of the samples showed that injecting media to the better micromixing port led to bigger size particles as shown in Figure 6.9. T-test on the mean cell volume, mean cell diameter and the shapes of particle distribution curves are very significantly different (Table 6.3). This data shows that better micromixing either leads to bigger yeast or a higher percentage of budded cells (or high specific growth rate) since the coulter counter can not tell the difference between the budded and unbudded cells. This fact is in good agreement with Barford and Hall's work [117], the finding from von Meyenbury [118] and the results of Johnston [119].

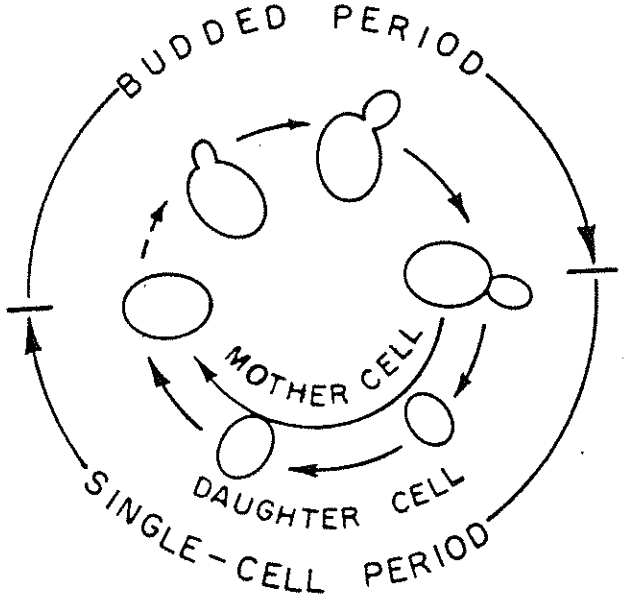

Figure 6.6a. Vegetative cell cycle of S. cerevisiae [116].

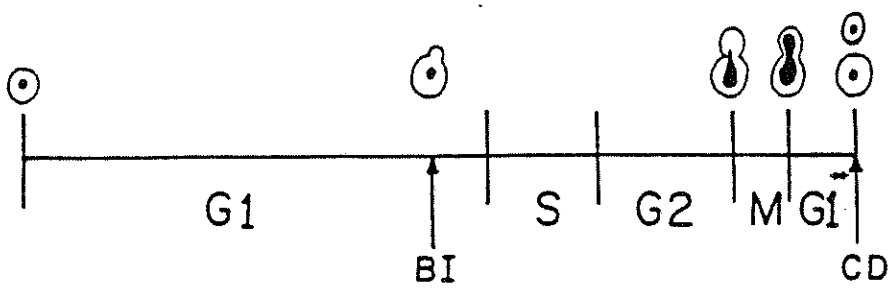

Figure 6.6b. Stages of the cell cycle [117]. G1, S, G2, and M phases, bud initiation (BI), and cell division (CD).

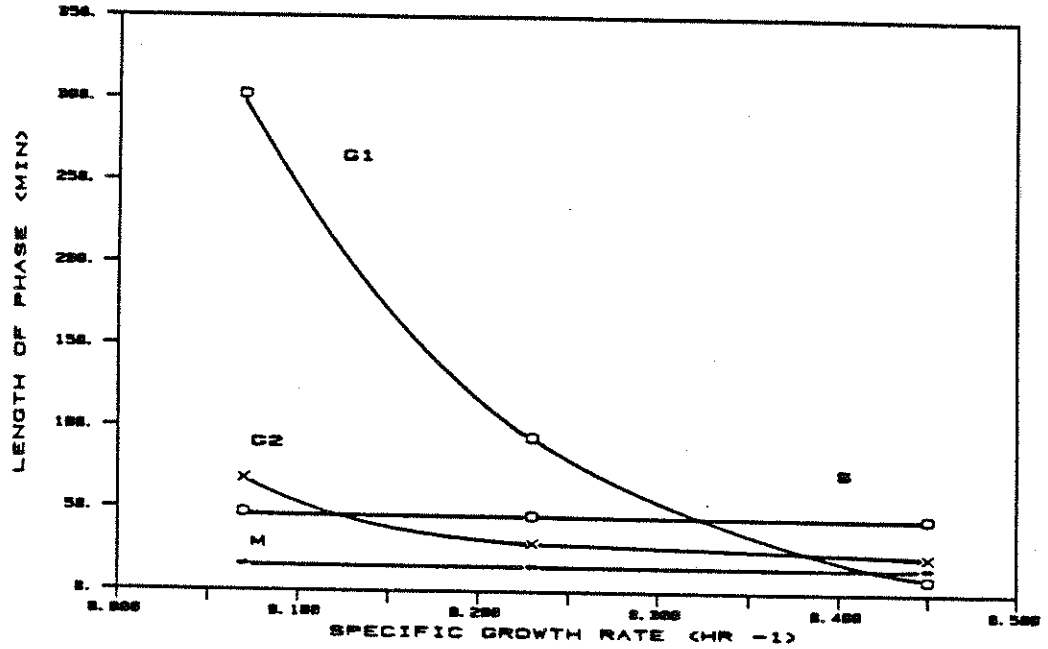

Figure 6.7. Variation in the lengths of cell cycle phases [117].

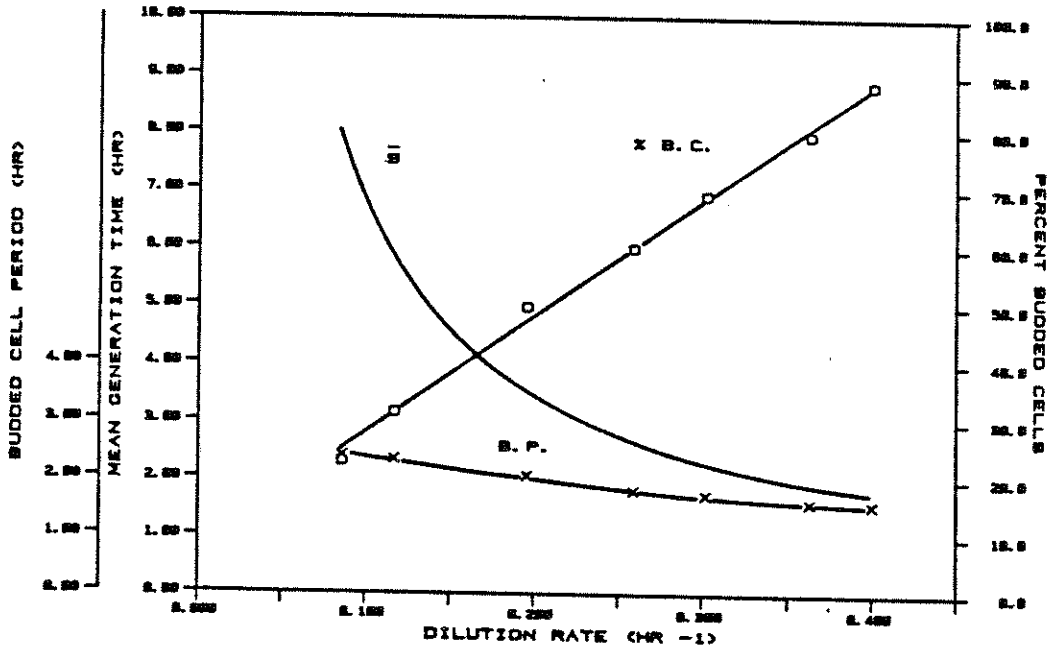

Figure 6.8. Dependence of the budded period and the percent budded cells on the steady state specific growth rate in continuous culture [118]. Mean generation time g, budded period B.P., and percent budded cells %B.C..

Table 6.3 Particle Size Distribution as Function of Eddy Size

	50 microns (stirrer side)	160 microns (bottom)	T-test	D.F.	Pr
mean cell vol. (micron³)	55, 53	38, 39	13.9	2	0.0018
mean cell dia. (micron)	4.73, 4.67	4.16, 4.22	12	2	0.0024
VAR	99, 100	134, 131	20.9	2	0.0008
STD	9.97, 10	11.6, 11.5	30	2	0.00045
3rd Moment	432, 447	1360, 1270	19.2	2	0.00095
4th Moment	13800,14800	38000, 36000	20.8	2	0.00082

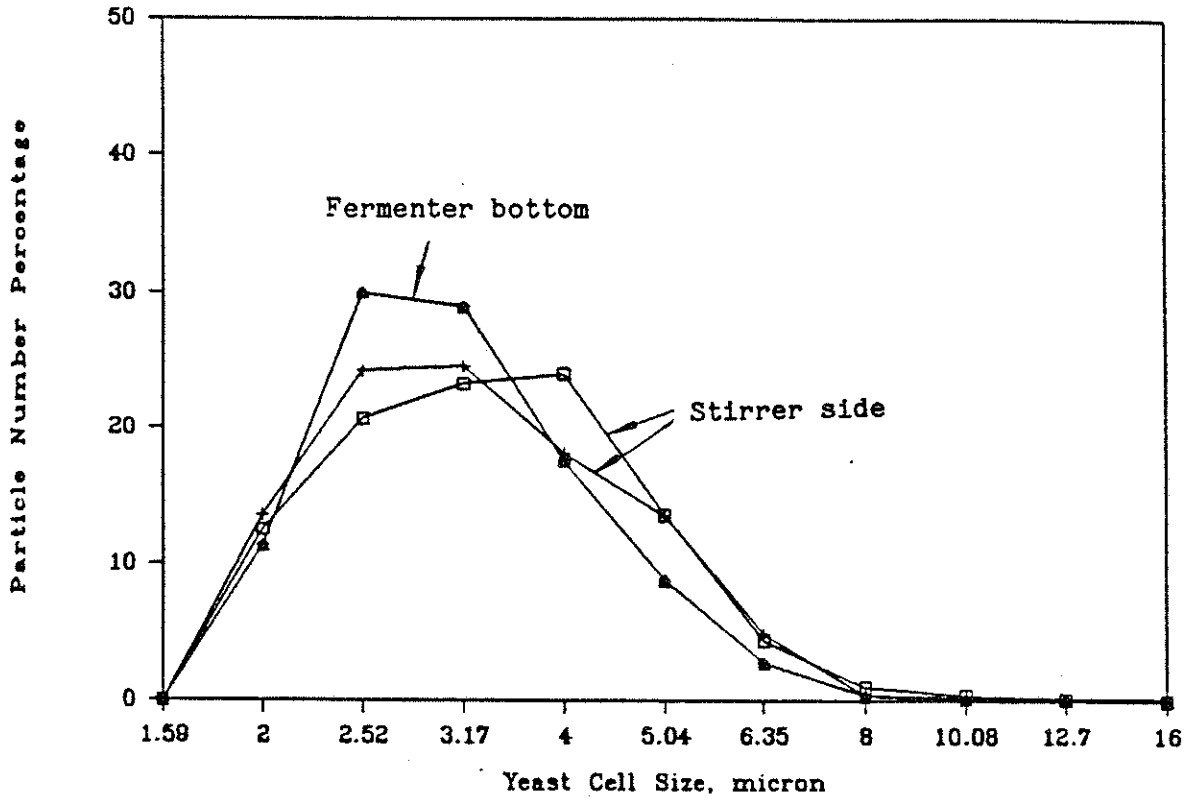

Figure 6.9. Particle size distribution as function of eddy size

6.3.4 Micromixing and Protein Synthesis as Well as Substrate Metabolism

Previous literature shows that the specific metabolic and physiological changes leading to the Crabtree effects include effects on enzyme synthesis and enzyme activity of TCA cycle enzymes, electron transport chain enzymes, and glyoxylate pathway enzymes [110]. In order to see if incomplete micromixing did stimulate the Crabtree effects, the samples from the different ports were disrupted and the cell contents were analyzed for total protein, aldolase and isocitrate dehydrogenase, so that the biological responses inside the cells can be obtained.

Figure 6.10 to 6.12 show that micromixing affected not only the total protein synthesis rate inside the yeast cells, but also enzyme activity such as aldolase and isocitrate dehydrogenase. Changes in the enzymes lead to different production level of some metabolites such as pyruvic acid within the TCA cycle (Figure 6.13). However, since all of the previous results from the literature only give qualitative answers and the enzyme patterns under glucose repression are very complicated (they are the nonlinear functions of specific growth rate and residual glucose level [100,110]) and less and no data available to explain the behavior, more work need to be done.

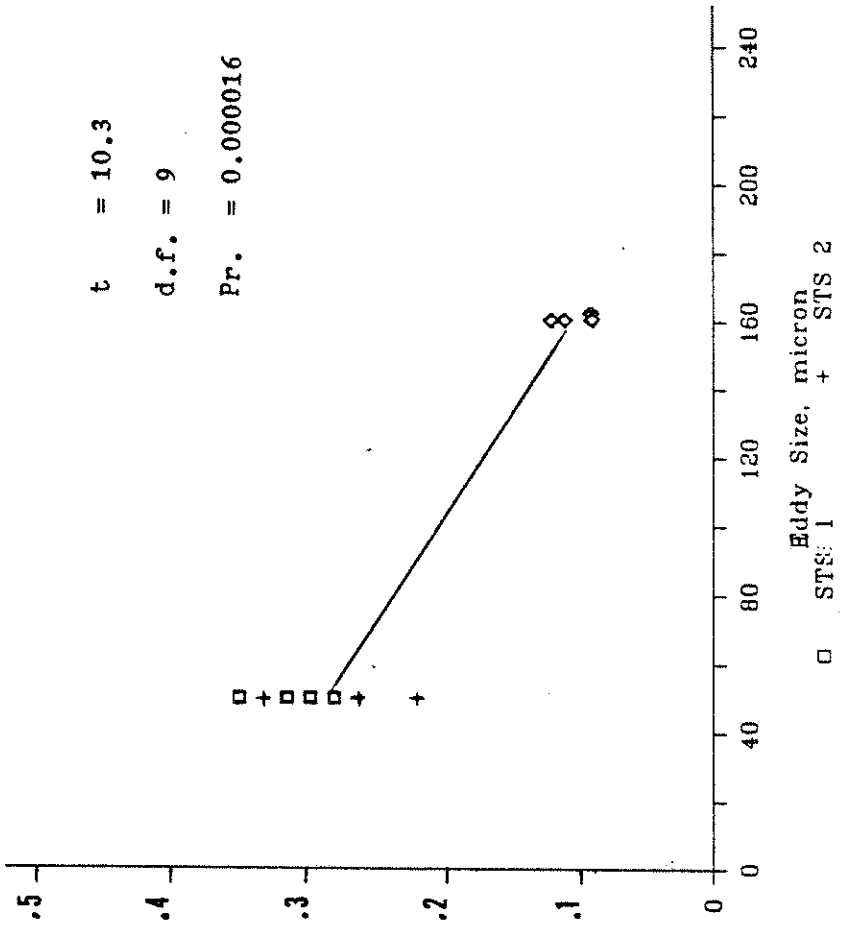

Figure 6.10. Total protein synthesis rate as function of eddy size

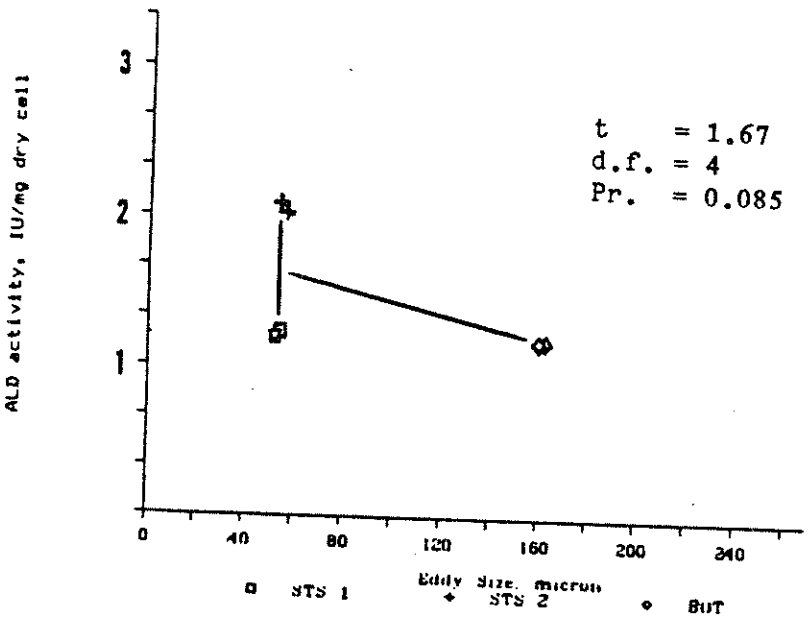

a)

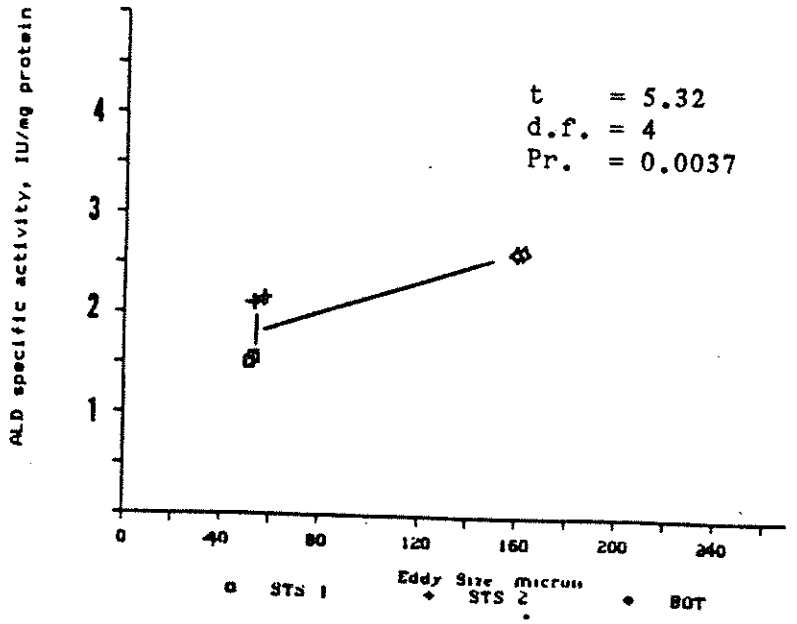

b)

Figure 6.11. Aldolase activity as function of eddy size. a). activity over biomass. b). activity over total protein.

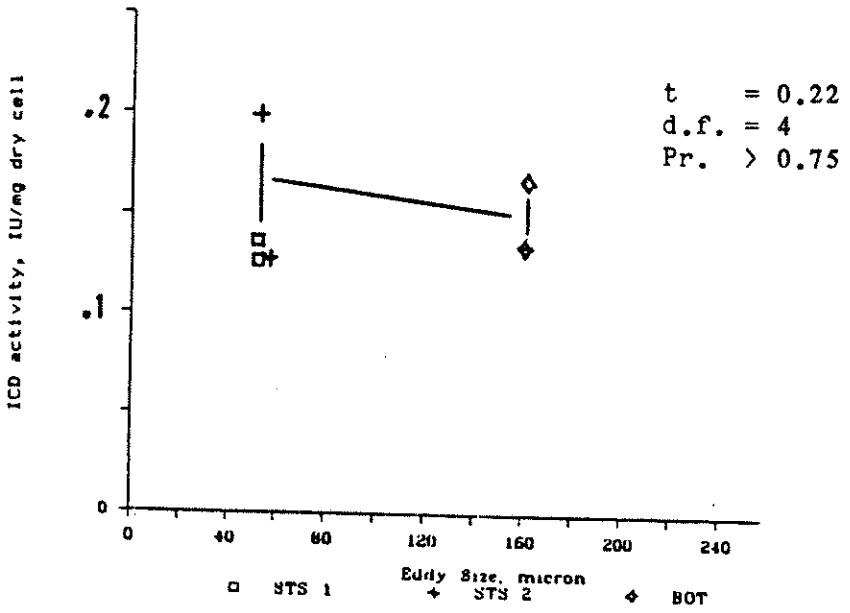

a)

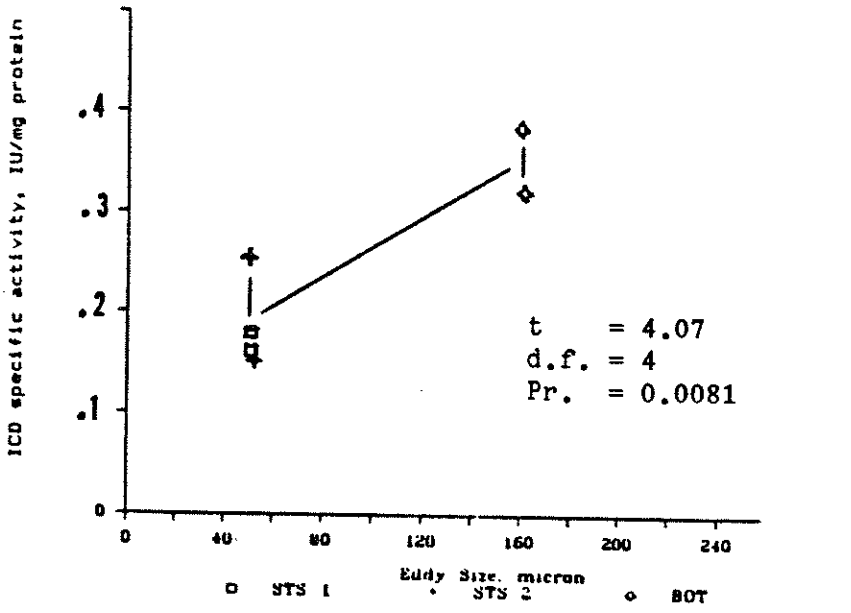

b)

Figure 6.12. Isocitrate dehydrogenase activity as function of eddy size. a). activity over biomass. b). activity over total protein.

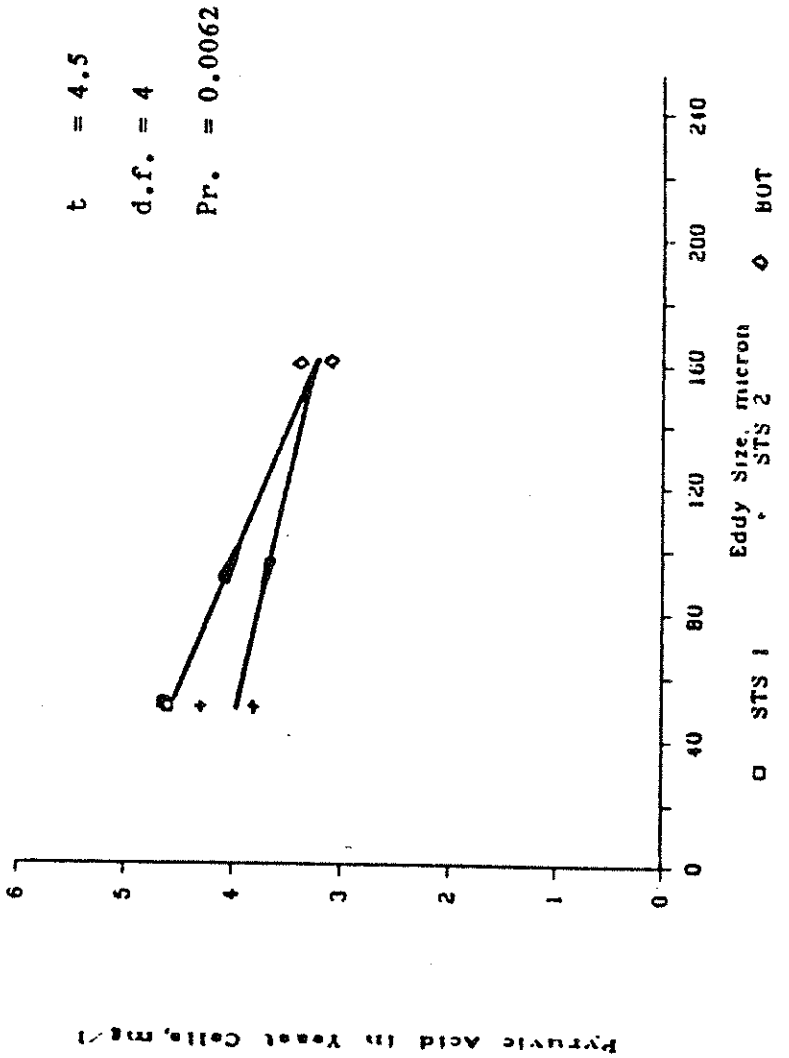

Figure 6.13. Pyruvic acid content in yeast cell as function of eddy size

6.3.5 Micromixing and Glucose Transport

In Chapter 5, it is shown from the previous literature that glucose uptake is the main regulatory substrate and glucose transport is the controlling step in glucose uptake. When macromixing-bulk mixing or turbulent mixing is perfect, micromixing is the controlling step. The experimental results of this work proved this. Under the experimental conditions, of which macromixing was shown to be substantially complete, it is shown that micromixing is important to the glucose uptake of Saccharomyces cerevisiae since the only difference between the stirrer side port and the fermenter bottom port is the degree of micromixing, which is expressed in terms of the zone size. The micromixing controlling in glucose uptake gave rise to all the biological responses described above. The complex responses have not been observed yet.

6.3.6 Comparison of Experiment Data and Mathematical Modelling

Figure 6.14 shows the comparison of the experimental data and the calculated values from the modelling in Chapter 5. The values of the parameters are taken from the experiments and literature (see Appendix 9.3). The data points fit the curve with $\gamma = 1.6 \pm 0.2$. It can be seen that although the model is simple, it shows good agreement with the experimental data. The data points(back up from 160 microns) departing the fitting curve suggests that after changing injection to the 160 micron port, some irreversible damage to the cells possibly resulted. The complicated changes inside the cells (enzymes, nuclear acid, etc.) need to be further investigated.

Since all the figures above only give two data points, more work need to be done to extend the results to an appropriate range of micromixing zone size.

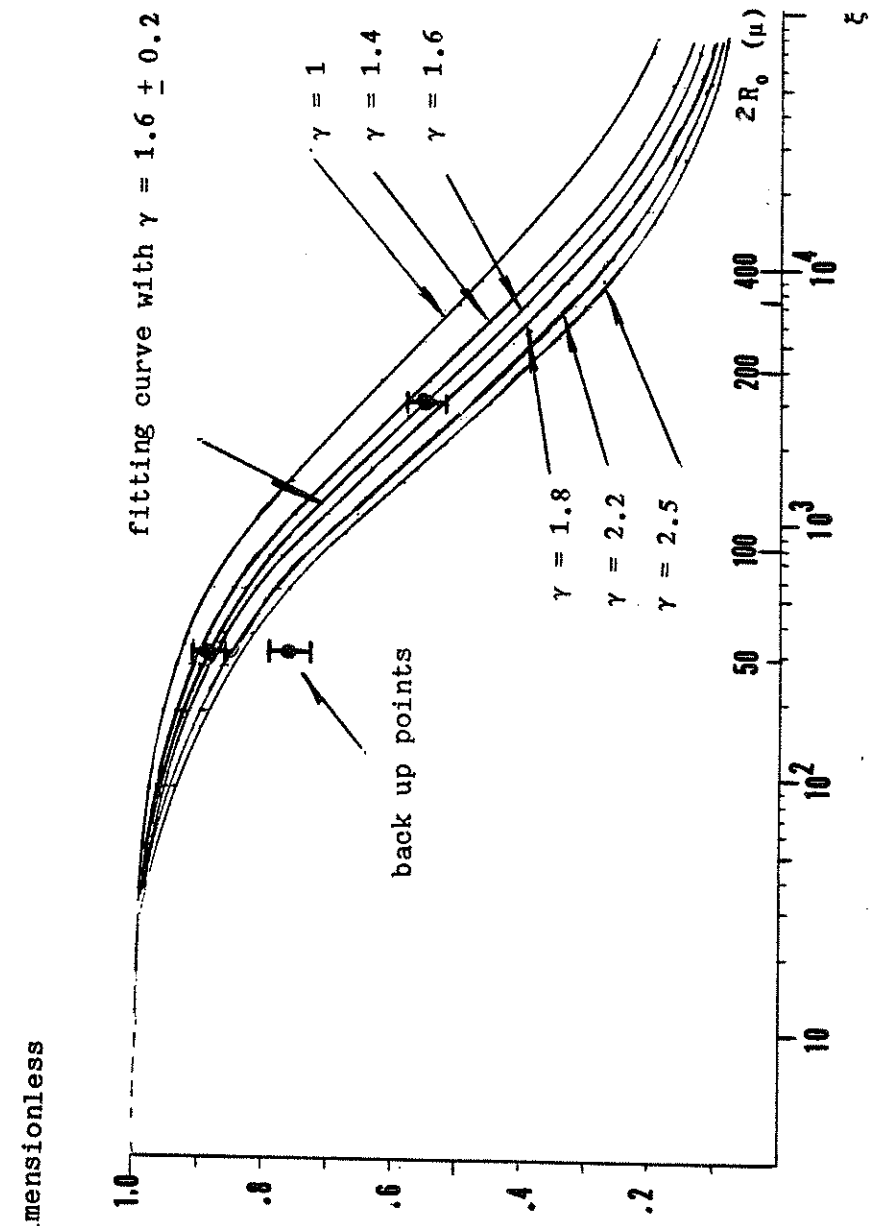

V_{max} = 0.0012 ggs, R_s=4 μ, X_{max} = 5g/l, S_o=0.03 g/l, K'=0.05 g/l

Figure 6.14. Comparison of the model and experimental data.

7. CONCLUSIONS AND FUTURE WORK

7.1 CONCLUSIONS

7.1.1 Characterization Technique

Azo coupling reaction of 1-naphthol and diazotized sulphanilic acid developed here is a useful technique in the gas-liquid-two-phase micromixing study. For the first time pure standards and better analytical technique are available for using the reaction initially developed by Bourne [26].

7.1.2 Micromixing in Gas-Liquid Two Phase Stirred Tank Fermenter

Mixing studies on a small stirred tank fermenter, which has higher energy input, multiple batch feed points and various agitation and gas feed rates, show that although macromixing is perfect, micromixing is still incomplete. The degree of micromixing of the system used is complex. Increasing agitation appears to always improve mixing whereas increasing gas rate can have either a beneficial or detrimental effect on mixing. The detrimental effect, which has not been previously recognized, is associated with feed points, or conditions, where gas bubble coalescence occurs.

An eddy-stretch model of Agnst, Bourne and Sharma [29] gives results that are semi-quantitatively representative (but much compressed) of the experimental results despite the fact that overall power dissipation results must be used rather than local values as are apparently measured by the chemical reactions. The stretching effects can be investigated from the slope of the relations between the micromixing index X_s, which is the final product yield, and the micromixing modulus M, which is the microtime and reaction time ratio.

The stirrer areas have much higher stretching effects but the baffle areas, on the other hand, show less influence of shearing.

7.1.3 Micromixing in Saccharomyces Cerevisiae Aerobic Fermentation

For the first time, it has been shown experimentally that aerobic fermentation of Sacchromyces cerevisiae with glucose-diffusion-limitation is significantly effected by micromixing. The important effects are expressed in terms of not only the oxygen and glucose transfer but also the protein synthesis, the productionsof metabolites and cell budding. When media were fed by the 50 micron good micromixing port, biomass yield was high and glucose was quickly uptaken by the yeast. The protein synthesis was also high. However, when media were fed by the 160 micron poor mixing port, glucose transport was deteriorated so by poor molecular diffusion or incomplete micromixing that the growth of yeast actually had a relatively poor microenvironment. Lower biomass production, lower protein synthesis rate and lower isocitrate dehydrogenase concentration, and lower production of pyruvic acid resulted. These phenomena showed that incomplete micromixing of the fermenter controls glucose transport, deteriorates glucose uptake of the yeast, and leads to:

1. poorer carbon conversion and biomass yield;
2. lower protein synthesis rate;
3. different enzyme activity and metabolite level;
4. poorer budding and growth;
5. different respiratory patterns.

The mathematical equation based upon micromixing control of glucose uptake shows good agreement with the experimental data.

7.2 FUTURE WORK

Although the experiment results showed that the fermentation was performed at the edge of Crabtree effects in Sacchromyces cerevisiae, more work need to be done to explain the nature of micromixing effects (on glucose repression).

Since the results of this study only give two data points on the effects of eddy size on fermentation, future work will extend the data to five injection ports (or five different degree of micromixing at stirrer side, stirrer bottom. front of baffle, between baffles and fermenter bottom ports) and a series dilution rates. The effects of micromixing will be evaluated in much more detail from:

1. carbon conversion and biomass yield;
2. respiratory pattern of yeast and oxygen utilization;
3. yeast budding;
4. protein synthesis rate, enzyme activity change and metabolite production;
5. change of nucleic acid level.

The mathematical model will be again evaluated by the biomass concentration results from the experiments.

8. ACKNOWLEDGEMENTS

I would like to express my gratitude to Professor Eric H. Dunlop for his invaluable guidance and encouragement during the pursuit of this work.

I would like to thank Dr. Wendell Iverson , Dr. Robert E. Sparks and Dr. Milorad Dudukovic for their advice in this wrok.

Support for this work was provided by a grant from the Anheuser-Busch Companies. The Virtis fermenter used was donated by Ralston Purina. The Coulter Counter was provided by the Anheuser-Busch Companies and the Cary spectrophotometer was provided by the Department of Chemistry. These are also greatly appreciated.

I would also like to thank Dr. Moshe M. White, Barbara Beard, Jeff Fowler, and Rick Dauer for providing various forms of support.

Finally I would like to especially thank my parents, although they are far away in China, and my wife for their great support and encouragement.

9. APPENDICES

APPENDIX 9.1

PH and Ionic Effects on Azo-coupling Reaction

Azo-coupling reactions have complex pH and ionic effects. Conant and Peterson [61] demonstrated that the rate of coupling of a series of naphtholsulphonic acids was proportional to the OH^- concentration in the range of pH of 4.50 to 9.15. It is now realized that the rate of coupling depends greatly upon the acidity of the medium and for every combination of components there exists an optimum pH range. This shows that the rate constant k_s is being affected by an acid-base equilibrium in one of the two reactants.

Eleven years later it was pointed out by Wistar and Bartlett [65] that not only the diazo, but also the substrate is subject to acid-base equilibrium. Thus:
For the diazo compounds:

$$Ar\text{-}N_2^+ + OH^- \rightleftharpoons Ar\text{-}N{=}N\text{-}OH \qquad (9.1)$$

For the substrate,

naththols, phenols: $$ROH \rightleftharpoons RO^- + H^+ \qquad (9.2)$$

amines: $$RNH_3^+ \rightleftharpoons RNH_2 + H^+ \qquad (9.3)$$

and there are four possible reactions that can be occuring. Bartlett proved that in coupling to amines it is the free amine and not the ammonium ion which entered into the substitution step proper and that the reacting form of the electrophilic component was not the diazohydroxide, but the diazonium ion. For the coupling of 1-naphthol and diazotized sulphanilic acid, the reaction species and the corresponding equilibria are:

$$AOH \rightleftharpoons AO^- + H^+ \qquad (9.4)$$

$$ArN_2^+ + H_2O \rightleftharpoons ArN_2OH + H^+ \rightleftharpoons ArN_2O^- + 2H^+ \qquad (9.5)$$

In the secondary reaction, the reactive species are the naptholate form of R, viz. RO^-, and the diazonium ion ArN_2^+:

$$ROH \rightleftharpoons RO^- + H^+ \qquad (9.6)$$

The concentrations of reactive species can be related to the total concentrations of A and B via equilibria of Eqn (9.4) and (9.5):

$$[AO^-] = \frac{[A]}{1 + 10^{(pK_A - pH)}} \qquad (9.7)$$

$$[ArN] = \frac{[B]}{1 + 10^{(2pH - pK_1 - pK_2)}} \qquad (9.8)$$

For the primary reaction, azo coupling is an electrophilic aromatic substitution proceeding via an intermediate which reacts with bases to form the final product. The reaction mechanism is:

$$AO^- + ArN_2^+ \underset{k_{-1},s}{\overset{k_1,s}{\rightleftharpoons}} \text{Complex} \underset{\text{base}}{\overset{k_2,s}{\rightleftharpoons}} RO^- \qquad (9.9)$$

Steady-state approximation shows:

$$r_1 = \frac{k_1,s\ k_2,s\ [\text{base}]}{k_{-1},s + k_2,s\ [\text{base}]}\ [AO^-]\ [ArN_2^+] = k_1',s\ [AO^-][ArN_2^+] \qquad (9.10)$$

and it is evident from equations (9.4) and (9.5) that a decrease in pH raises the concentration of reactive diazonium ions, but reduces that of the naptholate ions. There exists therefore an optimum pH at which the product of the concentrations of the reactive species is maximized and thus, according to equation (9.10), the reaction rate is a maximum for given total reagent concentrations.

By analogy, Putter [62] applied Bartlett's method to several naphtholsuphonic acids, which differed greatly in the equilibrium constant for the dissociation of their phenolic group. The kinetic determinations carried out with these combinations in the range of pH 7.4 to 9.8 showed the proportionality expected between the rate and the concentration of the naptholate ion, but none with that of the undissociated naphthol. However, semiquantitative experiments using coupling in very acid media (60% to 80% sulphuric acid) suggest that the undissociated phenol too is capable of reaction [63,64], but the rate of coupling to it is at least 10^{10} times less than that to phenolate and so remains practically undetectable even in moderately acid solution. This situation is shown in Figure 9.1.

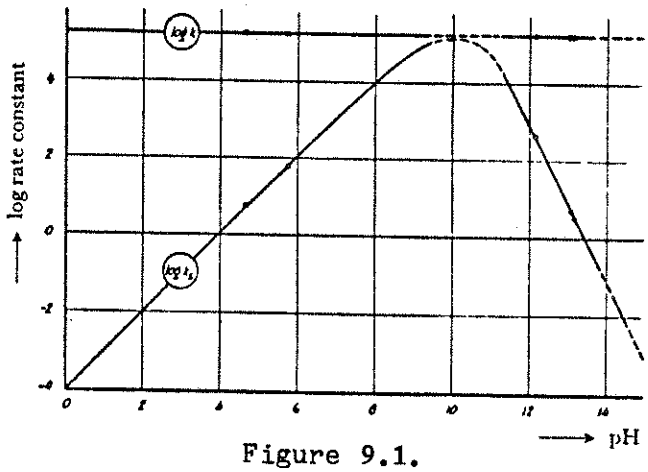

Figure 9.1.

pH dependence of the rate constants of coupling diazotized metanilic acid to 2-naphthol-6-sulphonic acid [66]

On the other hand for the function of the diazonium ion in the reaction, Zollinger [66] investigated the dependence of the rate of coupling on the ionic strength of the medium for the interaction of 2-naphthyl-amine-6-sulphonic acid with three diazo components in order to determine the sign and magnitude of the ionic charge on the latter. Bronsted's equation for primary salt effects takes the form as follows for the case of azo coupling:

$$\log k_I = \log k_o + \frac{2 Z_D Z_C \alpha I^{1/2}}{1 + \beta\alpha I^{1/2}} \qquad (9.11)$$

where α and β are constants.

It becomes apparent that increasing ionic strength would cause a decrease in the rate of reaction in the case of the diazonium ion (negative salt effect), but an increase in the case of the diazotated ion (positive salt effect). When the diazohydroxide or another electrically neutral species of diazo compound, such as the diazoacetate, is the reacting entity, the rate of coupling should be independent of the ionic strength. For the azo-diazo coupling reaction of 1-naphthol and diazotized sulphanilic acid, considering Eqn. (9.10), frequently k_2,s [base] >> k_1,s so that $k'_1,s = k_1,s$. Since the reactive species are ions, k'_1,s will generally depend upon ion strength (primary salt effect). Figure 9.2 illustrates this general salt effect.

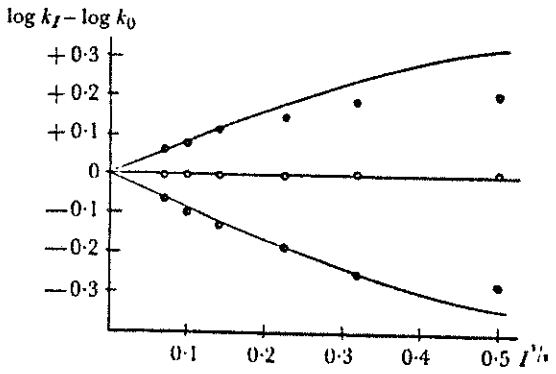

Figure 9.2.

Dependence of the rates of reaction of couplings to 2-naphthylamine-6-sulphonic acid on the ionic strength [66]

Circles indicate constants determined experimentally; the curves are those calculated according to Brönsted's equation

◐ 4-diazotoluene ○ diazobenzene-4-sulphonic acid ◑ diazobenzene-2,5-disulphonic acid

APPENDIX 9.2

Derivation of the Slab Diffusion-Reaction Equations

The continuity of species i, which we presume to be generated by reaction term R_i, over the control volume eddy, shows

$$\frac{\partial c}{\partial t}i = -\left(\frac{\partial N}{\partial x}ix + \frac{\partial N}{\partial y}iy + \frac{\partial N}{\partial z}iz\right) + R_i \tag{9.12}$$

This is the equation of continuity which describeds the change of molar concentration of the component i with respect to time at a fixed point in space. This change results from the motion of species i and its chemical reaction.

$$\frac{\partial c}{\partial t}i = -\left(\nabla \cdot \bar{N}_i\right) + R_i \tag{9.13}$$

The vector differential operator is defined in reatangular coordinates as

$$\nabla = \bar{\delta}_x \frac{\delta}{\delta x} + \bar{\delta}_y \frac{\delta}{\delta y} + \bar{\delta}_z \frac{\delta}{\delta z} \tag{9.14}$$

In order to obtain the equation which is generally used to describe diffusion, the molar flux $\bar{N}_i$ is replaced by the appropriate expression (9.19) which includes the concentration gradient.

$$\bar{N}_i = c_i \bar{v}_i = x_i \sum_{j=1}^{n} \bar{N}_j + \bar{J}_i \tag{9.15}$$

$$x_i = \frac{c}{\sum_{j=1}^{n} c_j} i = \frac{c}{c} i \tag{9.16}$$

$$x_i \sum_{j=1}^{n} \bar{N}_j = c_i \frac{\sum_{j=1}^{n} c_j \bar{v}_j}{\sum_{j=1}^{n} c_j} = \bar{c}v \tag{9.17}$$

$$\bar{J}_i = -c D_i \nabla x_i \tag{9.18}$$

$$\bar{N}_i = c_i \bar{v} - c D_i \nabla x_i \tag{9.19}$$

Equation (9.15) shows that the diffusion flux $\bar{N}_i$ relative to stationary coordinates is the resultant of two vectors, namely the vector given by equation (9.17) which is the molar flux of i resulting

from the bulk motion of the fluid and the vector given by equation (9.18) which, in turn, is the molar flux of i resulting from the diffusion superimposed on the bulk flow.

When equation (9.19) is substituted into (9.13) we get the following diffusion equation:

$$\frac{\partial c}{\partial t}i = -(\nabla \cdot c_i \vec{v}) + (\nabla \cdot cD_i \nabla x_i) + R_i \qquad (9.20)$$

Equation (9.20) describes the concentration profiles of the species i in a diffusing system. The only restriction is the absence of thermal, pressure and forced diffusion.

Assumption of Constaant c and D_i

Usually the experimental work is carried out with dilute solutions, thus the concentration of the solvent is much greater than that of the solutes and remains constant for an incompressible fluid. The sum of all concentrations, i.e. c, may be taken as constant. If D_i is also assumed to be constant, equation (9.20) becomes:

$$\frac{\partial c}{\partial t}i = -c_i(\nabla \cdot \vec{v}) - (\vec{v} \cdot \nabla c_i) + D_i \Delta c_i + R_i \qquad (9.21)$$

Assumption of Zero Molar Velocity inside the Slab and the Effect of Convection

For dilute solution, the molar velocity within the slab can be assumed zero :

$$\frac{\partial c}{\partial t}i + \vec{v} \cdot \nabla c_i = D_i \Delta c_i + R_i \qquad (9.22)$$

where Δ is Laplacian operator ∇^2:

$$\nabla^2 = \Delta = \frac{\partial^2}{\partial x^2} + \frac{\partial^2}{\partial y^2} + \frac{\partial^2}{\partial z^2} \qquad (9.23)$$

Assumption of One Dimensional Concentration Gradient

For the slab used in the simulation, only x-direction concentration gradient is considered:

$$\frac{\partial c}{\partial t}i + U \frac{\partial c}{\partial x}i = D_i \frac{\partial c^2}{\partial x^2}i + R_i \qquad (9.24)$$

APPENDIX 9.3

Parameters for Model-Experiment Comparison

The parameters for modelling are partially taken from the literature [126]. The values of the parameters for model-experiment comparison are:

V_{max} = 0.0012 g glucose/g cell.sec.

K' = 0.0504 g/l

R_s = 2 μm

S_o = 0.03 g/l

X_{max} is estimated from the glucose consumption and maximum yield. Under steady state,

glucose consumption = $F(S_{in} - S_{out}) \doteq FS_{in}$ $(S_{in} >> S_{out})$

cell production = $F(X_{out} - X_{in}) = FX_{out}$ (when $X_{in} = 0$)

Since in well mixed fermenters, $X_{out} = X$ (in the fermenter), therefore, yield of biomass, Y, is,

$$Y = \frac{\text{cell production}}{\text{glucose consumption}} = \frac{FX}{FS_{in}} = \frac{X}{S_{in}}$$

or,

$$X = YS_{in}$$

From the maximum yield and the feeding amount of glucose , we have,

$$X_{max} = Y_{max}S_{in}$$

The maximum yield varies from 0.45 to 0.5 [100, 111-114], and Y_{max} = 0.45 is taken here. The X_{max} then is,

$$X_{max} = 0.45 \times 11 \text{ (g/l)} = 0.495 \text{ (g/l)}$$

The values of R_s and S_o are estimated from the experimental measurements (see p. 89 Table 6.3 and p. 78 Table 6.1). Since X_{max} is neither affected very much by the values of S_o (in the range of 0.03 to 0.05 g/l) and those of X_{max} (4 to 5.5 g/l, Figure 5.4 and 5.5), nor by the values of R_s (in the range of 2 to 10 μm, $\xi=(R_o/R_s)^{0.5}-1$), the small variations in setting the values of S_o, X_{max} and R_s will not affect the results for modelling significantly.

10. NOTATION

A	1-naphthol
B	Diazotized sulphonate acid
BA1	Front of baffle port
BA2	Between baffle feed port
BOT	Fermenter bottom
C_i	Dimensionless concentration of species i, mol/m³
c_i	Concentration of species i, mol/m³
D	Diameter of fermenter, mm; or dilution rate, 1/hr; or diffusivity, m²/sec.
D'	Effective diffusivity, m²/sec
D_i	Diffusivity of species i, m²/sec
D_v	Diameter of vessel, mm
d	Thickness of quartz cell, cm; or diameter of stirrer, mm
F	Feeding rate of media, l/sec.
I	Ion strength, g ion/m³
IP	Injection port of reactant B
$\vec{J}_i$	Mass flux of component i relative to the molar average velocity mol/cm².sec
K'	Michaelis constant for glucose uptake, g/l
k_i	Rate constant of order i, m³/mol.sec
k_I	Rate constant at ionic strength I, m³/mol.sec
k_o	Rate constant at ionic strength 0, m³/mol.sec
ks	Stoichiometric rate constant, m³/mol.sec
$k'_{i,s}$	Rate constant of order i based on reactive species, m³/mol.sec
M	$k_2\delta_0^2 c_{B0}/D$, dimensionless micromixing modulus or segregation number
L	Characteristic length, m
N	Agitator speed, rpm
N_A	Mole of reactant A
N_B	MOle of reactant B
Nix, Niy, Niz	Rectangular components of the molar flux vector $\vec{N}$, mol/cm².sec
n	Reaction order
n_o	Minimum agitation speed for gas dispersion, rpm
OD	Optical Density
P	Power dissipation, W
P_g	Power dissipation in gased system, W
R	Monoazodye (azodye) or addition rate of B, cc/min
RQ	Respiratory Quotient, mole carbon dioxide formed/mole oxygen consumed
Q	Gas flow rate, liter/min
R_i	Generation of species i by reaction, mol/sec
$\bar{R}_k$	Radius of Kolomogroff eddy, m
R or r	Radius of sphere
S	Diazodye; or substrate concentration, g/l

S_o Substrate concentration in bulk fluid,
S_s Substrate concentration on cell surface,
STB Stirrer bottom port
STS Stirrer side port
SUR Surface port
T Dimensionless time
t Time, second
$\bar{t}_c$ Mean circulation time, second
U Velocity in x-direction component, m/sec
V Volume of liquid in fermenter, m^3;
$\bar{v}$ Glucose uptake rate of yeast, g glucose/g cell.sec
$\bar{v}$ Mole average velocity, cm/sec
v_i Velocity of species i, cm/sec
X Reaction extent or dimensionless distance, or cell density g/l
X_s Yield of S or micromixing index, dimensionless
x, y, z Rectangular coordinate
x_i Mole fraction of species i
Y^i Biomass yield, grams of biomass formed/gram glucose consumed
Z_D Charges on the reactive forms of diazo
Z_C Charges on the coupling components

Greek Letter

α Volume ratio of reactant A and B or constant
β Stretching parameter
$\bar{\delta}$ Instantaneous thickness of reaction zone, m
$\bar{\delta}_x$, $\bar{\delta}_y$, $\bar{\delta}_z$ Unit vectors associated with the x, y, z-coordinates
ε Energy dissipation rate, W/kg
ε_i Absorbence of species i
γ Rate of laminar shear, $second^{-1}$; or power constant
Kinematic viscosity or effectiveness factor for growth
μ Specific growth rate, /hr
λ Ratio constant
λ_k Kolmogoroff velocity microscale, m
τ Mean residence time, second

Subscripts

A 1-naphthol
B Diazotized sulphonate acid
D Diffusion
i Species i, or operation index
j Operation index
m Mixing
R Reaction, or monoazodye
S Diazodye
s Stretching, or surface
x, y, z Component in x, y, z direction of rectangular coordinate
o Initial time, or bulk conditions
1/2 Half-life

11. BIBLIOGRAPHY

1. R.S.Brodkey, Turbulence in Mixing Operations: Theory and Application to Mixing and Reactions, Academic Press, (1975)

2. R.S.Brodkey, The Phenomena of Fluid Motions, Addison-Wesley Publishing Co. Inc., Reading, Mass., (1967)

3. J.Rushton and J.Y.Oldshue, Chem.Eng.Prog., 49, 161, (1953)

4. J.M. Coulson and J.F. Richardson, Chemical Engineering Volume 3. Chemical Reactors Design, Biochemical Reaction Engineering including Computational Techniques and Control, Pergamon Press, Oxford (1979)

5. M.P.Dudukovic, 'Micromixing Effects on Multiple Steady States in Isothermal Chemical Reactors,' Chemical Engineering Science, 32, 985 (1977)

6. O. Levenspiel, Chemical Reaction Engineering, New York, John Wiley and Sons, 326, (1972)

7. P.V.Danckwerts, Appl. Sci. Research, 3, 279, 1952

8. P.V.Danckwerts, Chem.Eng.Sci., 7, 116, (1957)

9. J.W.Hiby, Chem.Eng.Technik, 51, 704, (1979)

10. H.Kramers, 'Physical Factors in Chemical Reaction Engineering, ' Chemical Engineering Science, 8,45 (1958)

11. P.V.Danckwerts, 'The Effects of Incomplete Mixing on Homogeneous Reactions,' Chemical Engineering Science,8,93 (1958)

12. T.N.Zwietering, 'The Degree of Mixing in Continuous Flow Systems,' Chemical Engineering Science,11,1 (1959)

14. H.Weistein and J.Adler, 'Micromixing Effects in Continuous Chemical Reactors,' Chemical Engineering Science,22,65 (1967)

15. J.Villermaux and A.Zoulalian,'Etat de melange du fluide dans un réacteur continu. A propos d'un modèle de Weinstein et Adler,' Chemical Engineering Science,24, 1513 (1969)

16. C.Aubry and J.Villermaux, 'Representation du Melange Imparfait de Deux Courants de Reactifs Dans un Reacteur Agite Continu,' Chemical Engineering Science,30, 457 (1975)

17. E. B. Nauman, 'The Droplet Diffusion Model for Micromixing,' Chemical Engineering Science,30, 1135 (1975)

18. K.T.Troung and J.C.Methot, 'Etude Expérimentale du Micromélange a l'aide d'untraceur Non-réctif Dans un Réactur Agité,' Canadian Journal of Chemical Engineering, 52, 767 (1974)

19. R.J. Ott and P.Rys, 'Chemical Selectivities Disguised by Mass Diffusion I. A Simple Model of Mixing-Disguised Reactions in Solutions,' Helvetica Chimica Acta, 58, 2074 (1975)

20. F.Nabholz, R.J.Ott and P.Rys, 'Chemical Selectivities Disguised by Mass Diffusion II. Mixing-Disguised Nitrations of Aromatic Compounds with Nitronium Salts,' Helvetica Chimica Acta, 58, 2093 (1975)

21. F.Nabholz, R.J.Ott and P.Rys, 'Chemical Selectivities Disguised by Mass Diffusion III. A Comparison of Two Versions of a Simple Model of Mixing-Disguised Reactions in Solution,' Helvetica Chimica Acta, 60, 2926 (1977)

22. F. Nabholz and P.Rys, 'Chemical Selectivities Disguised by Mass Diffusion IV. Mixing-Disguised Nitrations of Aromatic Compounds with Nitronium Salts,' Helvetica Chimica Acta, 60, 2937 (1977)

23. J.R.Bourne, E.Crivelli and P.Rys, 'Chemical Selectivities Disguised by Mass Diffusion V. Mixing-Disguised Azo Coupling Reactions,' Helvetica Chimica Acta, 60, 2944 (1977)

24. J.R.Bourne and F.Kozicki, 'Mixing Effects During the Bromination of Resorcin,' Chemical Engineering Science, 32, 1538 (1977)

25. F.Kozicki, 'Selektivitat Mischungsmaskierter Reaktionen in Ruhrkesseln,' Dissertation no. 6618, Eidgenossischen Technischen Hochschule, Zurich, Switzerland (1980)

26. J.R.Bourne, F.Kozicki and P.Rys, 'Mixing and Fast Chemical Reaction I. Test Reaction to Determine Segregation,' Chemical Engineering Science, 36, 1643 (1981)

27. H.Belevi, J.R.Bourne, and P.Rys, 'Mixing and Fast Chemical Reaction II. Diffusion-Reaction Model for the CSTR,' Chemical Engineering Science, 36, 1649 (1981)

28. J.R. Bourne, F.Kozicki, U.Moergeli and P.Rys, 'Mixing and Fast Chemical Reaction III. Model-Experiment Comparisons,' Chemical Engineering Science, 36, 1655 (1981)

29. W. Angst, J.R.Bourne, and R.N.Sharma, 'Mixing and Fast Chemical Reaction IV. The Dimensions of the Reaction Zone,' Chemical Engineering Science, 37, 585 (1982)

30. W. Angst, J.R.Bourne, and R.N.Sharma, 'Mixing and Fast Chemical Reaction V. Influence of Diffusion within the Reaction Zone on Selectivity,' Chemical Engineering Science, 37, 1259 (1982)

31. O. Bolaern and J.R.Bourne, 'Mixing and Fast Chemical Reaction VI. Extension of the Reaction Zone,' Chemical Engineering Science, 38, 999 (1983)

32. J.C.Hill, Ann.Rev.Fluid Mech., 8, 135, (1976)

33. A.Berker and S.Whitaker, Chem.Eng.Sci., 33, 889 (1978)

34. B.W.Ritchie and A.H.Tobgy, 'General Population Balance Modelling of Unpremixed Feedstream Chemical Reactors: A Review,' Chem.Eng.Commun., 2, 249 (1978)

35. J.Villermaux and J.C.Devillon, Proc.Sec.Int.Symp. Chem.React.Eng. B1-13, Elstvier, Amsterdam (1972)

36. A.Zoulalian and J.Villermaux, Adv.Chem.Ser., 133, 348 (1974)

37. J. Beer,Jr and R.S.Miller, Chemical Engineering Progress Symposium Series, 55, 23 (1959)

38. S. Middleman, Fundamentals of Polymer Processing, Chapter 12., McGraw Hill, New York (1977)

39. J.M. Ottino, W.E.Ranz and C.W.Macosko, 'A Lamellar Model for Analysis of Liquid-Liquid Mixing,' Chemical Engineering Science, 34, 877 (1979)

40. J.F.Brodberge, Thesis, Inst.Nat.Polytech.Lorraine (1981)

41. J.P. Barthole, J.Maisonneuve, J.N.Genoe, R.David and J.Villermaux, 'Measurement of Mass Transfer Rates, Velocity and Concentration Fluctuations in an Industrial Stirred Tank Reactor,' Chemical Engineering Fundamentals, A European Quarterly, 1, 17 (1982)

42. A.Bennani, J.N.Gence, J.Mathien, C.R.Acad.Sci., Paris, 293, Ser. II, 791 (1981)

43. J. Villermaux, 'Mixing in Chemical Reactors,' Laboratoire Des Sciences du Génie Chimique, CNRS-ENSIC Institut National Polytechnique De Lorraine, Nancy-France (in press)

44. S.J.Ye, 'Micromixing in Biochemical Reactors: Characterization of Virtis Fermenter Model 43-100,' Master Thesis, Department of Chem.Eng., Washington University, St.Louis, MO 63130 (1984)

45. R.C.Kinter, 'Drop Phenomena Affecting Liquid Extraction,' Advances in Chemical Engineering, 4, 52 (1963)

46. E.B.Naumann and B.A.Buffham, Mixing in Continuous Flow Systems, John Wiley and Sons, New York, (1983)

47. H. Kramers and K.R.Westerterp, Elements of Chemical Reactor Design and Operation, Academic Press, New York, (1963)

48. J. Paca, P. Ettler and V. Gregi, 'Hydrodynamic Behaviour and Oxygen Transfer Rate in a Pilot Plant Fermenter,' Journal of Applied Chemistry and Biotechnology, 26, 309 (1976)

49. N. Blakebrough and K.Sambamurphy,'Mass Transfer and Mixing Rates in Fermentation Vessels,' Biotechnology and Bioengineering, 7,25 (1966)

50. A. Einsele and R.K.Finn,'Influence of Gas Flow Rates and Gas Holdup on Blending Efficiency in Stirred Tanks,' Industry and Engineering Chemistry Process Design and Development, 19, 600 (1980)

51. H. Hofmann, 'Interaction of Fluid Flow and Chemical Kinetics in Homogeneous Reaction,' AIChE National Meeting, Houston, Texas (1963)

52. J.B. Joshi, A.B.Pandit and M.M.Sharma, 'Mechanically Agitated Gas-Liquid Reactors,' Chemical Engineering Science, 37, 813 (1982)

53. L.L. Tavlarides and M.Stamatoudis, 'The Analysis of Interphase Reactions and Mass Transfer in Liquid-Liquid Dispersions,' Advances in Chemical Engineering, 11, 199 (1981)

54. L.L. Tavlarides, 'Modelling and Scaleup of Dispersed Phase Liquid-Liquid Reactors,' Chemical Engineering Communications, 8, 133 (1981)

55. K. Rietema, 'Segregation in Liquid-Liquid Dispersions and Its Effect on Chemical Reactors,' Advances in Chemical Engineering, 5, 237-303 (1964)

56. J.T. Davies, 'Mass Transfer and Interfacial Phenomena,' Advances in Chemical Engineering, 4, 1 (1963)

57. A.Einsele, D.L.Ristroph and A.E.Humphrey, 'Mixing Times and Glucose Uptake Measured with a Fluorometer,' Biotechnology and Bioengineering, 20, 1487 (1978)

58. G.S. Hansford and A.E.Humphrey, 'The Effect of Equipment Scale and Degree of Mixing on Continuous Fermentation Yield at Low Dilution Rates,' Biotechnology and Bioengineering, 8, 85 (1966)

59. M.S.K. Chen, 'The Theory of Micromixing for Unsteady State Flow Reactors,' Chemical Engineering Science, 26, 17 (1971)

60. J.R.Bourne, 'Mixing on the Molecular Scale (Micromixing),' Chem. Eng. Sci., 38, No 1., 5, 1983

61. J.B. Conant and W.D.Peterson, 'The Rate of Coupling of Diazonium Salts with Phenols in Buffer Solutions,' Journal of the American Chemical Sociaty, 52, 1220 (1930)

62. R. Putter, 'Beitragzum Mechanismns der Azokupplung,' Angewandte Chemie, 63, 188 (1951)

63. Z.J. Allan, 'Aromatic Diazocompounds II. Coupling in Concentrated Sulphuric Acid,' Collection of Czechorlovak Chemical Communications,16-17, 620 (1952)

64. H. Zollinger, 'Zurkenntinis der Kupplungsreaktion. V: Die Reaktionsfahigkeit des Undissoziierten Phenols. Kupplungen in Hochkonzentrierten Schwefelsauren,' Helvetica Chimica Acta, 36, 1070 (1953)

65. R. Wistar and P.D.Bartlett, 'Kinetics and Mechanism of the Coupling of Diazonium Salts with Aromatic Amines in Buffer Solutions,' Journal of the American Chemical Sociaty, 63, 413 (1941)

66. H. Zollinger, Azo and Diazo Chemistry-Aliphatic and Aromatic Compounds, Interscience Publishers, Inc. (1961)

67. S. Nagata, Mixing, Principles and Applicaitons, Halsted Press, 341 (1975)

68. O. Levenspiel, THe Chemical Reactor Omnibook, OSU Book Stores, Inc. (1979)

69. J.Bryant, 'The Characterization of Mixing in Fermenters,' Advances in Biochemical Engineering, 5, 101 (1977)

70a. R.J. Freund and R.C. Littell, SAS for Linear Models, Cary, NC: SAS Institute (1981)

70b. R.A.Waller and D.B.Duncan, 'A Bayes Rule for the Symmetric Multiple Comparison Problem,' Journal of the American Statistical Associations, 64, 1484 (1969)

71. A.A.Ray, J.P.Sall and M.Saffer, SAS User's Guide: Basics, 1982 edition, SAS Institute Inc. (1982)

72. A.A.Ray, J.P.Sall and M.Saffer, SAS User's Guide: Statistics, 1982 edition, SAS Institute Inc. (1982)

73. V.W. Uhl and J.B.Gray, Mixing Theory and Practice, Academic Press, 133 (1966)

74. J.R.Bourne and S.Rohani, 'Mixing and Fast Chemical Reaction VII. Deforming Reaction Zone Model for the CSTR,' Chemical Engineering Science, 38, 911 (1983)

75. R.C.Waggoner and G.K.Patterson, 'Effect of Imperfect Mixing on th Performance and Control of Batch and Semibatch Reactors,' ISA Transactions, 14, 331 (1975)

76. D.P.Rao and L.L.Edwards, 'Mixing Effects in Stirred Tank Reactors: A Comparison of Models,' Chem. Eng. Sci., 28, 1179 (1973)

77. J.T.Davies, Turbulence Phenomena, New York, Academic Press, (1972)

78. J.Bulicka, 'Mass Transfer between Two Turbulent Liquid Phases,' Chemical Engineering Science, 31, 137 (1976)

79. A.J.Madden et al, AIChE J., 8, 233 (1962)

80. P. H. Calderbank, 'Physical Rate Processes in Industrial Fermentation,' Institution of Chemical Engineers, Transactions (London) 36, 443 (1958)

81. K. R. Westerterp, 'Design of Agitators for Gas-Liquid Contacting,' Chemical Engineering Science, 18, 495 (1963)

82. P.V.Danckwerts, Chemical Engineering Science, 2, 1 (1953)

83. A.Kattan and R.J.Adler, Chemical Engineering Science, 27, 1013 (1972)

84. J.M.Douglas, Chemical Engineering Progress Symp. Series, 60(48), 1 (1965)

85. Y.Nishimura and M.Matsubara, Chemical Engineering Sicence, 25, 1785 (1970)

86. K.B.Bischoff, Can. J. Chem.Eng., 44, 281 (1966)

87. L.T.Fan, B.I.Tsai and L.E.Erickson, AIChE J., 17(3), 689 (1971)

88. L.A.Dohan and H.Weinstein, Ind.Eng.Chem.Fund., 12(1), 64 (1973)

89. M.P.Dudukovic and H.Lamba, 68th AIChE Annual Meeting, Los Angeles, Nov. 1975, Microfiche No. 35, Paper No. 55c

90. R.B.Bird, W.E.Steward and E.N.Lightfoot, Transport Phenomena, New York, John Wiley and Sons, (1976)

91. T.T.Szabo and E.B.Nauman, AIChE J., 15, 575 (1969)

92. J.C.Mecklenburgh, Can.J.CHem.Eng., 48, 279 (1970)

93. E. Plasari, R.David and J.Villermaux, 'Micromixing Phenomena in Continuous Stirred Reactors Using a Michaelis-Menten Reaction in the Liquid Phase,' American Chemistry Science (ACS Symposium Series-Chemical Reaction Engineering) 65, 125-139 (1978)

94. E. Plasari, R.David and J.Villermaux, J.Nouveau J.Chim., 1, 49 (1977)

95. S.B.Hanna, E.Hunziker, T.Saito and H.Zollinger, Helvetica Chimica Acta,52, 1537 (1969)

96. D.I.C. Wang, C.L.Cooney, A.L.Demain, P.Dunnill, A.E.Humphrey, and M.D.Lilly, Fermentation and Enzyme Technology (Wiley, New York, 1979)

97. J.Oldshue, Biotechnol. Bioeng., 89, 3 (1966)

98. H.Taguchi, 'The Nature of Fermentation Fluids,' in Adv. in Biochem.Eng., 1, 1 (1971)

99. P.R. Fields and N.K.H.Slater, 'The Influence of Fluid Mixing upon Respiratory Patterns for Extended Growth of a Methylotroph in an Air-Lift Fermenter,' Biotechnology and Bioengineering, 26, 719-726, (1984)

100. A.Fiechter, 'Continuous Cultivation of Yeasts,' in D.M.Prescott ed., 'Methods in Cell Biology,' 11, 97, Academic Press (1975)

101. R.K.Bajpai and M.Reuss, Can.J.Chem.Eng., 60, 384 (1982)

102. J. Lievense and H.Lim, 'The Growth and Dynamics of Saccharomyces Cerevisiae', in G.Tsao, 'Annual Reports on Fermentation Processes,' 5, 211, Academic Press (1982)

103. A.Fiechter, G.F.Fuhrmann and O.Kappeli, 'Regulation of Glucose Metabolism in Growing Yeast Cells,' ETH, Zurich Switzerland

104. A.Einsele, 'Die Funktion de Stofftransportes in Bioreaktoren beim Mikrobiellen Kohlen wasserstoffabbau,' Diss. No. 4900, ETH, Zurich (1972)

105. T.Egli and A.Fiechter, J.General Microbiology, 123, 365 (1981)

106. J.E.Bailey and D.F.Ollis, Biochemical Engineering Fundamentals, McGraw-Hill Book Company New York (1977)

107. P.R.Stewart, 'Analytical Methods for Yeasts,' in D.M.Prescott, 'Methods in Cell Biology,' 12, 111, Academic Press, New York (1975)

108. D.Herbert, P.J.Phipps and R.E.Strange, 'Chemical Analysis of Microbial Cells,' in J.R.Norris and D.W.Ribbons ed., 'Methods in Microbiology,' 5B, 209, Academic Press, New York (1971)

109. E.D. Korn and D.H.Northcote,'Physical and Chemical Properties of Polysaccharides and Glycoproteins of the Yeast-Cell Wall,' Biochem. J., 75, 12 (1960)

110. K.von Meyenburg, 'Catabolite Repression and the Germination Cycle of Saccharomyces Cerevisiae,' University Institute of Microbiology, Oster Farimagsgade 2A, Copenhagen K, Denmark (unpubished)

111. H.P.Knopfel, 'Zum Crabtree-Effekt bei Saccharomyces cerevisiae und Candida tropicalis,' Diss. No. 4906, ETH, Zurich (1972)

112. A.Fiechter and H.K.von Meyenburg in Proc. 2nd Int. Symp. Yeast, Bratislava,' (A Kockova-Kratochrilova, ed.), p. 387, Slovenskej Akademie Vied (1966)

113. H.K.von Meyenburg, in 'Continuous Cultivation of Microorganisms, 4th Symp. Prague,' (I.Malek, K.Beran, Z.Fencl, V.Munk, J.Ricica, and H.Smrckova, eds.), p. 129, Academic Press, New York (1968)

114. C.Beck and H.K.Meyenburg, J. Bacteriology, 96, 479 (1968)

115. H.K.von Meyenburg and A.Fiechter, in Proc. 2nd Int. Symp. Yeast, Bratislava, (A Kockova-Kratochrilova, ed.), p. 377, Slovenskej Akademie Vied (1966)

116. S.Bartnicki-Garcia and I.McMurrough, in 'The Yeasts (Vol.2): The Physiology and Biochemistry of Yeasts,' (A.H.Rose, and J.S.Harrison, eds.), 441, Academic Press, New York (1971)

117. J.P.Barford and R.J.Hall, Exp.Cell Research 102, 276 (1979)

118. H.K.von Meyenburg, Path. Microbiol. 31, 117 (1968)

119. G.C.Johnston, C.W.Ehrhardt, A.Lorincz and B.L.A.Carter, 'Regulation of Cell Size in the Yeast Saccharomyces cerevisiae,' J. Bacteriology, 137, 1 (1979)

120. W.Woehrer and M.Roehr, Biotech. Bioeng., 23, 567 (1981)

121. F.Bergter and W.A.Knorre, Z. Allg. Mikrobio., 12, 613 (1972)

122. P.Peringer, H.Blachere, C.Corrieu and A.G.Lane, Biotech. Bioeng. Symp. No.4, 27 (1973)

123. P.Peringer, H.Blachere, C.Corrieu and A.G.Lane, Biotech. Bioeng. 16, 431 (1974)

124. A.H.Bijkerk and R.J.Hall, Biotech. Bioeng., 19, 267 (1977)

125. N.B.Pamment, R.J.Hall and J.P.Barford, Biotech. Bioeng., 20, 349 (1978)

126. J.P.Barford and R.J.Hall, Biotech. Bioeng., 23, 1735 (1981)

127. R.J.Hall and J.P.Barford, Biotech. Bioeng., 23, 1763 (1981)

128. T.B.Young and H.R.Bungay, Biotech. Bioeng., 15, 377 (1973)

129. T.B.Young, 'A Dynamic Analysis of Microbial Growth in a Chemostat Continuous Culture,' Ph.D. Thesis, Clemson University, Clemson, South Carolina (1971)

130. E.J.Conway and M.Downey, Biochemical Journal, 47, 347 (1950)

131. A.Rothstein, In 'Protoplasmatologia. Handbuch der Protoplasmaforschung' (L.V.Heilbrunn and E.Weber, eds.), Bd. II E 4, p.1, Springer-Verlag, Vienna (1954)

132. C.F.Heredia, A.Sols and G.DelaFuente, European Journal of Biochemistry, 5, 321 (1968)

133. A.Sols, In 'Aspects of Yeast Metabolism' (A.K.Mill and H.A.Krebs, eds.), p. 47, Blackwell Scientific Publication, Oxford (1968)

134. J.van Stevenick and A.Rothstein, J.Gen.Physiol., 49, 235 (1965)

135. G.K. Batchelor, 'Small Scale Variation of Convected Quantities like Temperature in Turbulent Fluid. Part 1. General Discussion and the Case of Small Conductivity,' Journal of Fluid Mechanics, 5, 113 (1959)

136. J.Villermaux and R.David, 'Recent Advances in the Understanding of Micromixing Phenomena in Stirred Reactors,' Chemical Engineering Communications, 21, 105 (1983)

137. G. Stephenson, Mathematical Methods for Science Students, 2nd Ed., Longman Group Limited (1979)

12. VITA

Biographical items on the author of the thesis, Mr. Shao-Jian Ye,

1) Born August 1, 1954

2) Technician, Department of Research and Development, Guangzhou Food Industry Corporation, September 1972 to March, 1977.

3) Attended the South China Institute of Technology from March, 1977 to June, 1980. Received the degree of Bachelor of Science in Industrial Fermentation/Chemical Engineering in June, 1980.

4) Microbial Engineer, Department of Research and Development, Guangzhou Food Industry Corporation, June, 1980 to September, 1980.

5) Attended Graduate School of the South China Institute of Technology from September, 1980 to December, 1981. Majored in Microbial Engineering/Chemical Engineering.

6) Attended Washington University from January, 1982 to August, 1984. Received the degree of Master of Science in Chemical Engineering in August, 1984.

7) Attended Washington University from September, 1984 to the present date.

January, 1985